Functional characterization of R294X and C-terminal *MECP2* mutations in Rett syndrome

By

Bridget Erran Collins

Dissertation
Submitted to the Faculty of the
Graduate School of Vanderbilt University
in partial fulfillment of the requirements
for the degree of

DOCTOR OF PHILOSOPHY
in

Neuroscience

May 31, 2022

Nashville, Tennessee

Approved:

Lisa Monteggia, Ph.D.

Colleen Niswender, Ph.D.

Danny Winder, Ph.D.

Jeffrey L. Neul, M.D. Ph.D.

ACKNOWLEDGMENTS

I must first acknowledge and thank the funding sources that have supported my doctoral training and this dissertation work: the National Institutes of Health (NIH) through Vanderbilt's Medical Scientist Training Program (T32GM007347), my Ruth L. Kirschstein National Research Service Award (F30MH122064), and Dr. Jeffrey L. Neul's R01HD083181, U54HD083211, and P50HD103537.

I would like to next acknowledge the Vanderbilt Medical Scientist Training Program (MSTP) for their continual support and advice. Additionally, this dissertation work would not have been possible without the training environment provided by the Vanderbilt Brain Institute, the Neuroscience Graduate Program, and Vanderbilt Cores (Mouse Neurobehavioral Core, Flow Cytometry Core, and Cell Imaging Shared Resource). I am especially thankful to Dr. John Allison in the Mouse Neurobehavioral Core for teaching me the art of behavior, for advice on experimental design and data analysis, for many fun political discussions, and for not-so-gently reminding me to not over-apologize.

I am so thankful for my thesis committee: Drs. Lisa Monteggia, Colleen Niswender, and Danny Winder. Your thoughtful feedback and encouragement have continually moved this work forward. I am especially thankful to Dr. Colleen Niswender, who welcomed me into RTT meetings with her lab, providing me with greater scientific guidance and support. I am particularly delighted to acknowledge and thank my mentor, Dr. Jeffrey Neul, for welcoming me as a wayward second-year graduate student and providing support through challenging times. His feedback and guidance were essential to my graduate training and professional development. His patience, positivity, and pursuit of translationally relevant research questions are an inspiration.

To my lab mates, current and former – you have all become some of my best friends. Thank you for welcoming me into the lab. To Dr. Jonathan Merritt – thank you for your time and patience in teaching me how to think carefully about experimental design and technique. Your encouragement and critical eye have irrevocably shaped my development as a scientist. Thank you too for keeping secret stashes of reagents and sharing them. To Katie Baugh and Željka Miletić – thank you for your friendship, many laughs, and our cat picture text group. I feel so lucky to work alongside such wonderful humans every day. To Kirsty Erickson – thank you for so many laughs and many helpful discussions about mouse behavior. (Thank you, too, for letting Hossein, Apollo, and I welcome Pluto into our life!)

To my family – my parents, sisters Mary and Patsy, and brothers Liam and Aidan. You have made life so fun, even when I'm so far away from home. Thank you for encouraging my training, even though it involves nearly a decade away from Chicago.

And finally, to my husband, Hossein. Thank you for your unwavering support, your kind understanding of late nights, your encouraging pushes to make me think, and your willingness to talk data over dinner. You make me a better person, and you make me a better scientist, and I'm grateful to have gone through this journey with you.

TABLE OF CONTENTS

Page

LIST OF TABLES

Table Page

LIST OF FIGURES

Figure Page

AMPA	α-amino-3-hydroxy-5-methyl-4-isoxazole propionic acid
ASD	autism spectrum disorder
BDNF	brain-derived neurotrophic factor
bFGF	basic fibroblast growth factor (FGF2, FGF-β)
BMP	bone morphogenetic protein
BRM	BRAHMA
BSA	bovine serum albumin
cAMP	cyclic adenosine monophosphate
CGI	CpG island
CNS	central nervous system
CRH	corticotropin-releasing hormone
CRISPR	clustered regularly interspaced short palindromic repeats
CTD	C-terminal domain
DAT	dopamine transporter
dbcAMP	dibutyryl cAMP
DNA	deoxyribonucleic acid
DNMT	DNA methyltransferase
DRD2	dopamine receptor D2
EGFR	epidermal growth factor receptor
EPSC	excitatory postsynaptic current
EPSP	excitatory postsynaptic potential
ESC	embryonic stem cell
FACS	fluorescence-activated cell sorting
FLNA	Filamin A
FoSTeS	fork stalling and template switching
GABA	γ-aminobutyric acid
GAPDH	glyceraldehyde-3-phosphate dehydrogenase
GDI1	GDP dissociation inhibitor 1
GDNF	glial cell-derived neurotrophic factor
GFP	green fluorescent protein
GPE	glycine-proline-glutamate
HDR	homology directed repair
HIER	heat-induced epitope retrieval
HP1	heterochromatin protein 1
ID	interdomain
I/O	input-output
IGF1	insulin-like growth factor 1
iPSC	induced pluripotent stem cell
IPSC	inhibitory postsynaptic current
KO	knockout
L1CAM	L1 cell adhesion molecule

LCR	low copy repeat
L-DOPA	L-3,4-dihydroxyphenylalanine (levodopa)
LOF	loss-of-function
LTD	long-term depression
LTP	long-term potentiation
LUHMES	Lund human mesencephalic
MBD	methyl-binding domain
MDS	*MECP2* duplication syndrome
MeCP2	methyl-CpG-binding protein 2
MMBIR	microhomology-mediated break-induced replication
MPP^+	1-methyl-4-phenylpyridinium
MRE	microRNA response element
N2a	Neuro-2a
NCoR	nuclear receptor co-repressor
NHEJ	non-homologous end joining
NID	NCoR/SMRT interaction domain
NL3	neuroligin-3
NMDA	N-methyl-D-aspartate
NPTII	neomycin phosphotransferase II
NTC	no template control
OPRM1	opioid receptor mu (μ) 1
PAM	protospacer adjacent motif
PBS	phosphate buffered saline
PFA	paraformaldehyde
PHF14	PHD finger protein 14
PI	propidium iodide
PLO	poly-L-ornithine
PNS	peripheral nervous system
PPF	paired-pulse facilitation
RAB39B	Ras-related protein Rab-39B
RNA	ribonucleic acid
RT-qPCR	quantitative reverse transcription PCR
RTT	Rett syndrome
sgRNA	single guide RNA
SMRT	silencing mediator of retinoid and thyroid hormone receptors
SRPK3	SRSF protein kinase 3
ssODN	single-stranded oligodeoxynucleotide
TBP	TATA-binding protein
TET	ten-eleven translocation
TH	tyrosine hydroxylase
TRD	transcription repression domain
TSS	transcription start site
WT	wild type

YBX1	Y-box binding protein 1
YY1	Yin Yang 1
XCI	X-chromosome inactivation

CHAPTER 1

Introduction

One afternoon in Vienna in 1965, pediatrician Andreas Rett walked into the waiting room of his clinic for children with disabilities and noticed two girls sitting in their mothers' laps, both with their arms gently restrained[1]. The mothers, by happenstance, released their grip simultaneously and both girls began to make unusual, stereotyped movements. With further research, Rett found that these girls shared similar developmental and clinical histories, and, upon analysis of the clinic's records, identified an additional six girls that did too. Rett believed he was observing a previously unrecognized syndrome and reported his findings in a little-known German journal one year later, in 1966[2]. This seminal article, titled "On a remarkable syndrome of cerebral atrophy associated with hyperammonemia in childhood," would remain virtually unrecognized for 15 years, until a group of European researchers would give a name to what pediatric neurologists now recognize as Rett syndrome.

Rett syndrome (RTT)

Andreas Rett's 1966 report described 22 young girls, each with an uncomplicated birth history and typical development until approximately 1 year of age[2]. However, at this age, Rett noted that the girls exhibited a consistent pattern of disruption in typical development, including shared characteristics of absent speech, motor dysfunction, apraxic gait, hand stereotypies, and epilepsy. Rett termed this syndrome "cerebral atrophy associated with hyperammonemia" and published his findings to raise awareness in the pediatric neurology community. Unfortunately, Rett's work was not widely read in the German journal *Wiener Medizinische Wochenschrift*, and his finding of hyperammonemia was not easily replicated by others, preventing broad acknowledgement of this childhood syndrome. Broad acknowledgement came only in 1983, when Swedish neurologist Bengt Hagberg and colleagues published a synthesis of 35 cases of "developmental stagnation…followed by rapid deterioration of higher brain functions" in young girls from France, Portugal and Sweden[3]. Noting similarities to the cases described in Rett's 1966 report, Hagberg termed this clinical pattern Rett's syndrome.

In the years following Hagberg's report, growing attention to this disorder led to the need for improved clinical characterization. With his broad expertise, Hagberg proposed a four-stage system describing the temporal progression of the disease: (1) early onset, (2) rapid deterioration, (3) plateau, and (4) late motor deterioration (**Figure 1**)[4]. Prior to onset of symptoms, children with Rett syndrome (RTT) undergo apparently typical development. In the first stage, early onset, girls with RTT may show delays in growth and, specifically, decreased head circumference (acquired microcephaly). The second stage of the disease, rapid deterioration, involves developmental regression with loss of previously acquired skills pertaining to language and hand use. This stage also includes the onset of hand stereotypies such as hand

wringing/squeezing and gait abnormalities. Children with RTT may also develop respiratory abnormalities (e.g. hyperventilation, apneas) at this time. Following this, cognitive function stabilizes while other medical conditions, such as seizures, arise in the plateau stage around 3-10 years of age. Finally, in the late motor deterioration stage, individuals with RTT may experience decreasing mobility, onset of parkinsonian features, and scoliosis, leading to significant motor disability.

RTT is diagnosed clinically, according to a set of guidelines published in 2010 by the RettSearch Consortium (**Table 1**)[5]. Typical, or classic, RTT is defined by the presence of a period of regression followed by recovery or stabilization, as well as the loss of acquired purposeful hand skills, the loss of acquired spoken language, gait abnormalities, and hand stereotypies. With the broader recognition of RTT, clinicians have also identified individuals that display some, but not all, of the features of typical RTT. These individuals are described to have atypical, or variant, RTT. Atypical RTT is defined by the presence of a period of regression followed by recovery or stabilization, as well as at least 2 of the main 4 criteria for typical RTT and at least 5 out of the 11 supporting criteria (e.g. breathing disturbances when awake, peripheral vasomotor disturbances, intense eye communication – "eye pointing"). Though diagnostic criteria have varied over the almost four decades since RTT was recognized globally, researchers have been able to glean epidemiologic data as to the incidence of RTT. RTT is a rare neurodevelopmental disorder, occurring with a cumulative incidence of 1.09 per 10,000 females by age 12 years[6].

The nearly exclusive occurrence of RTT in girls led the research community to predict that the disease is caused by an X-linked dominant mutation with lethality in males, the first part of which turned out to be true[3,7–11]. Extensive gene mapping of rare familial cases of RTT narrowed down the genetic region of interest to the Xq28 region, and in 1999 Ruthie Amir and colleagues identified a causative gene[10–15]. Using a systematic gene screening approach in sporadic cases of RTT, Amir et al. identified disease-causing mutations in the *MECP2* gene encoding methyl-CpG-binding protein 2 (MeCP2). Since then, it has been found that *MECP2* mutations account for over 95% of typical RTT cases and approximately 75% of atypical RTT cases[16,17]. *MECP2* mutations occur largely in a sporadic manner; however a small percentage of RTT cases occur in a familial manner through parental *MECP2* mutations[18,19].

The discovery of a genetic basis to RTT provided insight into the disease's marked manifestation in girls and women. While the notion of male lethality continues to mistakenly permeate the literature, genotyping of affected individuals and their parents led to the discovery that de novo *MECP2* mutations nearly exclusively derive from the paternal X-chromosome[18,20,21]. Consistently, a large portion of *MECP2* mutations involve C→T transitions at CpG sites, which, when methylated, are prone to spontaneous deamination and conversion to thymine[22]. Male germ cells are highly methylated on the X-chromosome, providing more chance for CpG mutation[23]. As the paternal X-chromosome is only inherited by female

children, RTT occurs nearly exclusively in girls and women. Occasionally, the *MECP2* mutation is inherited on the maternal X-chromosome[9,13,24]. In this case, mothers typically carry one allele with a *MECP2* mutation and have skewed X-chromosome inactivation in preference of the non-mutant allele. These mothers often do not fulfill criteria for RTT but may display mild cognitive impairment or a learning disability.

While most individuals with RTT are female, *MECP2* mutations do cause disease in males with an array of clinical phenotypes[9]. These mutations manifest disease in males in one of three ways: (1) inheritance of two X-chromosomes (47XXY, Klinefelter syndrome)[25,26], (2) development of a postzygotic *MECP2* mutation with resulting somatic mosaicism[27], and (3) rarely, inheritance of a *MECP2* mutation leading to RTT[28]. The array of *MECP2* mutations that causes disease in males also differs from those causing disease in females. For example, the A140V mutation is not considered to be associated with RTT in females, but can cause cognitive, motor, and psychiatric manifestations in males[29]. *MECP2*-associated disease in males ranges from cognitive impairment to typical and atypical RTT, progressive encephalopathy, and neonatal encephalopathy. Overall, disease tends to be more severe in males than in females, with males more commonly exhibiting abnormal initial development, ventilator dependency, and early death[30]. To better classify the different presentation and progression of *MECP2*-associated disease in males, the term "male RTT encephalopathy" has been proposed to describe the subset of males that meet criteria for RTT[30].

MECP2 Duplication Syndrome (MDS)

In the mid-2000s came the clinical discovery that overexpression of MeCP2 in people causes a different *MECP2*-related disorder, called *MECP2* duplication syndrome (MDS)[31,32]. Specifically, Meins et al. reported on a boy with severe intellectual disability and features of RTT who was determined to have a submicroscopic ~430 kb duplication within the Xq28 region containing the *MECP2* gene[31]. Following this, Van Esch et al. reported on four boys with intellectual disability that had duplications 400-800 kb in size containing several genes, including at least *L1CAM* (L1 cell adhesion molecule) and *MECP2*[32]. Several lines of evidence pointed specifically to *MECP2* as the genetic cause of MDS. First, the duplication of the individual described by Meins et al. did not involve *L1CAM*, suggesting that *MECP2* duplication is sufficient to cause MDS. Second, mouse modeling work suggested that MeCP2 overexpression leads to a progressive neurological disease involving seizures, spasticity, and premature death, and that higher MeCP2 level is associated with more severe disease[33].

The duplications that cause MDS are thought to occur via several molecular mechanisms[34,35]. The described *MECP2* duplications are non-recurrent, meaning that duplications have variable breakpoints and do not span the same genomic interval across unrelated individuals. In general, the Xq28 region has higher GC content and higher *Alu* repeat density compared to random sequences of the genome, possibly increasing regional genomic instability[34]. Furthermore, most

duplications have a distal breakpoint within a 215 kb genomic interval (47 kb telomeric to *MECP2*) that contains complex low copy repeat (LCR) sequences, suggesting that these LCRs may have a role in the origin of genomic rearrangement. Analysis of individual duplication breakpoints suggests that multiple mechanisms may be involved. For example, the *MECP2* duplication of one individual was proposed to occur via non-homologous end joining (NHEJ) due to the presence of proximal and distal microhomology[34]. However, the duplications of other individuals have been proposed to occur via complex rearrangements, which can result in embedded triplicated segments, segments of non-duplicated sequence within the duplicated region, and inversion of the duplicated sequence. These complex rearrangements may occur via Fork Stalling and Template Switching or, more generally, microhomology-mediated break-induced replication (FoSTeS/MMBIR), a replication-based mechanism that involves stalled replication forks switching templates through complementary template microhomology[36]. Further complicating this, duplicated segments of the Xq28 region have been found in tandem on the X-chromosome (Xq-Xp rearrangements), on the Y-chromosome (Xq-Yq translocations), as well as on autosomes (X-autosome translocations)[37].

Despite the wide variation of *MECP2* duplication events in mechanism of origin, genetic content, and genomic location, they collectively result in a consistent clinical MDS phenotype[37,38]. Individuals with MDS typically have severe developmental delay from birth, accompanied by microcephaly, hypotonia and acquired spasticity, feeding difficulties, and recurrent respiratory infections[38]. While developmental delay and hypotonia are commonly observed in neurodevelopmental disorders, the predisposition to infection distinguishes MDS, with many individuals requiring mechanical ventilatory support at some point. Infections range from otitis media to pneumonia, pyelonephritis, and meningitis[38]. While incompletely understood, gastroesophageal reflux and immune dysfunction may contribute to infection risk[39]. As individuals with MDS age, they may meet formal criteria for autism spectrum disorder (ASD) with gaze avoidance, restricted interests, and use of repetitive language[40,41]. Most individuals do not develop spoken language[42]. Seizures are also present in about half of individuals, with very variable onset. Overall, MDS is a severely debilitating disorder that requires lifelong specialized care. Often, recurrent infections coupled with refractory epilepsy and neurological deterioration lead to early death[42].

While individual *MECP2* duplication events are rare, MDS accounts for as much as 1% of unexplained X-linked intellectual disability[43]. Most *MECP2* duplications are transmitted to male children from a carrier mother[32]. Carrier mothers typically exhibit extreme (>90%) skewing with preference for the X-chromosome bearing one copy of *MECP2* and are asymptomatic or exhibit neuropsychiatric symptoms. Girls who inherit a *MECP2* duplication and do not have extreme skewing can manifest variable degrees of MDS-like symptoms, ranging from mild cognitive disability to severe disease similar to that

observed in males[44,45]. *MECP2* duplication can also occur de novo in males and females. In this case, males and females are affected similarly because the *MECP2* duplication is often expressed on an autosome[37,42].

Due to the rarity of MDS, clinical characterization and genotype-phenotype correlations in MDS are limited. However, work by Peters et al. showed that larger duplication size is correlated with increased severity across total clinical severity and motor behavioral assessment inventory scores[46]. Additionally, some evidence suggests that duplication of neighboring genes contributes to additional clinical phenotypes. For example, Filamin A (*FLNA*) gene duplication has been proposed to contribute to intestinal and bladder dysfunction and development of distinct facial features amongst individuals with MDS[47]. Furthermore, other genes that can be duplicated with *MECP2* have been associated independently with disease: GDP dissociation inhibitor 1 (*GDI1*, cognition), Ras-related protein Rab-39B (*RAB39B*, intellectual disability), and SRSF protein kinase 3 (*SRPK3*, muscle degeneration)[48–50].

DNA Methylation and Methyl-CpG-Binding Protein 2 (MeCP2)

DNA methylation is an epigenetic mark defined by the addition of a single methyl (-CH_3) functional group onto the 5-position of DNA base cytosine (5-methyl-cytosine, 5mC). DNA methylation is integral for many cellular processes in the developing and developed organism, including cellular differentiation, genomic imprinting, X-chromosome inactivation (XCI), and silencing of repetitive DNA[51,52]. Approximately 1% of all DNA bases and 70-80% of all CpG dinucleotides are symmetrically methylated in somatic cells of the vertebrate genome[53]. DNA methylation occurs at high levels in constitutive heterochromatin, where MeCP2 is also densely localized[54]. Other regions of the genome are methylated as well, including transcription start sites (TSS), gene bodies, enhancer elements, insulator elements, and intergenic regions[52]. DNA methylation functions differently at each of these regions, making for a complex system of epigenetic regulation. For example, the TSS of most active genes contain unmethylated CpG islands (CGIs); however, promoters of inactive genes often contain methylated CGIs, and these are associated with long-term stability of a repressed transcriptional state (e.g. imprinted genes, genes on the inactive X-chromosome)[55]. In contrast, gene body methylation is not associated with repression and is instead positively correlated with gene expression[56]. These examples illustrate the context-dependency of DNA methylation.

In addition to CpG methylation, non-CG methylation (mCH, where H=adenine, cytosine, or thymine) occurs in an asymmetric manner throughout the genome, particularly in the developed brain of mice and humans[57,58]. mCH increases in brain tissue of mice and humans during early postnatal development, most rapidly during the period of synaptogenesis (2-4 weeks of age in mice; 2 years of age in humans)[59–61]. Intriguingly, MeCP2 levels also increase during this period of development[62]. mCH levels reach a maximum of ~1.5% of CH genome positions and is predominantly present in the mCA

context[57,59]. In another level of complexity, methylated cytosines can also be modified by ten-eleven translocation (TET) dioxygenase enzymes that are crucial for DNA demethylation[63,64]. During the demethylation process, intermediate hydroxymethylated cytosine residues (5hmC) are generated and retain the capacity to interact with DNA methylation reader proteins[65,66]. Like non-CG methylation, 5hmC residues accumulate in the brain during development and in a cell type-specific manner. 5hmC is enriched in gene bodies of active genes and is thought to "functionally demethylate" these regions (generate lower occupancy of MeCP2 via decreasing high-affinity mCG availability) while retaining capacity to interact with DNA methylation readers to mediate chromatin organization[67,68].

One of these DNA methylation readers is MeCP2, discovered and cloned in 1992[69]. A chromatin-associated protein, MeCP2 binds symmetrically methylated cytosines in a CpG context via a methyl-binding domain (MBD, amino acids 78-162)[70]. The MBD spans an 85-amino acid sequence at the N-terminal part of MeCP2 and has a DNA binding footprint of approximately 12 nucleotides (**Figure 2**). In addition to symmetric CpG methylation, MeCP2 can bind to methylated cytosines in a wider variety of non-CpG contexts when methylated in an asymmetric manner[71–73]. MeCP2 has particular affinity for mCA amongst mCH contexts, especially in a CAC sequence[71,73]. Structural work of the MBD shows that MeCP2 likely binds as a monomer to methylated DNA, recognizing the hydration in the major groove of methylated DNA[74,75].

Once bound to DNA, MeCP2 interacts with the transcriptional repressors and activators to modulate transcription. In a well-characterized interaction, MeCP2 binds to the transcriptional co-repressor nuclear receptor co-repressor/silencing mediator of retinoid and thyroid hormone receptors (NCoR/SMRT) through its 29-amino acid NCoR interaction domain (NID, amino acids 285-313) (**Figure 2**)[76–78]. However, MeCP2 has also been reported to interact with a variety of other binding partners, including transcriptional co-activators, other transcriptional co-repressors, chromatin remodelers, chromatin modifiers, and splicing factors (**Table 2**). While MeCP2 has been shown to act as a transcriptional repressor in an in vitro context[76], transcriptomics of mice with MeCP2 deficiency or MeCP2 overexpression have shown that not all differentially-expressed genes are upregulated in MeCP2 deficient mice or downregulated in MeCP2 overexpression mice, as would be expected for a pure transcriptional repressor[72,79,80]. Though it is not clear if these transcriptional changes are direct or indirect effects of MeCP2 dosage, further evidence of a complex transcriptional regulatory role for MeCP2 is provided by the finding that MeCP2 loss globally reduces (instead of elevates) transcription and translation in human embryonic stem cell (ESC) derived neurons[81].

A large portion, ~60%, of the MeCP2 sequence is disordered in solution, making structural analysis challenging[82,83]. However, in addition to the MBD and NID, MeCP2 contains three AT-hook-like domains. AT-hooks are short DNA-binding motifs that interact with the minor groove of AT-rich DNA with the consensus sequence RGRP[84]. The three AT-hook-like

domains in MeCP2 occur in 1) the interdomain (ID) between the MBD and NID at amino acids 184-195, 2) the transcription repression domain (TRD) at amino acids 264-273, and 3) the C-terminus of the protein at amino acids 341-364 (**Figure 2**). The second of these AT-hook-like domains has been shown to alter chromatin structure when MeCP2 is bound, suggesting that these regions can stabilize or modulate chromatin structure around MeCP2 binding sites[85,86].

MeCP2 is expressed predominantly in the central and peripheral nervous systems (CNS, PNS), particularly in postmitotic neurons and less so in glia[87]. As a nuclear protein, MeCP2 is localized to neuronal nuclei at levels approaching that of histone octamers[88]. With such high levels of protein, MeCP2 shows widespread binding throughout the genome and tracks the density of both mCG and mCH[72,88]. Predominant binding sites occur in intergenic and intronic regions of the genome, but MeCP2 can also interact with elements such as promoters, enhancers, and gene bodies[89]. The expanse of MeCP2's DNA footprint suggests that it functions in a highly context-dependent manner. As an example of this, MeCP2 decreases the rate of transcriptional initiation of highly methylated long genes via interaction of gene body MeCP2 with the TSS[90]. Further, at enhancers containing a high density of mCG and mCA, MeCP2 represses enhancer activity[91]. These functions are likely mediated by the repressive action of MeCP2 in a context-dependent manner. Adding to the complexity of MeCP2 function, several phosphorylation sites (S308, S421) are activity-dependent and may provide an additional level of transcriptional control. While MeCP2 S308 phosphorylation reduces interaction with NCoR/SMRT, MeCP2 S421 phosphorylation permits brain-derived neurotropic factor (*Bdnf)* transcription, dendritic growth, and spine maturation[92,93]. Interestingly, MeCP2 has also been found to alter chromatin structure and promote chromatin compaction, introducing the notion that MeCP2 functions outside of transcriptional repression[94,95].

MECP2 mutations in RTT and genotype-phenotype correlations

More than 95% of individuals with typical RTT and approximately 75% of individual with atypical RTT have a mutation in the *MECP2* gene[16,17]. Over 200 different *MECP2* mutations have been documented as causative of RTT (RettBase: http://mecp2.chw.edu.au). However, some mutations more commonly observed than others. Namely, there are 8 major point mutations that account for over 60% of all typical RTT cases: R106W, R133C, T158M, R168X, R255X, R270X, R294X, and R306C (**Figure 3**)[16]. Additionally, there is a subset of C-terminal mutations, predominately small deletions, that accounts for approximately 5-10% of typical RTT cases. Less common *MECP2* mutations include those in exon 1, short deletions, large deletions, insertions, mutations at splice sites, and other point mutations[17]. Apart from RTT, *MECP2* mutations have also rarely been associated with other neurodevelopmental disorders including ASD[96–99], Angelman syndrome[100,101], and X-linked intellectual disability[102].

A high degree of variability in clinical severity is observed within RTT, across domains such as language and motor function[16]. There are several possible contributors to this variability, including XCI status, *MECP2* mutation type, genetic modifiers of *MECP2* mutations, and environment. The first, XCI, occurs in a random manner as one X-chromosome is silenced in each cell during early female embryogenesis[103]. XCI status dictates relative expression of mutant to non-mutant MeCP2 across cell and tissue types in girls. Higher preference for the non-mutant *MECP2* allele is thought to contribute to lower clinical severity[13,19,104]. The second, *MECP2* mutation type, influences the degree to which MeCP2 function is preserved. Mutations that are partial loss-of-function (e.g. R133C, R294X) tend to yield a milder clinical course than mutations that are complete loss-of-function (e.g. R255X, large deletions)[16]. The third, genetic modifiers of *MECP2* mutations, may alter clinical phenotypes via direct effects on *MECP2* or indirect effects on MeCP2's function[105]. Finally, behavioral interventions such as environmental enrichment have the potential to reduce functional deficits in RTT[106,107].

Though it cannot explain the full complement of clinical variability, *MECP2* mutation type has emerged as a significant source for both typical and atypical RTT[16,17]. Generally, genotype-phenotype correlations map onto both typical and atypical RTT; however, the phenotypes tend to be more highly skewed in atypical RTT[17]. For example, complete loss-of-function mutations such as R255X and large deletions are associated with higher clinical severity in both typical and atypical RTT, but the degree of increase in severity is greater in atypical than typical RTT (and vice versa for partial loss-of-function mutations associated with lower clinical severity). Additionally, these correlations appear to affect the entire disease course, as individuals with mild *MECP2* mutations tend to have a later diagnosis and less severe disease as children (and vice versa). Despite this difference in baseline severity, clinical severity does increase with age across most mutations. The largest contributors to clinical severity are hand use and onset of stereotypies, with smaller contributions from growth, motor dysfunction, and communication dysfunction. Ultimately, these genotype-phenotype correlations denote a pattern, but individuals with RTT may not have disease that exactly ascribes to this pattern. Other factors, including XCI, genetic modifiers, and environment, can also alter disease course.

R294X and C-terminal *MECP2* mutations in RTT

MECP2 mutations associated with mild disease include R133C, R294X, and C-terminal mutations. The R133C mutation has been shown to partially disrupt binding to methylated DNA, particularly to hydroxymethylated cytosines, leading to partial loss-of-function of MeCP2[67,108,109]. In contrast, the later R294X and C-terminal mutations do not disrupt the MBD and instead disrupt the NCoR/SMRT interaction domain (NID) sequence (R294X) or the 3′ end of the transcript (C-terminal mutations). Recent work has shed light on the partial loss-of-function mechanism of R294X; however, the pathogenic mechanism of C-terminal mutations remains largely unknown.

The R294X mutation, one of the 8 common point mutations, occurs in approximately 6% of individuals with typical RTT and approximately 4% of individuals with atypical RTT[16,17]. R294X is an arginine-to-stop mutation that occurs within the NID sequence. It is predicted to retain methylated DNA binding capacity and interrupt binding to the transcriptional co-repressor complex NCoR/SMRT. Recent mouse modeling work has shown that male hemizygous *Mecp2*$^{R294X/Y}$ (R294X) mice exhibit RTT-like phenotypes with delayed onset and increased lifespan compared to mouse models of other *MECP2* mutations[110]. These mild RTT-like phenotypes are associated with production of stable truncated MeCP2, unlike other models of nonsense *MECP2* mutations. Collectively, this work suggests that the R294X mutation acts through partial loss-of-function to cause RTT. Molecular work confirmed that the R294X truncation product binds to chromatin; however, interestingly, the truncation product bears higher chromatin binding affinity compared to wild type (WT) MeCP2[110].

C-terminal domain (CTD) mutations are a class of *MECP2* mutation grouped by genomic location. They occur in approximately 9% of individuals with typical RTT and approximately 17% of individuals with atypical RTT[17]. CTD mutations span a region of more than 500 bp and are highly variable, with over 100 different C-terminal *MECP2* mutations reported (RettBase: http://mecp2.chw.edu.au). However, a hotspot of small deletion-frameshift mutations starting between c.1157-1164 comprises about 60% of all CTD mutations. Two of these hotspot mutations have been modelled in mice: c.1157_1197del41 and c.1164_1207del44[111]. Mice with the c.1157_1197del41 mutation displayed severe RTT-like phenotypes and reduced lifespan; correspondingly, mice expressed very low levels of truncated MeCP2. However, mice with the c.1164_1207del44 mutation did not display severe RTT-like phenotypes and had no difference in lifespan compared to WT mice. Interestingly, when the mouse c.1164_1207del44 *Mecp2* allele was "humanized" with several added point mutations around the mutation to more closely match the human c.1164_1207del44 *MECP2* allele, truncated protein levels were significantly reduced in a cellular model. This work suggested that human-specific sequences around the CTD mutation hotspot might impact protein stability. Other studies have implicated the C-terminus in facilitating chromatin binding and in directing chromatin architecture, suggesting that CTD mutations might impact function as well as stability[82,112]. Still, a clear picture of how specific CTD mutations affect MeCP2 function is needed.

Disease modeling of RTT

The first mouse models of RTT were developed in the early 2000s, from the labs of Adrian Bird and Rudolf Jaenisch[113,114]. Both models involved deletion of exons shared by the two isoforms of *Mecp2* (Bird null: exons 3-4; Jaenisch null: exon 3). Global deficiency of MeCP2 led to a constellation of RTT-like phenotypes that exhibited sex-specific onset. Hemizygous male *Mecp2*$^{-/Y}$ mice were significantly underweight from 4 weeks of age (on the C57BL/6 background) and developed stiff gait, decreased activity, and tremor between 3-8 weeks of age[113,114]. *Mecp2*$^{-/Y}$ mice also developed hindlimb clasping and irregular breathing, with early death at approximately 10 weeks of age. In contrast, heterozygous female *Mecp2*$^{+/-}$ mice

displayed a similar set of RTT-like phenotypes, including stiff gait, decreased activity, hindlimb clasping, and irregular breathing, beginning much later, at 3-4 months of age[113,114]. The phenotypes exhibited by mice with global MeCP2 deficiency recapitulate features of RTT in humans, permitting use of this system for disease modelling.

The predominance of neurological features in RTT suggested that the central nervous system may be the predominant site of MeCP2 dysfunction. To test this, both the Bird and Jaenisch labs crossed mice expressing a loxP-flanked *Mecp2* allele with Nestin-Cre driver mice. This cross results in deficiency of MeCP2 in the CNS and PNS, including neuronal and glial precursors. Nestin-Cre conditional mutant mice were indistinguishable from global knockout (KO) mice. While unexpected due to the broad expression of MeCP2 throughout the body, this result indicated that phenotypes of *Mecp2*$^{-/Y}$ and *Mecp2*$^{+/-}$ mice are attributable to loss of MeCP2 in the nervous system[113,114]. Furthermore, the Jaenisch lab crossed mice expressing a loxP-flanked *Mecp2* allele with CamK-Cre93 driver mice to yield MeCP2 deficiency in postnatal forebrain, hippocampus, and brainstem neurons. These CamK-Cre93 conditional mutant mice displayed typical development until 3 months, at which time they began to show similar RTT-like phenotypes of stiff gait and decreased activity[113]. This result suggested that RTT-like phenotypes are attributable to MeCP2 deficiency in neurons rather than glia. Consistently, follow-up work showed that astrocyte-specific reactivation of *Mecp2* in globally MeCP2 deficient mice partially rescued behavioral abnormalities and had very minimal effect on lifespan[115], while microglia-specific reactivation of *Mecp2* in globally MeCP2 deficient mice did not rescue behavioral abnormalities[116,117].

The Jaenisch lab's work suggested that MeCP2 deficiency in post-mitotic neurons is sufficient to cause disease. This was confirmed and extended by experiments that induced MeCP2 deficiency when mice reached maturity. Specifically, a tamoxifen-inducible *Mecp2* knockout strategy was applied to mice aged 60 days or older, eliminating MeCP2 only during adulthood[118]. These mice exhibited RTT-like phenotypes similar to germline *Mecp2* knockout mice, including hypoactivity, abnormal gait, hindlimb clasping, and premature death with similar median time to death after dosing (~10-12 weeks). This result demonstrated that MeCP2 expression is required continuously in the developed brain and argued that, though the onset of RTT correlates with neurodevelopment, the disease may not be attributable to disruption of the developing brain.

Given these findings, the field raised the reverse question of whether reactivation of *Mecp2* after symptom onset could provide therapeutic benefit. This was shown in a tamoxifen-inducible Cre recombination experiment, whereby a loxP-flanked stop sequence is excised upon administration of tamoxifen[119]. Reactivation of *Mecp2* after symptom onset in hemizygous male *Mecp2* mutant mice rescued phenotypic score, improved motor behavior and breathing phenotypes, and preserved survival up to 30 weeks of age[119,120]. Reactivation of *Mecp2* after symptom onset (~30 weeks of age) in heterozygous female *Mecp2* mutant mice similarly significantly rescued phenotypic score, representing observation of

activity, gait, hindlimb clasping, tremor, breathing, and coat condition[119]. Together, these experiments provided early hope for the potential of disease-modifying therapeutics, through reversal of MeCP2 loss after onset of symptoms and diagnosis in people.

Since then, numerous studies have used complex mouse genetics to achieve cell-type specific loss of MeCP2 in WT mice or reactivation of *Mecp2* in global knockout mice, to determine the cell types, brain regions, and circuits involved in RTT pathogenesis. Selective reduction of MeCP2 has been behaviorally characterized in multiple different brain regions, including postnatal forebrain[113,121], basal ganglia[122], hypothalamus[123], and cerebellum[124], as well as in specific cell types, including glutamatergic neurons[125], GABAergic neurons[126], dopaminergic and noradrenergic neurons[127], serotonergic neurons[127], parvalbumin-expressing interneurons[128], and somatostatin-expressing interneurons[128]. Though the details of behavioral consequences of region- and cell type-specific MeCP2 loss are beyond the scope of this dissertation, collectively this work demonstrates that MeCP2 function is critical across a variety of brain regions that, together, contribute to the complex behaviors observed in RTT.

Additionally, extensive work has gone into development of mouse models harboring common *MECP2* mutations to understand their pathophysiological mechanism. To date, mouse models of all 8 common *MECP2* point mutations – R106W, R133C, T158M, R168X, R255X, R270X, R294X, and R306C – have been generated (**Table 3**)[77,108,110,129–135]. These mutations fall into two categories – missense (R106W, R133C, T158M, R306C) and nonsense/truncating (R168X, R255X, R270X, R294X) mutations. Each of the missense mutations yield a protein product in mice at varying levels compared to full-length WT MeCP2. In comparison, amongst the nonsense mutations, R168X and R255X produce no detectable protein product while R270X and R294X mutations yield produce stable truncation products in mice. However, R270X truncation product was not detected in a human brain lysate from a heterozygous female individual with RTT, suggesting that features of the R270X mouse model may not reflect human pathophysiology[134]. Despite differences in protein production amongst the 8 common point *MECP2* mutations, they each cause RTT via complete or partial loss-of-function. In the latter case, mutations disrupting the MBD are predicted to decrease binding to methylated DNA, while mutations disrupting the NID are predicted to decrease interaction with transcriptional co-repressors. Furthermore, different mutations within the MBD differentially affect binding to methylated DNA[136]. For example, the R106W mutation nearly abolishes methylated DNA binding capacity, while R133C retains partial binding capacity. Apart from the 8 common point mutations, an additional 2 C-terminal mutations have been modelled in mice – c.1157_1197del41 (p.L386HfsX5) and c.1164_1207del44 (p.P389X) (**Table 3**)[111]. L386HfsX5 mice display RTT-like phenotypes and decreased survival, consistent with other models of *MECP2* mutation. However, P389X mice did not display RTT-like behavioral phenotypes and had survival comparable to WT mice up to 1 year. As discussed in the previous section, differences in the MeCP2 C-terminus between mice and humans may

explain this discrepancy; however, more work is needed to understand the mechanism underlying C-terminal *MECP2* mutation.

With the knowledge that *MECP2* loss-of-function predominantly affects neurons in the brain, the field moved to determine synaptic effects of MeCP2 loss. Basal synaptic transmission was first evaluated by input-output (I/O) curves, which correlate presynaptic volleys as input (representing depolarization of presynaptic terminals) with the slope of evoked field excitatory postsynaptic potentials as output (field EPSPs). At Schaffer collateral-CA1 synapses, male *Mecp2*$^{-/Y}$ and female *Mecp2*$^{+/-}$ mice have I/O ratios unchanged from WT, indicating similar basal synaptic transmission[119,137]. MeCP2 loss does, however, affect presynaptic function. One metric of this is paired-pulse facilitation (PPF), a form of short-term plasticity. PPF is measured by delivering two stimuli within a short millisecond interstimulus interval and measuring field EPSP responses. Typically, the second recorded field EPSP is enhanced due to elevated presynaptic calcium concentration following the first stimulus, leading to a greater release of synaptic vesicles following the second stimulus. Pre-symptomatic *Mecp2* mutant mice do not display differences in PPF compared to WT littermates; however, symptomatic *Mecp2* mutant mice display decreased PPF, suggesting increased release probability[137–139]. This PPF phenotype may be caused by direct effects of MeCP2 protein level on calcium concentration in the presynaptic terminal or indirect alterations of presynaptic proteins involved in neurotransmitter release, that take effect only during postnatal development[140].

Long-term potentiation (LTP) and long-term depression (LTD) are forms of long-term synaptic plasticity in which different frequency stimulations cause a persistent increase or decrease in synaptic strength. Male hemizygous *Mecp2*$^{-/Y}$ and female heterozygous *Mecp2*$^{+/-}$ mice both show attenuated LTP and LTD in the CA1 region of the hippocampus[119,137,138]. Of note, and consistent with the LTP phenotype, *Mecp2*$^{-/Y}$ mice express lower levels of N-methyl-D-aspartate (NMDA) receptor subunit NR2A and higher levels of subunit NR2B compared to WT[137]. The NR2B subunit is expressed predominantly at immature synapses, and the NR2A subunit is more efficient than NR2B in generating NMDA receptor-dependent LTP at adult CA1 synapses[141]. A final form of plasticity affected by MeCP2 loss is homeostatic plasticity, the ability of neurons to restore their activity to a setpoint following changes to network activity. One specific form of homeostatic plasticity is synaptic scaling, characterized by cell-wide changes in synaptic strength following neuronal activity. MeCP2 deficiency prevents an activity-dependent decrease in the α -amino-3-hydroxy-5-methyl-4-isoxazole propionic acid (AMPA) receptor subunit GluR2 expression and synaptic scaling in hippocampal cultures[142], as well as synaptic scaling in the neocortex after sensory deprivation[143].

Loss of *MECP2* expression is also associated with changes to synaptic structure. Mouse and human neurons deficient in MeCP2 have smaller neuronal cell size and increased density of neurons[81,113,144,145]. Additionally, post-mortem brain tissue

and mouse neurons deficient in MeCP2 show low dendritic spine density and decreased dendritic branching complexity[87,144,146,147]. These results argue that MeCP2 is involved in the structural maturation of neurons, including dendritic spine development and dendritic arborization.

Disease modeling of MDS

With the successful generation of mouse models of RTT, two mouse models of MDS were subsequently developed. The first, Tg(*MECP2*)1Hzo (Zoghbi TG), was created by the Zoghbi lab via the introduction of the human *MECP2* genomic sequence (including the original promoter and proximal regulatory sequences) into an autosome, effectively globally duplicating protein levels throughout the life of the animal (**Table 3**)[33]. Zoghbi TG mice demonstrate typical development until approximately 10-12 weeks of age, at which time they show forepaw clasping, enhanced motor learning, and enhanced fear response in a contextual fear conditioning paradigm. As they age, these Zoghbi TG mice develop seizures, hypoactivity, and spasticity with early death. Importantly, analysis of several transgenic lines with differing MeCP2 protein levels found that increasing levels of MeCP2 protein correlated with increased severity of MDS-like phenotypes, reinforcing the notion that *MECP2* gene dosage drives MDS. A second mouse model of MDS, *Mapt*$^{\text{tm1(}Mecp2\text{)Jae}}$ (Jaenisch TG), was created by the Jaenisch lab via the introduction of the mouse *Mecp2* coding sequencing in-frame into the first exon of the *Tau* gene, effectively globally duplicating the gene in post-mitotic neurons (**Table 3**)[148]. This tau-MeCP2 fusion protein contains the first 31 amino acids of Tau followed by the MeCP2 E2 protein and, when combined with endogenous mouse MeCP2, yields approximately twice the typical levels of MeCP2 in the brain[148,149]. The Jaenisch TG mice display motor dysfunction, increased anxiety-like behavior, and enhanced fear response in contextual and cued conditioning paradigms.

Both Zoghbi and Jaenisch MDS mouse models have behavioral phenotypes redolent of MDS features, including deficits in motor coordination and increased anxiety-like behavior. However, there are differences between the two; for example, the Jaenisch TG mice do not display decreased lifespan while the Zoghbi TG mice do display decreased lifespan. Discrepancies such as this may be attributed to differences in transcriptional control of the transgene (i.e. the native *MECP2* human promotor and regulatory sequences vs. those of mouse *Tau*) or differences in function of the protein (i.e. human MeCP2 E1 and E2 vs. tau-MeCP2-E2 fusion). Complicating this picture, the Zoghbi model of MDS has been reported to show mouse strain-specific phenotypes, indicating that background affects phenotypic expression. To circumvent this, several studies have used F1 hybrid mice with success[129,150,151]. Due to these complicating issues, the contributions of specific cell types and brain regions to MDS-like phenotypes has not been as thoroughly dissected as in RTT. However, one study showed reversal of social recognition deficits in MDS model mice via normalization of MeCP2 levels in the medial prefrontal cortex[152]. Additionally, elevated anxiety-like behavior and decreased social approach in MDS model mice were reversed by genetic reduction of corticotropin-releasing hormone (CRH) or opioid receptor mu (μ) 1 (OPRM1), respectively[151].

Apart from MDS-like behavior, mouse models have provided insight into the synaptic underpinnings of the disease. Electrophysiological analysis of TG mouse hippocampal brain slices showed impairments in synaptic plasticity. These experiments found normal I/O curves, indicating that Schaffer collateral input onto CA1 neurons is intact[149]. However, PPF, a form of short-term synaptic plasticity, was enhanced in hippocampal slices of both Zoghbi and Jaenisch TG mice, suggesting a presynaptic effect of MeCP2 overexpression leading to a decrease in release probability[33,149]. Consistently, some cognitive and motor behavioral phenotypes and synaptic dysfunction can be normalized by treatment with a non-competitive $GABA_A$ receptor antagonist, picrotoxin[153]. Additionally, TG mice show differences in LTP in the hippocampus[33,149]. While hippocampal LTP was enhanced in Zoghbi TG mice, hippocampal LTP was attenuated in Jaenisch TG mice; these differences may be due to pattern of MeCP2 expression and require further study. Spontaneous neurotransmission was evaluated alongside evoked neurotransmission in the Jaenisch TG mice. Recordings from cultured hippocampal neurons found increased resting excitatory drive, with enhanced mini-excitatory postsynaptic currents (mEPSCs) and no changes to mini-inhibitory postsynaptic currents (mIPSCs)[149]. Collectively, these studies of neurotransmission suggest that MeCP2 overexpression causes alterations to excitatory neurotransmission in the hippocampus, with increased resting excitatory drive.

While the molecular mechanism for these electrophysiological alterations is not well understood, MeCP2 overexpression has been associated with alterations to structural features of synapses. For example, in mouse hippocampal CA1, MeCP2 overexpression leads to increased glutamatergic synaptic density during early postnatal development[154]. Consistently, cortical neurons derived from several different *MECP2* duplication induced pluripotent stem cell (iPSC) lines show increased synaptogenesis and dendritic complexity[155]. However, overexpression of WT *MECP2* in rat hippocampal pyramidal slices leads to a transient decrease in the density of spines, specifically of mature spines, without affecting dendritic complexity or length[146]. These studies suggested that the structural effects of MeCP2 overexpression are model- and timepoint-dependent. Follow-up work used the Zoghbi TG mouse model to study L5 pyramidal neurons in the barrel cortex (region of somatosensory cortex that receives input from whiskers via the thalamus) in vivo[156]. In this model, dendritic spine density was initially increased until 12 weeks of age, after which point TG animals showed decreased dendritic spine density compared to WT littermates. Interestingly, spontaneous spine turnover remains increased in aged TG animals, with higher spine gain and loss rates biased towards spine loss.

In addition to baseline differences in spine density, the structural plasticity of spines is also affected by MeCP2 overexpression. In WT mice, rotarod motor training induces an increase in bouton elimination rate in the motor cortex[157,158]. MeCP2-overexpressing mice do not exhibit this increase in bouton elimination, and instead show excessive formation and

stabilization of dendritic spine clusters, consistent with the behavioral phenotype of motor overperformance. These molecular and behavioral changes are reversible by pharmacological inhibition of ERK, suggesting that Ras-ERK signaling hyperactivity contributes to these phenotypes in TG animals[159]. Collectively, this work supports the notion that excessive MeCP2 contributes to inappropriate consolidation of clustered synaptic connections during motor learning, in addition to having baseline effects on spine density.

Therapeutics for RTT

The reversibility of RTT-like phenotypes in mouse models after symptom onset has provided hope that disease-modifying treatment could be developed for individuals diagnosed with RTT. Rescue experiments have shown that elevation of MeCP2 levels in symptomatic mice significantly improves, but does not fully rescue, overall RTT-like phenotypes, survival, and respiratory and motor function[119,120]. The lack of complete rescue may be due to incomplete restoration of MeCP2 levels across the brain, but further work is needed to determine this. Regardless, a cautious but hopeful outlook for RTT therapy has spurred preclinical work and clinical trials in this space.

One of the first targets of RTT therapeutic development was BDNF, an important mediator of neuronal and synaptic maturation. In heterozygous female mouse models of RTT and in humans with RTT, *BDNF* transcript is downregulated with loss of functional MeCP2[160]. Further, overexpression of *BDNF* in *Mecp2* null male mice extends survival, rescues specific motor deficits, and reverses electrophysiological abnormalities[161]. Therapeutic efforts were directed towards increasing BDNF levels as an indirect method of restoring MeCP2 function. One of these methods was treatment with ampakines, drugs that enhance glutamatergic AMPA receptor activity to upregulate endogenous BDNF. Chronic treatment of hemizygous male *Mecp2*$^{-/Y}$ mice with the ampakine CX546 was able to restore normal breathing rate and minute volume/weight[162]. Another drug shown to increase endogenous BDNF is fingolimod, a sphingosine-1 phosphate receptor agonist that crosses the blood brain barrier, and administration of fingolimod to hemizygous male *Mecp2*$^{-/Y}$ mice normalized rotarod motor performance and extended lifespan by approximately 1 month[163]. A clinical trial assessing the safety and efficacy of oral fingolimod in children older than 6 years found that the drug is safe but found no evidence of an effect on clinical, laboratory, or imaging measures of disease (FINGORETT; NCT02061137)[164].

Unfortunately, the blood brain barrier penetrance of BDNF is low, making its application as a therapeutic challenging. Insulin-like growth factor 1 (IGF1), however, confers similar effects on neuronal survival and maturation through overlapping signaling pathways and crosses the blood brain barrier, especially through its metabolite glycine-proline-glutamate (GPE)[165–167]. Treatment of hemizygous male *Mecp2*$^{-/Y}$ mice with GPE showed distinct benefits after initiating dosing from a young age (P15-P18)[168]. Specifically, GPE promoted survival, improved structural brain abnormalities (e.g.

brain weight, spine density), and improved behavioral and physiological abnormalities (e.g. breathing irregularity, activity). Additionally, treatment of adult female heterozygous *Mecp2*$^{+/-}$ mice with GPE stabilized cortical plasticity to WT levels[168]. This encouraging data provided the impetus for further preclinical studies of IGF1, GPE, and GPE analogues like trofinetide in RTT. Trofinetide, the proline-methylated analogue of GPE, harbors an improved pharmacokinetic profile compared to GPE and a phase II clinical trial in individuals with RTT showed that oral trofinetide is generally safe and well-tolerated (NCT01703533)[169]. Promisingly, trofinetide at 200 mg/kg twice daily in children/adolescents with RTT improves core features across multiple disease domains as assessed by clinicians and caregivers (NCT02715115)[170]. Analysis of a Phase III trial of trofinetide in children and adolescents with RTT is ongoing (NCT04181723).

Another modulator of the BDNF signaling pathway is the NMDA receptor antagonist ketamine. Previous work in mouse models has shown that ketamine can act through NMDA receptor antagonism to release a translational block of *Bndf*[171]. Additionally, acute systemic treatment with ketamine in female heterozygous *Mecp2*$^{+/-}$ mice normalizes pre-pulse inhibition of acoustic startle[172]. A Phase II clinical trial of oral ketamine in RTT is ongoing (NCT03633058). Apart from modulation of BNDF signaling, therapeutic efforts for RTT have also targeted other downstream mediators of MeCP2 function, such as neurotransmitter systems (e.g. GABA, dopamine, serotonin) with variable success in mouse models[173].

Direct methods to restore MeCP2 function aim to elevate functional MeCP2 protein. These include 1) gene therapy, 2) X-chromosome reactivation, 3) genome editing, and 4) RNA editing strategies. First, gene therapy employs viral delivery of the *MECP2* gene to permit increased protein expression. Numerous studies have evaluated the safety and efficacy of modelled gene therapy in hemizygous *Mecp2*$^{-/Y}$ mice and have demonstrated rescue of survival, body weight, and select behavioral phenotypes[174–179]. However, only one study thus far has evaluated the safety and efficacy of gene therapy in heterozygous *Mecp2*$^{-/+}$ mice, where authors demonstrated that systemic viral delivery in adulthood rescued gross phenotypic progression as well as motor and cognitive behavioral phenotypes[174]. Collectively these studies have also identified potential barriers to the use of gene therapy in people, most prominently hepatotoxicity occurring with systemic delivery[176,179]. Second, X-chromosome reactivation aims to pharmacologically de-repress *MECP2* transcription from the inactive X-chromosome in female neurons[180]. Third, genome editing aims to correct the mutant *MECP2* allele to via approaches such as CRISPR/Cas9 (clustered regularly interspaced short palindromic sequences)[181]. Finally, RNA editing employs adenosine deaminase enzymes to program site-specific adenine-to-inosine editing of RNAs and correction of G>A mutations in *Mecp2* at the transcript level[182,183].

Summary and project rationale

Rett syndrome, an X-linked neurodevelopmental disorder caused predominantly by mutations in the gene encoding chromatin modulator methyl-CpG-binding protein 2 (*MECP2*), is a leading genetic cause of disability in girls worldwide. Affected individuals develop typically for a period of 6-18 months, at which time the disease causes developmental regression with loss of purposeful hand movements, loss of speech, hand stereotypies, and gait abnormalities. Treatment options are currently limited to symptomatic management, making the development of novel therapeutic approaches critically important. 10% of disease-causing *MECP2* mutations arise in its C-terminal domain. However, despite the high prevalence of mutations in this region, few studies have investigated their pathophysiological mechanism(s). Furthermore, proposed therapeutic strategies for RTT focus largely on remedying loss-of-function (LOF) mutations that occur in other domains of MeCP2 - the methyl-binding and NCoR-interaction domains. Previous work suggests that the C-terminus may alter local chromatin binding and conformation, but thorough functional studies of different types of C-terminal mutations are lacking. This dissertation aims to determine the effect of the R294X mutation on MeCP2 function (Chapter II) and elucidate the functional significance of the C-terminal domain (Chapter III). This work involves the development of an in vitro framework to probe C-terminal *MECP2* mutations in functional assays, as well as the use of dual molecular and behavioral approaches to dissect the pathogenic mechanism of the prevalent R294X mutation. This research provides mechanistic insight into the complex neurodevelopmental disorder Rett syndrome, as well as assists clinical decision-making by identifying the viability of proposed therapies for individuals with R294X *MECP2* mutations.

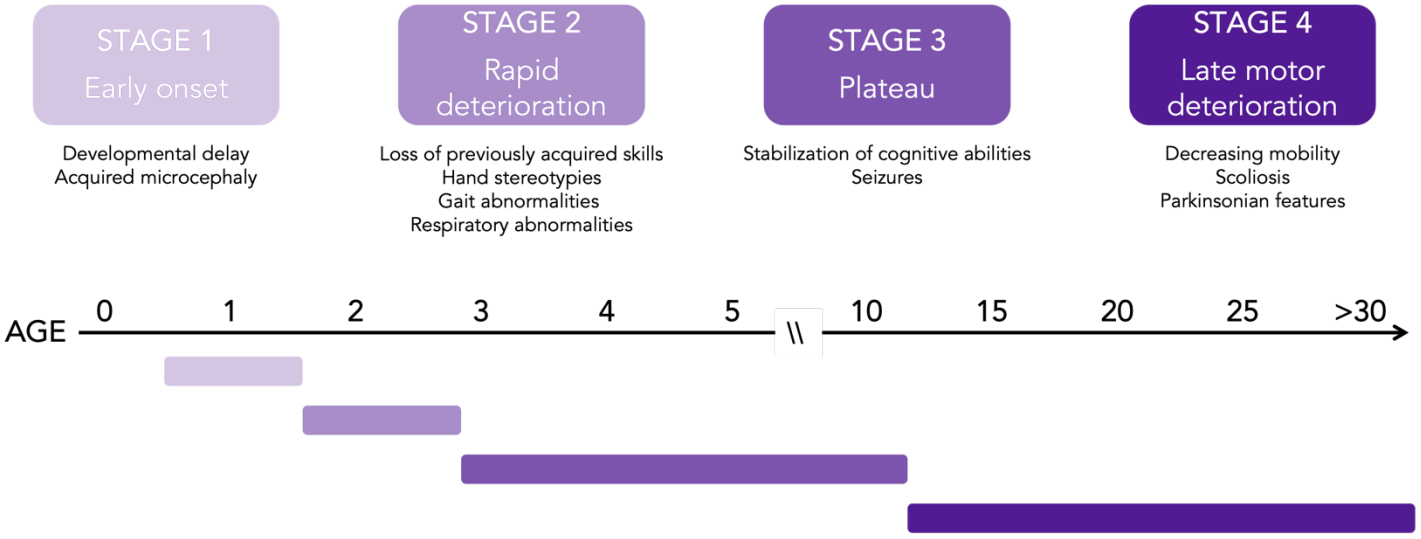

Figure 1. Disease stages in Rett syndrome

The progression of Rett syndrome can be described in four stages of disease. In Stage 1 (early onset), children develop mostly typically with possible acquired microcephaly and developmental delay. In Stage 2 (rapid deterioration), children undergo developmental regression over the course of weeks, months, or years with loss of previously acquired skills including purposeful hand movements and spoken language. Children also begin to develop breathing and gait abnormalities during this period. In Stage 3 (plateau), children usually experience stabilization of cognitive abilities and have onset of other medical conditions such as seizures. In Stage 4 (late motor deterioration) individuals with RTT experience decreasing mobility and may develop parkinsonian features.

Table 1. Diagnostic criteria for Rett syndrome Adapted from Neul et al. *Ann Neurol* 2010[5].

Typical (classic) RTT	Atypical (variant) RTT
A period of regression followed by recovery or stabilization and: Main criteria (must fulfill all 4) 1. Partial or complete loss of acquired purposeful hand skills 2. Partial or complete loss of acquired spoken language 3. Gait abnormalities: Impaired (dyspraxic) or absence of ability 4. Stereotypic hand movements such as hand wringing/squeezing, clapping/tapping, mouthing, and washing/rubbing automatisms Exclusion criteria (must fulfill none) 1. Brain injury secondary to trauma (peri- or postnatally), neurometabolic disease, or severe infection that causes neurological problems 2. Grossly abnormal psychomotor development in the first 6 months of life	A period of regression followed by recovery or stabilization and: Main criteria (must fulfill at least 2 out of 4) 1. Partial or complete loss of acquired purposeful hand skills 2. Partial or complete loss of acquired spoken language 3. Gait abnormalities: Impaired (dyspraxic) or absence of ability 4. Stereotypic hand movements such as hand wringing/squeezing, clapping/tapping, mouthing, and washing/rubbing automatisms Supportive Criteria (must fulfill at least 5 out of 11) 1. Breathing disturbances when awake 2. Bruxism when awake 3. Impaired sleep pattern 4. Abnormal muscle tone 5. Peripheral vasomotor disturbances 6. Scoliosis/kyphosis 7. Growth retardation 8. Small cold hands and feet 9. Inappropriate laughing/screaming spells 10. Diminished response to pain 11. Intense eye communication – "eye pointing" Exclusion criteria (must fulfill none) 1. Brain injury secondary to trauma (peri- or postnatally), neurometabolic disease, or severe infection that causes neurological problems 2. Grossly abnormal psychomotor development in the first 6 months of life

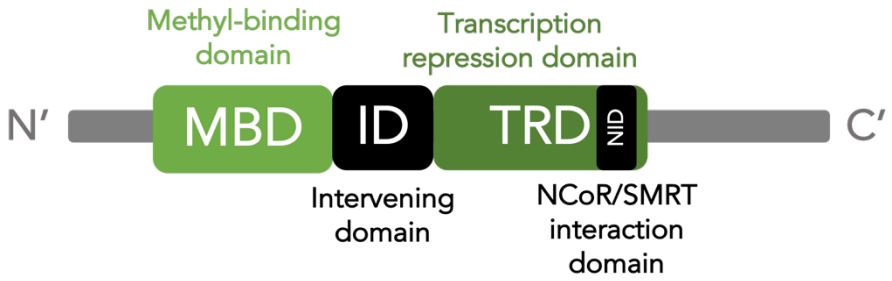

Figure 2. Schematic of MeCP2 functional domains

Schematic illustration of MeCP2 protein from the N-terminus (right) to C-terminus (left). The two main protein domains are indicated in shades of green: methyl-binding domain (MBD) and transcription repression domain (TRD). The location of the NCoR/SMRT interaction domain (NID) within the TRD is indicated in black. The intervening domain (ID) between the MBD and TRD is also indicated in black.

Table 2. Proteins that interact with MeCP2

Binding Partner	Function	Binding site(s) on MeCP2	Reference(s)
ATRX	Chromatin remodeler	MBD, ID	184–186
BRM (BRAHMA)	Chromatin remodeler	Unknown	187
c-Ski	Transcriptional co-repressor	ID, TRD	188
CoREST	Transcriptional co-repressor	Unknown	189
CREB	Transcriptional activator	Unknown	80
DNMT1 (DNA methyltransferase 1)	Maintenance DNMT	MBD, ID, TRD	190
H3K9 methyltransferase	Chromatin modifier	Unknown	191
HP1 (Heterochromatin protein 1)	H3K9me3 reader involved in heterochromatin formation	N-terminus	192
mSin3a	Transcriptional co-repressor	MBD, ID, TRD	77,193,194
NCoR (Nuclear receptor co-repressor)	Transcriptional co-repressor	NID	77,188
PHF14 (PHD Finger Protein 14)	Histone-binding protein	MBD	195
YBX1 (Y-box binding protein 1)	Regulator of transcription, translation, splicing, and DNA repair	ID, TRD	196
YY1 (Yin Yang 1)	Transcription factor (dual activator/repressor)	ID, TRD	197

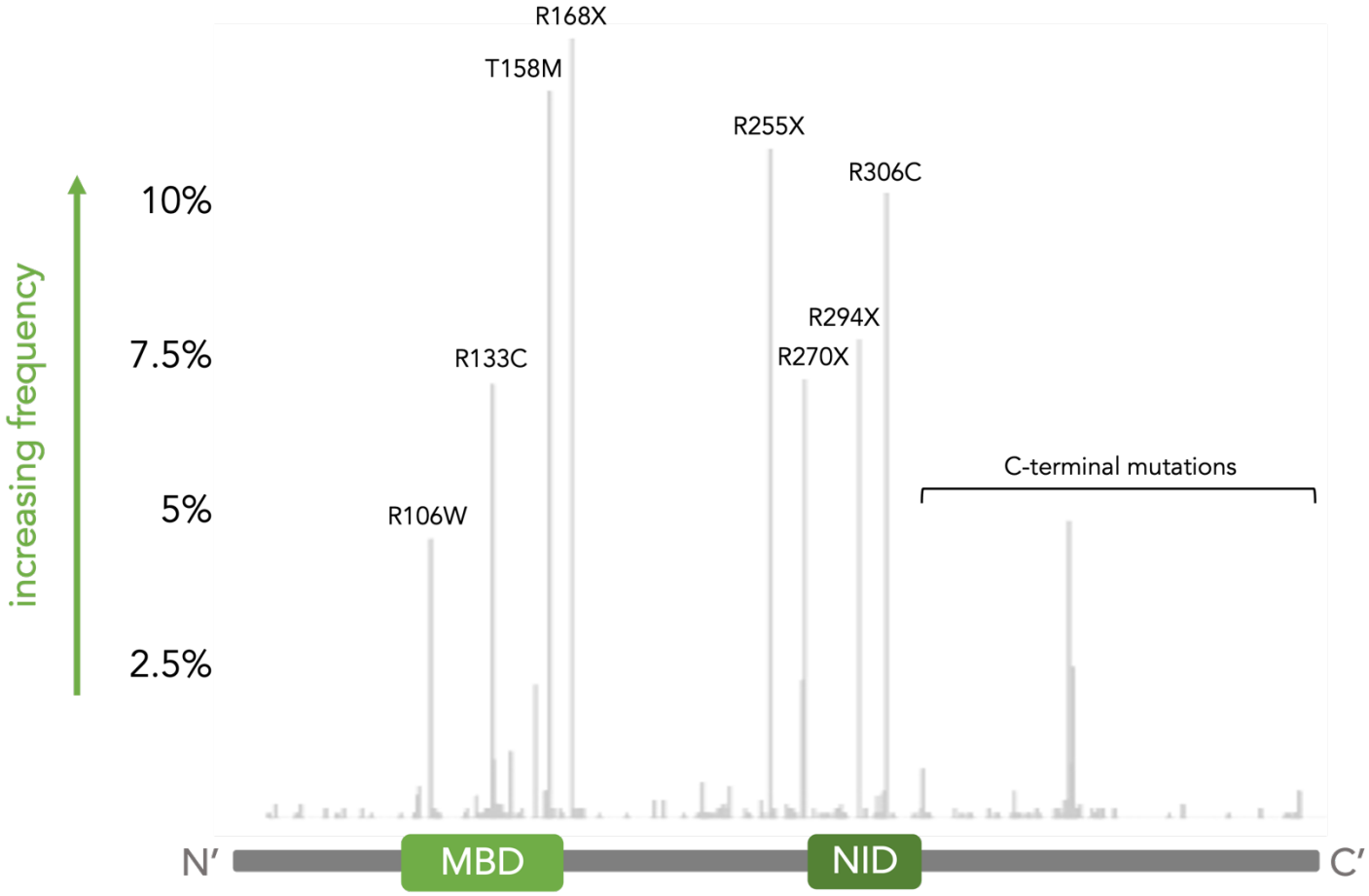

Figure 3. Common *MECP2* mutations in Rett syndrome

Frequency map of *MECP2* mutations identified in girls with RTT from the NIH Natural History Study of Rett Syndrome and Related Disorders (Study Director: Jeffrey L. Neul, MD PhD). Mutation frequency is depicted on the y-axis while the start of the mutation along the protein sequence is indicated on the x-axis. A schematic of the MeCP2 protein domains is provided for reference. The 8 common point mutations and set of C-terminal mutations are indicated.

Table 3. Mouse models of *MECP2* mutation and duplication

Line	Mutation	Description	Tags	Reference(s)
Mecp2$^{tm1.1Bird}$	Knockout	Cre-mediated excision of *Mecp2* exons 3 and 4	none	114,198
Mecp2$^{tm1.1Jae}$	Knockout	Cre-mediated excision of *Mecp2* exon 3	none	113
Mecp2$^{tm4.1Joez}$	R106W	Introduction of exon 3 containing R106W mutation and C-terminal Tavi tag	Tavi (C-terminal)	131
Tg(*MECP2**R111G/EGFP)1Hzo	R111G	Introduction of human *MECP2* gene with R111G mutation onto an autosome	EGFP (C-terminal)	129
Mecp2$^{tm6.1Bird}$	R133C	Introduction of exon 4 containing R133C mutation and C-terminal EGFP tag	EGFP (C-terminal)	108
Mecp2$^{tm1.1Vnar}$	A140V	Introduction of exon 4 containing A140V mutation	none	130
Mecp2$^{tm1.1Joez}$	T158A	Introduction of exon 4 containing T158A mutation	none	132
Mecp2$^{tm4.1Bird}$	T158M	Introduction of exon 4 containing T158M mutation and C-terminal EGFP tag	EGFP (C-terminal)	108
Mecp2$^{tm3.1Joez}$	T158M	Introduction of exon 4 containing T158M mutation and C-terminal Tavi tag	Tavi (C-terminal)	131
Mecp2$^{tm1.1Jtc}$	R168X	Introduction of exon 4 containing R168X mutation	none	199
Mecp2$^{tm1.1Hupp}$	R168X	Introduction of exon 4 containing R168X mutation	none	133
Mecp2$^{tm1.1Irsf}$	R255X	Introduction of exon 4 containing R255X mutation	none	134
Tg(*MECP2**R270X/GFP)AHzo	R270X	Introduction of exon 4 containing R270X mutation and C-terminal GFP tag	GFP (C-terminal)	85
Tg(*MECP2**G273X/GFP)AHzo	G273X	Introduction of exon 4 containing G273X mutation and C-terminal GFP tag	GFP (C-terminal)	85
Mecp2^{R294X}	R294X	CRISPR/Cas9-mediated engineering of the R294X mutation	none	110
Mecp2$^{tm2.1Meg}$	R306C	Introduction of exon 4 containing R306C mutation	none	77
Mecp2$^{tm5.1Bird}$	R306C	Introduction of exon 4 containing R306C mutation and C-terminal EGFP tag	EGFP (C-terminal)	108
Tg(*MECP2**R306C/EGFP)1Hzo	R306C	Introduction of human *MECP2* gene with R306C mutation and a C-terminal EGFP tag onto an autosome	EGFP (C-terminal)	129
Mecp2^{tm1Hzo}	T308X	Introduction of exon 4 containing T308X mutation	none	200
Mecp2^{L386HfsX5}	L386HfsX5	CRISPR/Cas9-mediated engineering of the L386HfsX5 mutation	none	111
Mecp2^{P389X}	P389X	Introduction of exon 4 containing P389X mutation	none	111

Mapt$^{tm1(Mecp2)Jae}$	*Mecp2* duplication	Introduction of mouse *Mecp2* cDNA sequence into exon 1 of the tau gene, in-frame with the endogenous tau start codon	none	148,149
Tg(*MECP2*)1Hzo	*MECP2* duplication	Introduction of human *MECP2* gene sequence onto an autosome	none	33

CHAPTER 2

Safety and efficacy of genetic *MECP2* supplementation in the R294X mouse model of Rett syndrome

This chapter is adapted from "Safety and efficacy of genetic *MECP2* supplementation in the R294X mouse model of Rett syndrome" published in *Genes, Brain, and Behavior* and has been reproduced with the permission of the publisher and my co-authors Jonathan K. Merritt, Kirsty R. Erickson, and Jeffrey L. Neul.

Citation: Collins BE, Merritt JK, Erickson KR, Neul JL. Safety and efficacy of genetic *MECP2* supplementation in the R294X mouse model of Rett syndrome. *Genes Brain Behav*. e12739 (2021).

Introduction

Rett syndrome (RTT) is an X-linked neurodevelopmental disorder caused predominantly by de novo mutations in the *MECP2* gene encoding transcriptional modulator methyl-CpG-binding protein 2 (MeCP2)[2,12]. Because *MECP2* mutations are largely paternally inherited, RTT occurs mostly in females[18]. However, males with *MECP2* mutations manifest a variety of clinical phenotypes as well[30]. Individuals with RTT experience typical development until approximately 18-30 months, at which age affected individuals experience developmental regression with loss of previously acquired skills such as expressive language and purposeful hand use, as well as onset of hand stereotypies and gait abnormalities[3,5]. RTT can also cause a variety of associated clinical features including seizures, breathing dysfunction, and autonomic abnormalities[201–203]. Promisingly, restoration of MeCP2 pre- or post-symptomatically has been shown to rescue premature death and gross RTT-like phenotypes in mice, providing hope that disease-modifying therapies could be developed for RTT[119,174,175,204]. While early clinical trials have shown some therapeutic promise, no disease-modifying therapies are currently available[169,170].

One proposed therapeutic approach for RTT is supplementing the *MECP2* mutant allele with a WT *MECP2* allele to produce typical levels of functioning protein, including specific strategies such as gene therapy and reactivation of *MECP2* on the inactive X-chromosome. Gene therapy achieved via viral delivery of *MECP2*, for example, has shown rescue of survival, gross phenotypic development, and some behavioral phenotypes in mouse models of RTT[174–176,178,179]. One primary challenge to the realization of these therapies is that *MECP2* is a dosage-sensitive gene, and protein levels are tightly regulated bidirectionally in vivo. While loss of MeCP2 function causes RTT in humans, duplication and occasionally triplication of *MECP2* with resultant gain of protein function causes a related neurodevelopmental disorder called *MECP2* duplication syndrome (MDS)[32,205]. RTT and MDS share some clinical features such as motor dysfunction, stereotypic movements, gait abnormalities, and seizures. However, there are differences in onset and severity of these shared features[206]. MDS can also be differentiated from RTT by its predominance in males and associated immunodeficiency, which causes recurrent

respiratory infections in early life. Given this narrow therapeutic window of *MECP2* dosage, interventions for RTT that supplement full-length MeCP2 protein must do so without eliciting excess MeCP2 levels and MDS-like adverse effects.

The risk of MDS-like adverse effects is predicted to depend on baseline level of functioning MeCP2, with lower and higher levels decreasing and increasing risk, respectively. A main factor influencing baseline level of functioning MeCP2 is mutation type. Specific *MECP2* mutation type impacts clinical severity in humans, likely due to different mutations' impacts on protein function[16]. Mutations that cause significant disruption of DNA binding capacity (e.g., R106W) or do not produce any protein product (e.g., R255X) cause disease with higher clinical severity in people. Mutations that are predicted to retain partial DNA binding (e.g., R133C) or co-repressor interaction capacity (e.g., R294X) cause disease with lower clinical severity in people. These genotype-phenotype correlations have been recapitulated in mouse models and suggest that partial loss-of-function mutations would confer higher risk for MDS-like adverse effects with MeCP2 supplementation[108,110,131,134]. Previous work has evaluated MeCP2 supplementation in the context of loss-of-function mutations T158M, R255X, and R306C[129,134,176,207]. However, these studies focused largely on mutations associated with higher clinical severity and on rescue of RTT-like phenotypes in male mice. Further preclinical evaluation of the MeCP2 dosage therapeutic window in the context of partial loss-of-function mutations, particularly in female mice, is needed to determine the safety of therapeutic MeCP2 supplementation approaches.

To address this, we used a mouse model of the R294X *MECP2* mutation[110]. R294X is a common mutation that truncates the protein within the NID and eliminates the entire C-terminus[77]. In humans and in mice, the R294X mutation is associated with milder disease compared to other *MECP2* mutations, likely attributable to the presence of a stable truncated protein product[16,17,110]. Because this truncation product lacks the domain required for co-repressor interaction, the R294X mutation is predicted to cause RTT via partial loss-of-function. Moreover, the R294X truncation product binds chromatin more tightly than WT MeCP2, creating the potential for dominant negative interactions with supplementation of full-length MeCP2[110]. For these two reasons, the R294X mouse model is advantageous to study the feasibility of therapeutic approaches aimed at restoring levels of functional MeCP2.

A fundamental question for therapeutic development is whether approaches that restore MeCP2 function, such as gene therapy, are safe and efficacious in partial loss-of-function mutations that cause RTT, especially those that produce a truncated protein with both the ability and an increased avidity to bind DNA, such as R294X. To answer this question, we crossed mice harboring the R294X allele with mice carrying a human *MECP2* transgene on an autosome, as a model of idealized gene therapy. We found that addition of *MECP2* transgene normalized MeCP2 expression level in both male and female mice, and behavioral phenotypes due to MeCP2 loss-of-function were rescued in both sexes. We did not observe

adverse MDS-like behavioral phenotypes in male R294X animals. However, we observed MDS-like motor coordination and gait phenotypes in female R294X mice expressing the *MECP2* transgene. Collectively, these findings suggest that genetic supplementation of MeCP2 in the context of the partial loss-of-function R294X mutation is safe and effective in males, and largely so in females. However, careful consideration of baseline motor function and risk for potential adverse motor effects with MeCP2 supplementation therapy may be warranted for girls and women with RTT.

Materials and methods

Mouse Care and Breeding

All methods and animal care procedures were approved by the Vanderbilt Animal Care and Use Committee. Mice were housed in AAALAC-approved facilities at Vanderbilt University. All mice were bred on a C57BL/6J background. Male WT C57BL/6J mice were mated to female *Mecp2*$^{R294X/+}$;*MECP2*^{Tg} mice to generate male and female experimental mice, including *Mecp2*$^{+/Y}$ and *Mecp2*$^{+/+}$ (WT), *Mecp2*$^{R294X/Y}$ and *Mecp2*$^{R294X/+}$ (R294X), *MECP2*^{Tg} (TG), and *Mecp2*$^{R294X/Y}$;*MECP2*^{Tg} and *Mecp2*$^{R294X/+}$;*MECP2*^{Tg} (R294X TG) mice[33,110,134]. Mice were genotyped as previously described using allele-specific PCR[110]. All experiments were performed using WT littermates as controls.

Mouse Behavior

All behavioral experiments were performed in the Vanderbilt University Neurobehavioral Core Facility. Behavioral tests were performed using male and female mice. Mice were group housed (3-5 mice/cage) on a 12-hour light/dark cycle with food and water available *ad libitum*. Mice were transferred to test rooms and acclimated to the environment for 30 minutes prior to testing. Unless otherwise stated, all equipment was cleaned with 70% ethanol between trials to provide a standardized testing environment. All behavioral experiments were performed during the light phase.

Behavioral batteries were conducted across three independent cohorts for both males and females. Male mice underwent a behavioral battery at 20-22 weeks of age, including the following tests in order: elevated zero maze, open field, whole-body plethysmography, rotarod, Crawley 3-chamber, and fear conditioning. Female mice underwent a behavioral battery at 30-31 weeks of age, including the following tests in order: open field, whole-body plethysmography, rotarod, fear conditioning, and forced gait.

Physical Characterization

Mouse weights were measured prior to general phenotyping (described below). Mouse lengths were measured as distance from nose to base of the tail.

General Phenotyping

Mice were scored for development of Rett-like phenotypes based on Bird scoring[119]. Phenotypes including activity level, hindlimb clasping, tremor, breathing irregularity, coat condition, hunch, and gait were scored in a clean cage containing only bedding. Scores were recorded as 0, 1, or 2 for absent, present, or severe phenotype according to **Table 4**.

Elevated zero maze

Anxiety-like behavior was assessed using a white elevated zero maze (Stoelting: 50 cm inner diameter, 5 cm lane width, 15 cm closed arm wall height, 50 cm apparatus leg height). Illuminance was approximately 300 lux in open arms and approximately 70 lux in closed arms. Animals were selected in random order to minimize handling prior to testing. Animals were placed in the center of one open arm of the maze at the beginning of each trial. At the end of each trial, test mice were placed in a new cage to leave untested cage mates undisturbed. Each trial was recorded by a video camera mounted to the ceiling, and data was analyzed by ANY-maze software (Stoelting).

Open field

Spontaneous locomotor activity was assessed in MedAssociates 27x27x20.5 cm activity chambers placed within sound-attenuating 64x27x42 cm boxes that were light- and air-controlled. Locomotion was detected by the disruption of infrared beams with mouse body movement. Horizontal activity was measured by 32 photocells located 1 cm above the chamber floor (16 each in the X- and Y-directions). Vertical activity was measured by 16 photocells located 4 cm above the chamber floor (in the Z-direction). Mice were placed in the center of the activity chambers at the beginning of each trial, and their locomotion was tracked with Activity Monitor software for 30 minutes.

Unrestrained whole-body plethysmography

Respiratory function was assessed using unrestrained whole-body plethysmography. Mice were placed into plethysmography chambers (DSI: Buxco, ~500 ml in volume) with a continuous air flow rate of 1 L/minute. Breathing was recorded for 60 minutes, and raw breathing data was collected through Ponemah software. Concurrent time-locked chamber video data was collected to track mouse movement throughout the experiment. Between experiments, chambers were cleaned with water. A custom Python script was used to quantify movement and filter out segments of the experiment in which the mouse was active. The remaining "calm" segments were subjected to breathing waveform analysis. Derived parameters included breathing rate, breathing irregularity, and apnea count. Breathing irregularity was calculated as the instantaneous change in breath duration between adjacent breaths. Apneas were called as pauses that were greater than 0.5 seconds in duration and also greater than twice the local and overall average breath duration. Apnea count was

normalized to count per 1,000 breaths. A minimum of 200 total called breaths was required for inclusion in analyses. One male mouse (R294X) and three female mice (2 WT, 1 R294X TG) met exclusion criteria.

Rotarod

Motor coordination was assessed with a five-lane MedAssociates rotarod machine (ENV-574M). The rubber rotarod drum was 3.18 cm in diameter and textured to prevent slippage. The drum was located 30.68 cm above the apparatus floor. Mice were loaded onto the rotarod at a rotation speed of 4 rpm. Once all animals were loaded, the rotarod was set to initiate pre-programmed acceleration from 4 to 40 rpm over a period of 5 minutes. The time to fall was manually recorded for a maximum time of 5 minutes. To account for passivity on the rotarod, if an animal completed two passive rotations (i.e., underwent two full rotations without making a step forward) it was considered to have fallen. Animals completed three trials a day for three consecutive days, with at least 30 minutes rest between trials. Time to fall was averaged across trials for each mouse for each day.

Crawley 3-chamber

Social behavior was assessed using the Crawley 3-chamber assay[208]. The 3-chamber apparatus consists of a clear 60x42x22 cm box divided into three adjacent and equally sized compartments. Walls separating the compartments contained openings for mice to travel freely between compartments. Empty inverted wire pencil cups were placed in same-sided corners of each the left and right compartments. The test was conducted in three consecutive stages on a single day. In Stage 1 (Habituation), mice were allowed to freely explore the apparatus for five minutes. In Stage 2 (Sociability), an unfamiliar sex-, age-, and weight-matched WT mouse (Stranger 1) was placed under one of the pencil cups. Test mice were allowed to explore the apparatus for 7.5 minutes. The side of Stranger 1 was alternated between successive test mice and balanced across genotypes to account for potential side bias. In Stage 3 (Social Novelty Preference), another unfamiliar sex-, age-, and weight-matched WT mouse (Stranger 2) was placed under the remaining pencil cup. Test mice were again allowed to explore the apparatus for 7.5 minutes. Stranger 1 and Stranger 2 were always derived from different home cages and had no previous contact with any experimental mice. Additionally, all stranger mice were habituated to the wire pencil cups by placing them underneath for 30 minutes/day for two days prior to testing. After Stage 3, test mice were placed in a new cage, which prevented contact with untested cage mates. A camera mounted to the ceiling captured video data for all stages. Video data was manually scored for location of the mouse (left, center, or right chamber) for Stages 1, 2, and 3. Video data was also manually scored for interaction with pencil cups (left or right pencil cup) for Stages 2 and 3. Interaction was defined as sniffing, pawing, or rearing onto the cup. Scoring was performed with the free and open-source Behavioral Observation Research Interactive Software (BORIS v7.9.7). Discrimination indices were calculated for Stage 2 (Sociability) and Stage 3 (Social Novelty Preference) according to the following calculations:

Sociability Discrimination Index:

((time with social cup) – (time with empty cup)) / ((time with social cup) + (time with empty cup))

Social Novelty Preference Discrimination Index:

((time with novel cup) – (time with familiar cup)) / ((time with novel cup) + (time with familiar cup))

Fear Conditioning

Memory was assessed using the fear conditioning assay. The assay consisted of one training day and one test day. On training day, mice were acclimated for 30 minutes in a dedicated acclimation room adjacent to the test room. When ready for testing, mice were placed into 29.53x23.5x20.96 cm MedAssociates chambers equipped with stainless steel grid floors capable of delivering an electric shock. Mice were allowed to freely explore for 2 minutes and then a 30-second 90dB tone stimulus was administered, with the final 2 seconds accompanied by a 0.5mA foot shock. After an additional 2-minute period, this 30-second tone-shock pairing was repeated. Mice remained in the chamber for a final 1-minute period and were then removed. Mice were placed into a fresh cage to avoid contact with untested cage mates, within a recovery room adjacent to the test room. 24 hours later, mice were tested for context-dependent fear memory by re-introducing them to the training chamber for 4 minutes. 2 hours later, mice were tested for cue-dependent fear memory by placing them into an altered environment for 4 minutes, the final 2 minutes of which were accompanied by the 90dB tone stimulus. This altered environment included red lighting in the acclimation/test/recovery rooms, lack of white light in the chamber, a flat baseboard, rounded walls, and vanilla scent. In both tests, a video camera mounted to the front door of the chamber recorded mouse movement. Percentage of time spent freezing was recorded across the full 4-minute context test and the final 2 minutes of the cue test (when the tone stimulus was played). Freezing was defined as behavior below a motion threshold of 18 arbitrary units for 30 frames (1 second) minimum freeze duration and % time freezing was calculated using the default linear method.

Forced Gait Analysis

Mouse gait was assessed using the CleverSys TreadScan for forced gait analysis. The TreadScan apparatus consists of a treadmill chamber placed above a transparent belt treadmill illuminated by external light sources. A high-speed digital camera is placed underneath the treadmill chamber to capture ventral videos of mice on the treadmill. Mice were placed into the treadmill chamber and allowed to freely explore for 1 minute. The treadmill was turned on and off at a speed of 20 cm/s until the test mouse was continuously running. A 20-second video was then captured for footprint placement and movement analysis. Video files were automatically segmented using TreadScan software to include only periods of continual running. Video files were additionally manually clipped to eliminate periods when the mouse slowed running before a stop or exhibited lateral movement. This list of segments was subjected to footprint analysis with paw identification

training modules built in accordance with the manufacturer's instructions. All analyzed gait metrics were weighted by number of counted steps per foot.

MeCP2 Western blotting

Mice were humanely euthanized and perfused with ice-cold phosphate buffered saline (PBS) prior to isolation of brain tissue and dissection into hemibrains. Hemibrains were homogenized in buffer containing 10mM HEPES, 1.5mM $MgCl_2$, 10mM KCl, 0.05% NP-40, 0.5mM DTT, and 1x Mammalian Protease Inhibitor Cocktail (Sigma P8340), pH 7.9. The cytosolic fraction was removed following centrifugation and nuclear pellets were resuspended in buffer containing 5mM HEPES, 1.5mM $MgCl_2$, 0.2mM EDTA, 25% glycerol, 0.5mM DTT, and 1x Mammalian Protease Inhibitor Cocktail, pH 7.9. Suspended nuclei were treated with benzonase for 1 hour on ice (Sigma E1014). Following nuclease treatment, NaCl concentration was increased to 600mM, and nuclei were incubated on ice for 1 hour. Cellular debris was removed by high-speed centrifugation and nuclear protein concentration was determined with the 660nm Protein Assay Reagent (Pierce, Waltham, MA, USA). 5 μg of nuclear protein was loaded into individual wells of 10% house-made acrylamide SDS-PAGE gels and subjected to standard Western blotting procedures. An Odyssey CLx (LI-COR, Lincoln, NE, USA) imaging system was used for blot detection and quantification was performed in Image Studio Lite (LI-COR). Full-length MeCP2 was detected with an antibody specific to the carboxy terminus of MeCP2 (Cell Signaling, Danvers, MA, USA; D4F3, monoclonal rabbit anti-C'MeCP2, 1:5,000 dilution). R294X MeCP2 was detected with an antibody specific to the amino terminus of MeCP2 (Sigma; M7443, monoclonal mouse anti-N' MeCP2, 1:1,000 dilution). TATA-binding protein (TBP) was detected as a loading control (Full-length MeCP2 Westerns: abcam ab51841, monoclonal mouse anti-TBP, 1:2,000 dilution) (R294X MeCP2 Westerns: Cell Signaling 8515S, polyclonal rabbit anti-TBP, 1:2,000 dilution). Secondary antibodies used for detection were goat anti-rabbit 800CW (LI-COR 926-32211, 1:10,000 dilution) and goat anti-mouse 680RD (LI-COR 926-68070, 1:10,000 dilution).

Statistical analysis

Statistical analysis was performed within Prism 9 (GraphPad, San Diego, CA, USA). Behavioral data was analyzed with one-way ANOVA (factor = genotype) and Dunnett's post-hoc comparison to WT. Rotarod and fear conditioning training data were analyzed with two-way repeated measures ANOVA (factors = genotype, time) and Dunnett's post-hoc comparison to WT. Quantitative Western blots were analyzed with one-way ANOVA (factor = genotype) and Dunnett's post-hoc comparison to WT (**Figure 4A-B**) or unpaired t-test (**Figure 4C-D**). All plots display mean ± standard error of the mean. Statistical significance is represented in all plots as follows: *p<0.05, **p<0.01, ***p<0.001, ****p<0.0001.

Results

Gross RTT-like phenotypes are rescued with *MECP2* transgene in male and female R294X mice

We set out to determine whether genetically introducing full-length MeCP2 in the context of the partial loss-of-function R294X allele could rescue RTT-like phenotypes without eliciting adverse MDS-like effects. To do so, we drew on an established mouse model of MDS that expresses an autosomal human *MECP2* transgene under its native promoter[33]. These transgenic mice (*MECP2*^{Tg}) express full-length MeCP2 at levels approximately twice that of endogenous mouse MeCP2 in males and females (**Figure 4A-B**)[33,129]. *MECP2*^{Tg} mice display some phenotypes, such as those relevant to motor behavior and cognition, that are opposite to those observed in mice with *Mecp2* loss-of-function mutations, providing a behavioral readout of MeCP2 dosage[33,134,150,151]. We crossed mice harboring the *Mecp2* R294X allele with *MECP2*^{Tg} mice to generate *Mecp2*$^{+/Y}$ and *Mecp2*$^{+/+}$ (WT), *Mecp2*$^{R294X/Y}$ and *Mecp2*$^{R294X/+}$ (R294X), *MECP2*^{Tg} (TG), and *Mecp2*$^{R294X/Y}$;*MECP2*^{Tg} and *Mecp2*$^{R294X/+}$;*MECP2*^{Tg} (R294X TG) mice[110]. R294X mice of both sexes express truncated MeCP2, and this is supplemented by transgenic full-length MeCP2 in R294X TG animals (**Figure 4C-D**). We assayed and analyzed male and female cohorts separately because *MECP2* mutations cause RTT in females and variety of clinical phenotypes in males, including a subset with a more severe clinical course compared to females with RTT (RTT encephalopathy)[2,3,30].

We first evaluated gross physical features and symptomatic progression in male and female mice. Consistent with previous characterization, we found that male R294X mice have low body weight compared to WT littermates as early as 4 weeks of age (**Figure 5A**)[110]. Additionally, male R294X mice display progression of RTT-like symptoms (**Figure 5B**)[119]. Both of these phenotypes are rescued with addition of *MECP2* transgene, as male R294X TG mice are indistinguishable from WT littermates. Unlike the males, we found that female R294X mice do not have a low body weight phenotype (**Figure 5C**). However, female R294X mice do display progression of RTT-like symptoms, and these are also rescued to WT levels by addition of *MECP2* transgene (**Figure 5D**).

RTT-specific breathing phenotypes are rescued with *MECP2* transgene in male R294X mice

To test the hypothesis that MeCP2 supplementation provides safe and effective behavioral rescue in R294X mice, we conducted a behavioral battery including assays for RTT-specific phenotypes and assays for bidirectionally dosage-sensitive phenotypes. We evaluated these phenotypes at different ages for male (20-22 weeks old) and female mice (30-31 weeks old, with exception of gait performed at 34-40 weeks old), as male mice lacking MeCP2 function have an earlier onset of phenotypic abnormalities compared to female RTT mice. This is expected, as male *Mecp2* mutant mice are hemizygous for the mutation. Here we present results from the male mice as in this condition all somatic cells should express both the *Mecp2* R294X and *MECP2* TG alleles, providing a genetically homogenous readout of MeCP2 supplementation. The

batteries included tests for spontaneous locomotor activity, anxiety-like behavior, breathing function, motor coordination, sociability and social novelty preference, learning and memory, and gait (**Figure 6**).

Breathing disturbances are highly prevalent in RTT and, though complex and individually variable, often include bouts of hypoventilation alternating with irregular breathing or hyperventilation[209]. Mice with common *Mecp2* mutations also reproducibly display breathing dysfunction[110,133,134,207]. To investigate breathing function in the context of the R294X allele, we conducted unrestrained whole-body plethysmography experiments in male WT, R294X, TG, and R294X TG mice[210–212]. We found that male R294X mice display abnormal breathing function, which is not observed in R249X TG littermates (**Figure 7A**). Quantitatively, this abnormal breathing function reflects an increased basal breathing rate (**Figure 7B:** one-way ANOVA $F_{(3,55)} = 19.39$, $p<0.0001$; Dunnett's post hoc comparison to WT $p<0.0001$, $p=0.1359$, $p=0.6527$ for R294X, TG, and R294X TG respectively), increased breathing irregularity (**Figure 7C**: one-way ANOVA $F_{(3,55)} = 29.35$, $p<0.0001$; Dunnett's post hoc comparison to WT $p<0.0001$, $p=0.7114$, $p=0.7631$ for R294X, TG, and R294X TG respectively), and increased incidence of apneic events (**Figure 7D**: one-way ANOVA $F_{(3,55)} = 41.64$, $p<0.0001$; Dunnett's post hoc comparison to WT $p<0.0001$, $p=0.9971$, $p=0.9931$ for R294X, TG, and R294X TG respectively) compared to WT littermates. Each of these RTT-specific breathing phenotypes is rescued to WT levels with addition of *MECP2* transgene.

Bidirectionally dosage-sensitive behavioral phenotypes are normalized with *MECP2* transgene in male R294X mice

In addition to RTT-specific breathing phenotypes, we also assayed behaviors that are bidirectionally dosage-sensitive in male mice. One such behavior is spontaneous locomotor activity. Individuals with RTT have gross motor dysfunction and can experience motor deterioration in the late course of disease, with loss of ambulation and development of parkinsonian gait. Individuals with MDS display early onset of severe motor dysfunction, including infantile hypotonia and progressive spasticity[3,32,38,40,173]. Mice with *Mecp2* mutations and transgenic *MECP2* overexpressing mice have both been reported to display decreased spontaneous locomotor activity[77,110,133,150,207]. We observe a similar phenotype in male R294X and male TG mice, which display decreased total distance travelled in a 30-minute open field assay, compared to WT littermates (**Figure 8A**; **Figure 8B**: one-way ANOVA $F_{(3,55)} = 7.825$, $p=0.0002$; Dunnett's post hoc comparison to WT $p=0.0003$, $p=0.0156$, $p=0.6554$ for R294X, TG, and R294X TG respectively). The total distance that male R294X TG mice travelled is not different from that of WT littermates, indicating normalization of spontaneous locomotor activity.

To evaluate motor coordination, we performed the rotarod assay. Literature suggests that mice harboring *Mecp2* mutations generally underperform, while transgenic *MECP2* overexpressing mice generally overperform, relative to WT controls[33,77,108,110,133,134,150,207]. We too observe this difference, as male R294X mice display decreased latency to fall and male TG mice display increased latency to fall compared to WT littermates across all three days of the assay (**Figure 8C**: two-

way repeated measures ANOVA, Genotype $F_{(3,57)} = 73.58$ and $p<0.0001$, Day $F_{(2,114)} = 10.38$ and $p<0.0001$, Genotype x Day $F_{(6,114)} = 0.5766$ and $p=0.7483$). Addition of *MECP2* transgene normalizes motor coordination in males, as the latency to fall of male R294X TG mice is not different from that of WT littermates.

We assayed anxiety-like behavior using the elevated zero maze assay, as there is a high prevalence of comorbid anxiety in individuals with RTT and MDS[40,213,214]. Previous reports indicate that mice harboring common loss-of-function *Mecp2* mutations generally display decreased anxiety-like behavior, while transgenic *MECP2* overexpressing mice generally display increased anxiety-like behavior[108,110,133,134,150,151]. Consistently, we observe that male R294X mice spend more time in the open arms of the maze, while male TG mice spend less time in the open arms of the maze, compared to WT littermates, indicating decreased and increased anxiety-like behavior respectively (**Figure 8D**: one-way ANOVA $F_{(3,57)} = 30.49$, $p<0.0001$; Dunnett's post hoc comparison to WT $p<0.0001$, $p=0.0464$, $p=0.9945$ for R294X, TG, and R294X TG respectively). The time male R294X TG mice spend in the open arms of the maze is not different from that of WT littermates, demonstrating that addition of *MECP2* transgene normalizes anxiety-like behavior. As a complementary metric for anxiety-like behavior, we analyzed the percent distance travelled in the center of the open field arena during the open field assay. Male R294X mice travel a higher percentage of distance in the center compared to WT littermates, consistently indicative of decreased anxiety-like behavior (**Figure 9A**: one-way ANOVA $F_{(3,55)} = 6.108$, $p=0.0012$; Dunnett's post hoc comparison to WT $p=0.0002$, $p=0.0747$, $p=0.0504$ for R294X, TG, and R294X TG respectively). Both TG and R294X TG male mice travelled a percentage of distance in the center similar to WT littermates.

As an evaluation of social behavior, we used the Crawley 3-chamber assay for sociability and social novelty preference. Though social behavior phenotypes vary widely amongst mouse models of RTT depending on allele, mouse strain, and testing/analysis methods, some work has found elevated sociability and social novelty preference in *Mecp2* mutant mice and reduced sociability and social novelty preference in transgenic *MECP2* overexpressing mice[150–152,215,216]. We used a single-day protocol and evaluated the sociability of mice (preference to interact with an unfamiliar mouse over an empty cup) and social novelty preference (preference to interact with an unfamiliar mouse over a familiar mouse). We found that mice of all genotypes exhibited typical sociability, with positive mean discrimination indices (**Figure 10A**: one-way ANOVA $F_{(3,57)} = 1.642$, $p=0.1898$; Dunnett's post hoc comparison to WT $p=0.2486$, $p=0.9966$, $p>0.9999$ for R294X, TG, and R294X TG respectively). Additionally, mice of all genotypes exhibited typical social novelty preference (**Figure 10B**: one-way ANOVA $F_{(3,57)} = 0.0431$, $p=0.9880$; Dunnett's post hoc comparison to WT $p=0.9931$, $p=0.9821$, $p=0.9703$ for R294X, TG, and R294X TG respectively). These data suggest that neither R294X nor TG male mice show social behavior phenotypes in this assay.

Finally, we employed contextual and cued fear conditioning to investigate learning and memory. Previous reports have demonstrated that mice with *Mecp2* mutations display decreased freezing, while transgenic *MECP2* overexpressing mice display increased freezing, relative to WT controls across both tests[33,110,134,152]. We found that, during the training session, male TG mice displayed higher freezing levels than WT littermates, beginning and continuing after the first tone-shock pairing (**Figure 8E**: two-way repeated measures ANOVA, Genotype $F_{(3,55)} = 13.09$ and $p<0.0001$, Day $F_{(5,275)} = 59.19$ and $p<0.0001$, Genotype x Day $F_{(15,275)} = 11.38$ and $p<0.0001$). Neither R294X nor R294X TG male mice displayed freezing levels different from WT mice in the training session. Additionally, though not significant in the context recall test, male R294X mice displayed decreased freezing relative to WT mice during the cue recall test. Male TG mice displayed increased freezing relative to WT during both context and cue recall tests (**Figure 8F**: one-way ANOVA $F_{(3,56)} = 26.05$, $p<0.0001$; Dunnett's post hoc comparison to WT $p=0.0889$, $p<0.0001$, $p=0.8655$ for R294X, TG, and R294X TG respectively; **Figure 8G**: one-way ANOVA $F_{(3,56)} = 16.50$, $p<0.0001$; Dunnett's post hoc comparison to WT $p=0.0164$, $p=0.0016$, $p=0.9072$ for R294X, TG, and R294X TG respectively). Male R294X TG mice displayed freezing levels that were not different from WT during context and cue recall tests, indicating that addition of *MECP2* transgene normalizes fear memory.

RTT- and MDS-like behavioral phenotypes are rescued in female R294X TG mice

No adverse effects of MeCP2 supplementation were observed in our behavioral battery with male mice. However, we hypothesized that the therapeutic window for *MECP2* elevation might differ for female mice. Females with *MECP2* mutations are mosaic due to inactivation of either the WT or mutant *MECP2* allele in each somatic cell[217]. Most individuals with RTT have balanced XCI, but highly skewed XCI has been observed in some individuals with mild RTT and asymptomatic carriers of disease-causing *MECP2* mutations[218–220]. Importantly, while *MECP2* gene therapy in 46,XY males should lead to co-expression of endogenous mutant and exogenous WT alleles in all somatic cells, *MECP2* gene therapy in 46,XX females should lead to two populations of somatic cells – 1) cells that co-express endogenous mutant and exogenous WT alleles, as occurs in males, and 2) cells that express both endogenous and exogenous WT alleles. We hypothesized that modelling gene therapy in females would specifically address potential MDS-like adverse effects arising from this second population of somatic cells that are not present in males.

We began the female behavioral battery at 30 weeks with the open field assay to evaluate spontaneous locomotor activity. Similar to male mice, female R294X mice travelled decreased total distance compared to WT littermates over a 30-minute period (**Figure 11A**; **Fig. 11B:** one-way ANOVA $F_{(3,55)} = 5.186$, $p=0.0032$; Dunnett's post hoc comparison to WT $p=0.0028$, $p=0.2303$, $p=0.9705$ for R294X, TG, and R294X TG respectively). Unlike males, female MDS model mice did not display a phenotype in this assay, as female TG mice travelled a total distance that was not different from WT littermates. In female R294X TG mice, spontaneous locomotor activity was rescued to WT levels with addition of *MECP2* transgene. We next

analyzed breathing function through unrestrained whole-body plethysmography. Female R294X mice displayed an abnormal breathing pattern (**Figure 11C**), with an increased basal breathing rate (**Figure 11D:** one-way ANOVA $F_{(3,55)}$ = 6.516, p=0.0008; Dunnett's post hoc comparison to WT p=0.0081, p=0.9586, p=0.9267 for R294X, TG, and R294X TG respectively), increased breathing irregularity (**Figure 11E:** one-way ANOVA $F_{(3,55)}$ = 17.41, p<0.0001; Dunnett's post hoc comparison to WT p=0.0014, p=0.0089, p=0.9298 for R294X, TG, and R294X TG respectively), and increased incidence of apneic events (**Figure 11F:** one-way ANOVA $F_{(3,55)}$ = 15.27, p<0.0001; Dunnett's post hoc comparison to WT p=0.0020, p=0.0510, p=0.3989 for R294X, TG, and R294X TG respectively) compared to WT littermates. Unexpectedly, female TG mice also demonstrated relatively decreased breathing irregularity (increased regularity) (**Figure 11E**). These RTT-specific breathing phenotypes were each rescued by addition of *MECP2* transgene in R294X TG littermates. Finally, we assayed learning and memory with fear conditioning, an assay in which *Mecp2*$^{-/+}$ mice have been shown to exhibit deficits[198,221,222]. In the training session, female TG mice displayed increased freezing beginning and continuing after the first tone-shock pairing, similar to male TG mice (**Figure 11G:** two-way repeated measures ANOVA, Genotype $F_{(3,58)}$ = 16.13 and p<0.0001, Minute $F_{(5,290)}$ = 221.4 and p<0.0001, Genotype x Minute $F_{(15,290)}$ = 4.905 and p<0.0001). This phenotype is not observed in female R294X TG mice. In the contextual and cue recall tests, female TG mice again displayed increased freezing compared to WT littermates (**Figure 11H**: one-way ANOVA $F_{(3,58)}$ = 5.050, p=0.0035; Dunnett's post hoc comparison to WT p=0.8863, p=0.0114, p=0.6172 for R294X, TG, and R294X TG respectively; **Figure 11I:** one-way ANOVA $F_{(3,58)}$ = 2.320, p=0.0847; Dunnett's post hoc comparison to WT p=0.2994, p=0.0292, p=0.3981 for R294X, TG, and R294X TG respectively). However, the percentage of time that female R294X mice spent freezing was not different from WT mice. In female R294X TG mice, the MDS-like phenotypes were not apparent, demonstrating that transgenic *MECP2* supplementation does not elicit adverse hippocampal-dependent learning phenotypes in the context of the R294X allele.

Transgenic *MECP2* supplementation leads to an MDS-like motor coordination phenotype in female R294X mice

Our behavioral battery also evaluated a motor behavior that is bidirectionally dosage-sensitive in females – motor coordination – through the rotarod assay. Similar to findings in the male mice, female R294X mice displayed a decreased latency to fall while female TG mice displayed an increased latency to fall relative to WT littermates (**Figure 12A**: two-way repeated measures ANOVA, Genotype $F_{(3,59)}$ = 60.68 and p<0.0001, Day $F_{(2,118)}$ = 13.74 and p<0.0001, Genotype x Day $F_{(6,118)}$ = 0.5522 and p=0.7674). However, female R294X TG mice overperformed compared to WT mice, with an increased latency to fall mice that reached statistical significance on the second day of the assay. We wondered whether the enhanced motor coordination in female R294X TG mice stemmed from differences in gait function. To address this, we performed forced gait analysis in female mice aged 34-40 weeks. We found that front paw stride length was increased in both TG mice and R294X TG mice compared to WT littermates (**Figure 12B**: one-way ANOVA $F_{(3,58)}$ = 9.460, p<0.0001; Dunnett's post hoc comparison to WT p=0.1535, p=0.0354, p=0.0490 for R294X, TG, and R294X TG respectively). Rear paw stride length was

only increased in R294X TG mice compared to WT littermates (**Figure 12C**: one-way ANOVA $F_{(3,58)} = 8.361$, p=0.0001; Dunnett's post hoc comparison to WT p=0.2234, p=0.0522, p=0.0489 for R294X, TG, and R294X TG respectively). Because differences in gross physical features can impact forced gait performance, we measured body weight and length. While there were no differences in body weight across genotype, female R294X mice had decreased body length and female TG mice had increased body length compared to WT mice (**Figure 12D:** one-way ANOVA $F_{(3,58)} = 2.030$, p=0.1197; Dunnett's post hoc comparison to WT p=0.0787, p=0.9506, p=0.9791 for R294X, TG, and R294X TG respectively). Body length of female R294X TG mice was not different from that of WT mice (**Figure 12E**: one-way ANOVA $F_{(3,58)} = 13.46$, p<0.0001; Dunnett's post hoc comparison to WT p=0.0092, p=0.0092, p=0.6014 for R294X, TG, and R294X TG respectively).

Discussion

Within the past decade, preclinical evidence has emerged supporting MeCP2 supplementation as a viable therapeutic strategy for RTT. Promising among such approaches is gene therapy, with viral delivery of full-length *MECP2* to the CNS. Numerous studies have evaluated the safety and efficacy of gene therapy in hemizygous *Mecp2*$^{-/Y}$ mice and have demonstrated rescue of survival, body weight, and select behavioral phenotypes[174–179]. However, only one study thus far has evaluated the safety and efficacy of gene therapy in heterozygous *Mecp2*$^{-/+}$ mice, where authors demonstrated that systemic viral delivery in adulthood rescued gross phenotypic progression as well as motor and cognitive behavioral phenotypes[174]. Collectively these studies have also identified potential barriers to the use of gene therapy in people, most prominently hepatotoxicity occurring with systemic delivery[176,179]. However, MDS phenotypes, and subsequently the potential for MDS-like adverse effects due to excess MeCP2 in the CNS, have not been thoroughly evaluated in these experiments. Additional preclinical research into the therapeutic window of *MECP2* gene therapy in mice harboring partial loss-of-function *Mecp2* mutations, particularly in female mice, is needed to determine the safety of approaches involving MeCP2 supplementation.

We addressed both of these by genetically modelling MeCP2 supplementation in the context of the partial loss-of-function R294X allele and screening for behavioral evidence of excess MeCP2 in males and females separately. We found that male R294X TG mice express full-length MeCP2 at levels comparable to male WT littermates, indicating normalization of protein level. In comparison, female R294X TG mice express full-length MeCP2 at levels approximately 1.5x that of female WT littermates, consistent with random X-chromosome inactivation of endogenous WT and R294X alleles. We carried out a broad behavioral battery designed to evaluate rescue of RTT-like phenotypes observed in male and female R294X mice, as well as potential MDS-like adverse effects. We found that male R294X and female R294X mice share some RTT-like phenotypes, including decreased spontaneous locomotor activity, breathing dysfunction, and reduced motor coordination. Male and female TG mice displayed opposing phenotypes, notably enhanced motor coordination and enhanced fear

memory. RTT-specific phenotypes were rescued and phenotypes that are bidirectionally MeCP2 dosage-sensitive were normalized in male R294X TG mice. RTT-specific phenotypes were also rescued by addition of *MECP2* transgene in females. However, female R294X TG mice performed similarly to MDS model mice in assays for motor coordination and gait, suggesting that the underlying motor circuitry is particularly sensitive to MeCP2 dosage in females.

We chose to examine the partial loss-of-function R294X mutation, which we previously engineered into mice using CRISPR/Cas9 technology[110]. R294X is a common mutation in *MECP2* that truncates the coding sequence within the NID and eliminates the C-terminal portion of the protein. In mice, the R294X allele produces a truncated protein product, rendering it unique amongst the common RTT-causing *MECP2* truncation mutations. This truncation product retains DNA binding capacity with resultant partial functioning, likely the reason why R294X is associated with milder clinical disease in humans[16]. We replicated behavioral results in male R294X mice, finding that they display decreased spontaneous locomotor activity, elevated anxiety-like behavior, breathing dysfunction, reduced motor coordination, and impaired memory formation[110]. Our results in the fear conditioning assay differ slightly from previous findings in this model[110]. While we report significant differences between male WT and R294X mice in the cue but not context recall test at 20 weeks, Merritt et al. reported significant differences in both at 16 weeks. This difference might be due to experimental conditions and/or mouse age causing generally lower freezing in our WT mice. Additionally, we found that R294X mice do not display deficits in sociability or social novelty preference via the Crawley 3-chamber assay. Of note, social behavior phenotypes vary widely amongst mouse models of RTT depending on allele, mouse strain, and testing/analysis methods[223]. We evaluated a partial loss-of-function allele on a pure C57BL6/J background, using a single-day protocol and blinded manual scoring of interaction time from a video of the assay – any/several of which could account for differences between our results and previous reports.

We extended this work with behavioral evaluation of female R294X mice. Gross physical characterization revealed that, unlike many male models, female R294X mice do not have a low body weight phenotype. This is consistent with a report from *Mecp2*$^{R168X/+}$ mice, in which there was no statistically significant difference in body weight from WT until 10 weeks of age[133]. We also did not observe a high body weight phenotype, as was notably reported in *Mecp2*$^{R255X/+}$ mice beginning at 10 weeks of age. At 34-40 weeks, however, several individual female R294X mice displayed very high body weights, though the R294X genotype average did not reach statistically significant difference from WT. Genetic background strongly influences body weight phenotypes in RTT model mice, and it is possible that genetic variation mediates expression of this phenotype in individual mice[114]. As evidence of this, one study documented differences in body weight phenotypes amongst *Mecp2*$^{+/-}$ mice, noting elevated body weight in F1 FVB/N x 129S6/SvEv mice and reduced body weight in F1 FVB/N x C57BL/6 mice[198]. Differences in strain may account for variation between female R294X weight and that of

previous reports such as R255X females, given that the R294X data are derived from >10 generations of a backcross to C57BL/6J.

Behaviorally, we found that similar to males, the females demonstrated RTT-like phenotypes in assays for spontaneous locomotor activity, breathing function, and motor coordination. However, unlike the males, female R294X mice did not display deficits in fear learning. Contextual memory deficits have been reported in female *Mecp2*$^{-/+}$ mice on FVB/N x 129S6/SvEv F1, 129S6/SvEv x C57BL/6 F1, and C57BL/6 backgrounds but not, to our knowledge, in a model of a human point mutation[198,221,222]. We hypothesize that the lack of memory deficits in female R294X mice reflects the milder phenotype observed in people with the R294X mutation and can be attributed to partial functioning of the R294X truncation product. However, our experiments do not address the alternate possibility that memory deficits have a delayed manifestation in female R294X mice, past 30 weeks of age. Together, our behavioral evaluation of male and female R294X mice contributes insights into the behavioral consequences of partial loss-of-function *MECP2* mutations like R133C, R294X, and R306C[108,129]. Additionally, our work reinforces the utility of the R294X model, with relatively prolonged survival and delayed onset of RTT-like phenotypes, for preclinical work[110].

An important consideration for any RTT therapeutic in preclinical development is its effect on MeCP2 dosage. Several neuronal ASD-associated genes have been determined to be bidirectionally dosage-sensitive (*RAI1*, *SHANK3*, *UBE3A*) in addition to *MECP2*, meaning that both decreases and increases in gene function cause neurological disease in people[224]. Because of this, therapeutic approaches that elevate functional MeCP2 beyond typical levels, such as gene therapy and reactivation of *MECP2* on the inactive X-chromosome, have the potential for excess dosage-related adverse effects. We considered the potential for these dosage-related adverse effects by genetically modelling idealized gene therapy capable of fully restoring MeCP2, via supplementation of transgenic human MeCP2 in the context of the R294X allele. While this genetic approach permits precise control of MeCP2 dosage, one limitation is that it models MeCP2 supplementation pre-symptomatically, whereas putative gene therapy would be administered post-symptomatically. Post-symptomatic genetic and viral delivery of *MECP2* have both shown symptomatic benefit in mice, providing hope that this is achievable clinically[119,177,178]. However, the experimental paradigm used here does not address post-symptomatic MeCP2 supplementation.

We first assessed male mice because they develop RTT-like phenotypes with earlier onset compared to females and model genetically homogenous MeCP2 supplementation throughout the CNS. When assessed at 20 weeks, we found that addition of *MECP2* transgene in male R294X mice was sufficient to rescue RTT-specific breathing phenotypes. We additionally evaluated behaviors that are bidirectionally dosage-sensitive in males. At this age, male TG mice demonstrated phenotypes

in spontaneous locomotor activity, anxiety-like behavior, motor coordination, and fear memory assays, consistent with previous reports[134,150–152]. Unexpectedly, we also found that male TG mice had elevated freezing levels in the training session of the fear conditioning assay after the first tone-shock pairing. Yu et al. reported a similar phenotype in *MECP2* transgenic mice, as well as elevated freezing in a new context after training, suggesting elevated startle and generalization of learned contextual fear[152]. Male R294X TG mice do not display any of these MDS-like phenotypes, demonstrating that MeCP2 supplementation is safe in the male R294X model. Only one other study by Heckman et al. has evaluated the behavioral consequences of transgenic MeCP2 supplementation in the context of a partial loss-of-function *MECP2* mutation[129]. In this work, authors evaluated the common R306C mutation in male mice aged 5- and 11-weeks expressing mutant MeCP2 with a C-terminal GFP tag, finding that motor and cognitive behaviors were fully rescued with *MECP2* transgene. Our work complements these findings, supporting the notion that introduction of full-length MeCP2 to males is safe and effective. Specifically, we note that MeCP2 supplementation is effective even in the presence of a truncation product with DNA-binding capacity, alleviating potential concerns for dominant negative interactions.

We next assessed female mice, which undergo XCI and heterogeneously express WT or mutant MeCP2 throughout the CNS. XCI generates two considerations for MeCP2 supplementation that are specific to females. First, unlike the males, females with transgenic *MECP2* expression will have a population of neurons that co-express the full-length *MECP2* transgene and the endogenous WT allele. Second, XCI skewing can alter the predominance of this population of neurons. Though most individuals with RTT display balanced XCI, skewed XCI that occurs in a minority of individuals could decrease or increase severity depending on whether the WT or mutant allele predominates[218,220]. Together, mutation type and XCI status contribute to individual variation in functioning MeCP2 that likely impacts clinical severity, and both factors should be considered with therapeutic approaches involving MeCP2 supplementation. Though our experimental design could not evaluate different degrees of XCI skew, we were able to assess safety in the context of a partial loss-of-function allele. We found that, similar to males, RTT-specific phenotypes such as decreased spontaneous locomotor activity and breathing dysfunction were rescued by addition of *MECP2* transgene.

Females with *MECP2* duplications on the X-chromosome often display neuropsychiatric disease but not the MDS clinical phenotype seen in males. This is due to nearly 100% XCI skewing in favor of the WT allele, as measured in peripheral blood samples[40]. However, if the *MECP2* duplication is on an autosome or if there is unskewed XCI, females can manifest an abnormal phenotype to varying degrees, making this model relevant to females as well[225]. MDS-like phenotypes were milder in females as compared to males, as female TG mice displayed differences from WT only in assays for motor coordination and contextual learning. While enhanced freezing in fear conditioning was rescued by transgenic MeCP2 supplementation of the R294X allele in females, female R294X TG mice overperformed on the rotarod assay for motor

coordination, similar to female TG mice. Furthermore, both TG and R294X TG female mice displayed increases in stride length compared to WT littermates as determined by forced gait analysis. These changes in gait did not correlate with gross physical parameters across both genotypes, as there were no differences in weight and female TG mice, but not female R294X TG mice, had increased body length relative to WT controls. These results point to a potential sex-specific motor coordination side effect of MeCP2 supplementation in the female brain. MeCP2 supplementation of the R255X allele in female mice leads to similarly subtle overperformance, with significantly elevated latency to fall reported on the first of two test days compared to WT controls[134]. Because this has now been observed across both complete (R255X) and partial (R294X) loss-of-function mutations, we predict that MeCP2 supplementation of other RTT-causing mutations would elicit a similar motor coordination phenotype. One possible explanation is that this subtle MDS-like motor coordination phenotype is driven by the population of cells expressing both endogenous *Mecp2* as well as transgenic human *MECP2*. This population of cells is exposed to excess levels of full-length MeCP2 and may uniquely impact behavioral phenotypes in females, regardless of mutation type.

The circuitry underlying the enhanced motor coordination phenotype has been dissected by Rothwell et al. using a mouse model of autism-associated neurologin-3 (NL3) mutations[226]. The authors found that these mutations specifically decreased synaptic inhibition onto D1-expressing medium spiny neurons in the nucleus accumbens in ventral striatum, causing acquired repetitive motor behavior. Consistently, selective loss of MeCP2 from forebrain GABAergic neurons causes impaired motor coordination in male mice, and selective preservation of MeCP2 in forebrain GABAergic neurons in floxed-STOP-*Mecp2* female mice rescues this impaired motor coordination phenotype[122,126]. Interestingly, the latter study also found that female floxed-STOP-*Mecp2* mice with MeCP2 levels restored in the striatum overperformed on the rotarod when retested one month after the original test compared to WT controls[122]. Together with our findings, this data suggests that the striatal circuitry responsible for motor coordination is particularly sensitive to MeCP2 dosage in females, reinforcing the notion that MeCP2 dosage can have sex-specific effects and highlighting the importance of using female mice in preclinical studies for RTT[226].

Table 4. Scoring algorithm for RTT-like phenotypes in mice

Phenotype	Score of 0 (Absent)	Score of 1 (Present)	Score of 2 (Severe)
Activity	Typically responsive	Minimally responsive	Non-responsive
Hindlimb clasping	Legs typically spread	One leg held against body	Both legs held against body
Tremor	No tremor	Intermittent tremor	Continuous tremor
Breathing	Typical breathing	Hyperventilation or pauses in breathing	Gasps or panting
Coat condition	Typically groomed fur	Fur poorly groomed on close inspection (during handling)	Fur obviously poorly groomed (noticed immediately when cage is opened)
Hunch	No hunch	Hunch present on palpation	Hunch visualized without palpation
Gait	Typical gait	Wide stance or waddling gait	Uncoordinated or “hopping” gait

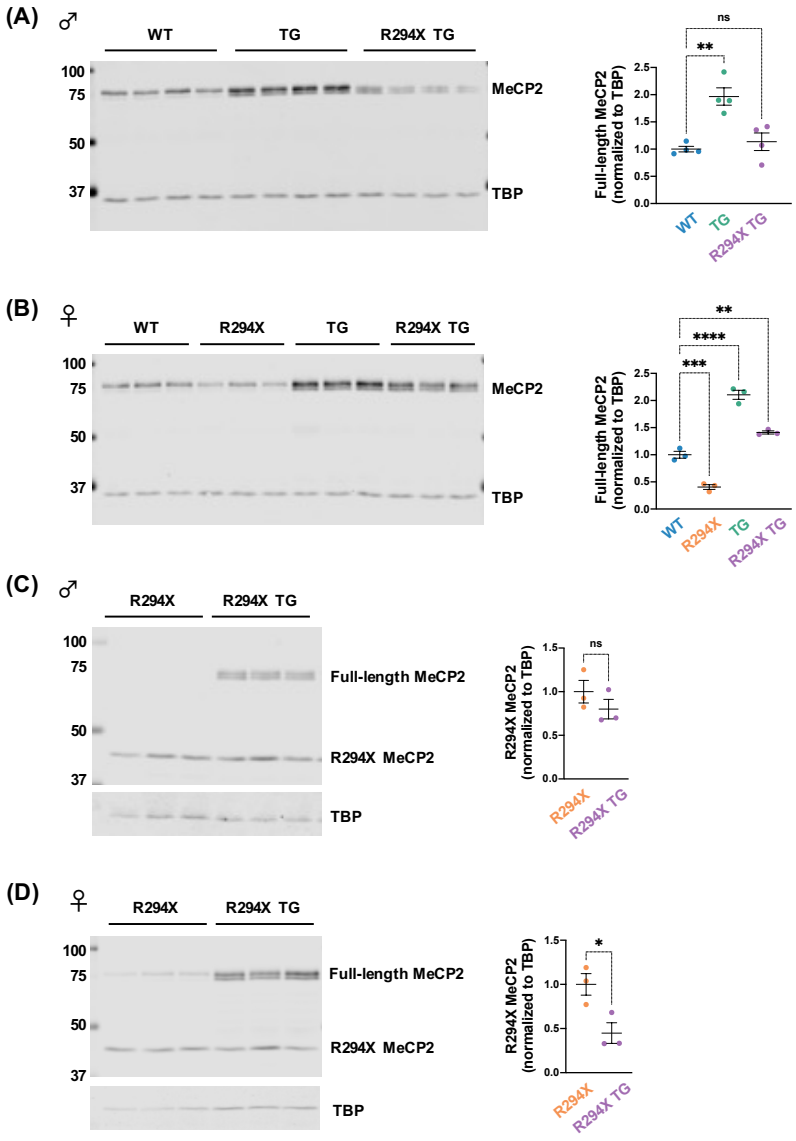

Figure 4. Full-length and truncated R294X MeCP2 are expressed in male and female mice

(A) Male TG mice express full-length MeCP2 at ~2x of WT levels. Male R294X TG mice express full-length MeCP2 at ~1x of WT levels. Representative Western blot of hemibrain nuclear lysates next to quantification. (Age: 24-25 weeks. WT n=4; TG n=4; R294X TG n=4) (B) Female R294X mice express full-length MeCP2 at ~0.5x of WT levels. Female TG mice express full-length MeCP2 at ~2x of WT levels. Female R294X TG mice express full-length MeCP2 at ~1.5x of WT levels. Representative Western blot of hemibrain nuclear lysates next to quantification. (Age: 36-39 weeks. WT n=3; R294X n=3; TG n=3; R294X TG n=3) (C) Male R294X and R294X TG mice express R294X truncation product at similar levels. Representative Western blot of hemibrain nuclear lysates next to quantification. (Age: 24-25 weeks. R294X n=3, R294X TG n=3) (D) Female R294X mice express R294X truncation product ~2x of R294X TG levels. Representative Western blot of hemibrain nuclear lysates next to quantification. (Age: 38-39 weeks. R294X n=3, R294X TG n=3)

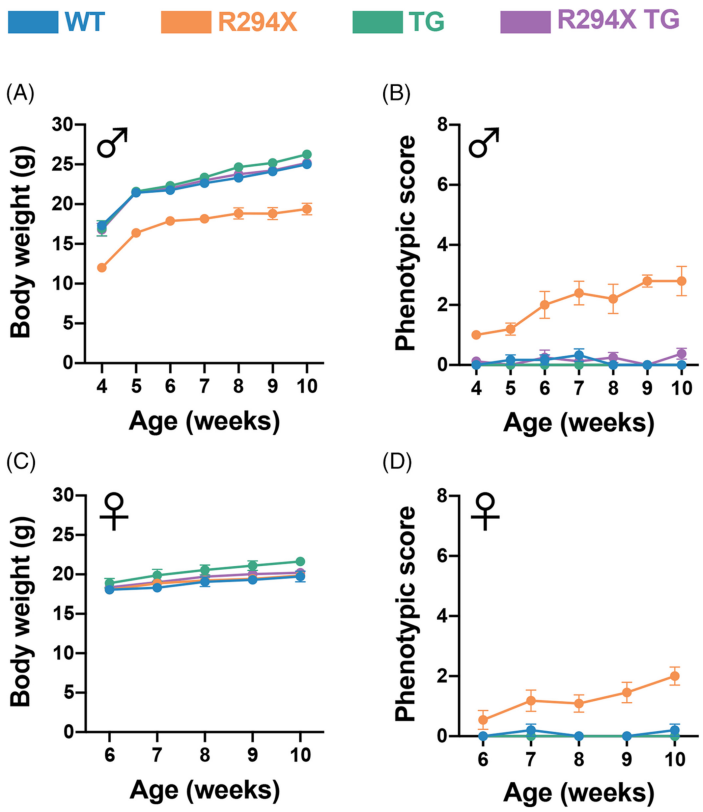

Figure 5. Gross RTT-like phenotypes are rescued with *MECP2* transgene in male and female R294X mice

(A) Body weights of male R294X mice are lower than that of WT littermates at 4 weeks of age and beyond. This phenotype is rescued by *MECP2* transgene in male R294X TG mice, whose body weights are not different from WT. (WT n = 6, blue; R294X n = 5, orange; TG n = 9, green; R294X TG n = 8, purple) (B) Male R294X mice exhibit progression of RTT-like phenotypes, as reflected by an increase in phenotypic score, which is rescued by *MECP2* transgene. (WT n = 6; R294X n = 5; TG n = 9; R294X TG n = 8) (C) Female R294X mouse body weights are not different from that of WT littermates. (WT n = 5; R294X n = 11; TG n = 7; R294X TG n = 9) (D) Female R294X mice exhibit progression of RTT-like phenotypes, as reflected by an increase in phenotypic score, which is rescued by *MECP2* transgene. (WT n = 5; R294X n = 11; TG n = 7; R294X TG n = 9)

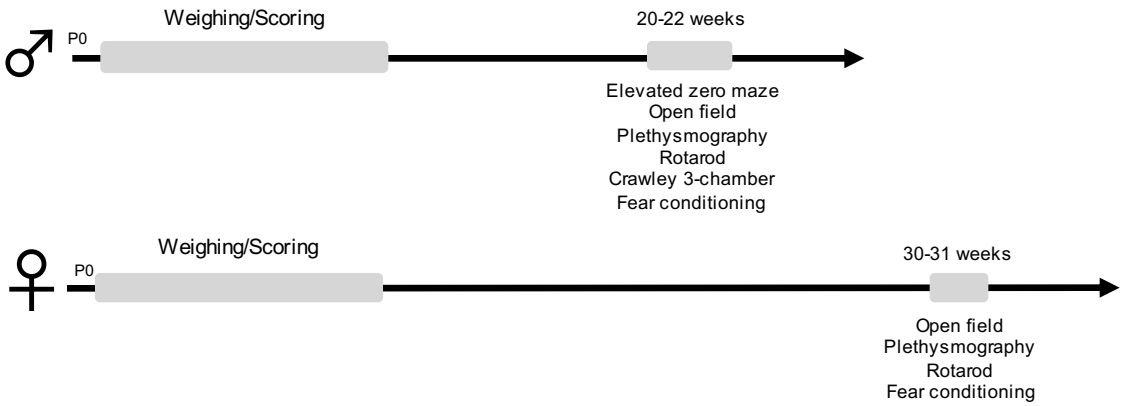

Figure 6. Timeline of mouse behavioral experiments

(Top) Three cohorts of male mice were weighed and phenotypically scored between weeks 4-14, and the behavioral battery run between weeks 20-22. The behavioral battery included the following tests in order: elevated zero maze, open field, plethysmography, rotarod, Crawley 3-chamber, and fear conditioning. (Bottom) Three cohorts of female mice were weighed and phenotypically scored between weeks 6-14, and the behavioral battery run between weeks 30-31. The behavioral battery included the following tests in order: open field, plethysmography, rotarod, and fear conditioning.

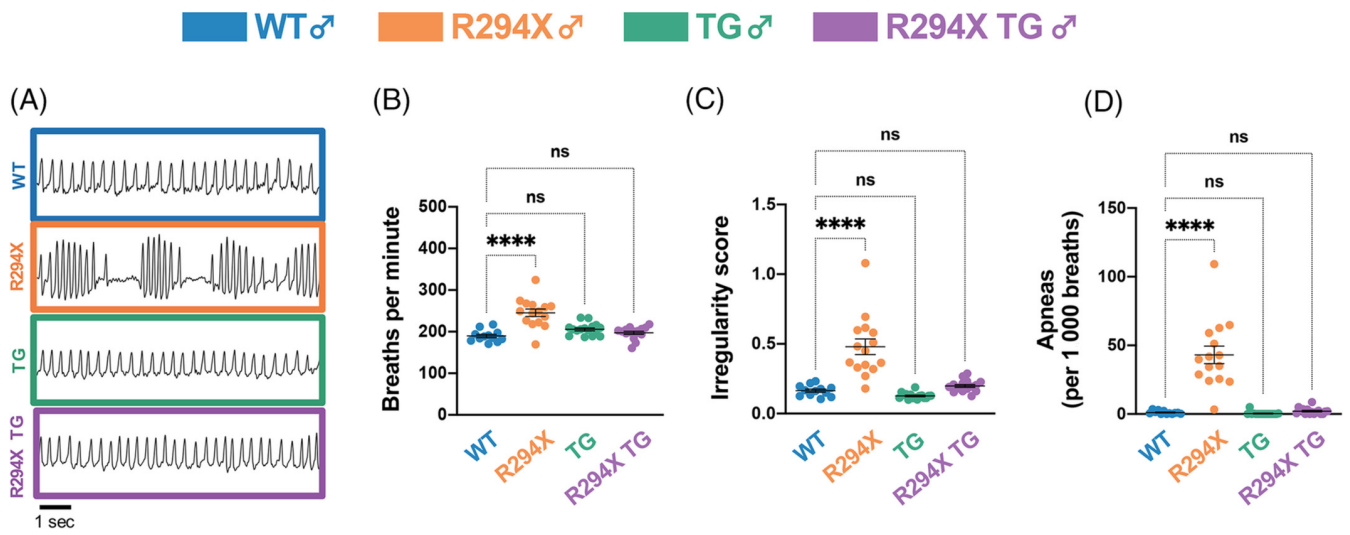

Figure 7. RTT-specific breathing phenotypes are rescued with *MECP2* transgene in male R294X mice

(A) Male R294X mice have an altered breathing pattern compared with WT littermates at 20 weeks of age, which is rescued by addition of *MECP2* transgene in male R294X TG mice. (B) Basal breathing rate is elevated in male R294X mice compared with WT littermates, which is rescued by addition of *MECP2* transgene. (Age: 20 weeks. WT n = 12; R294X n = 15; TG n = 16; R294X TG n = 16) (C) Breathing irregularity score, which reflects the instantaneous rate of change in total breath time, is elevated in male R294X mice compared with WT littermates. This phenotype is rescued by addition of *MECP2* transgene in male R294X TG mice. (Age: 20 weeks. WT n = 12; R294X n = 15; TG n = 16; R294X TG n = 16) (D) Male R294X mice have increased apneic events compared with WT littermates, which is rescued by addition of *MECP2* transgene. (Age: 20 weeks. WT n = 12; R294X n = 15; TG n = 16; R294X TG n = 16)

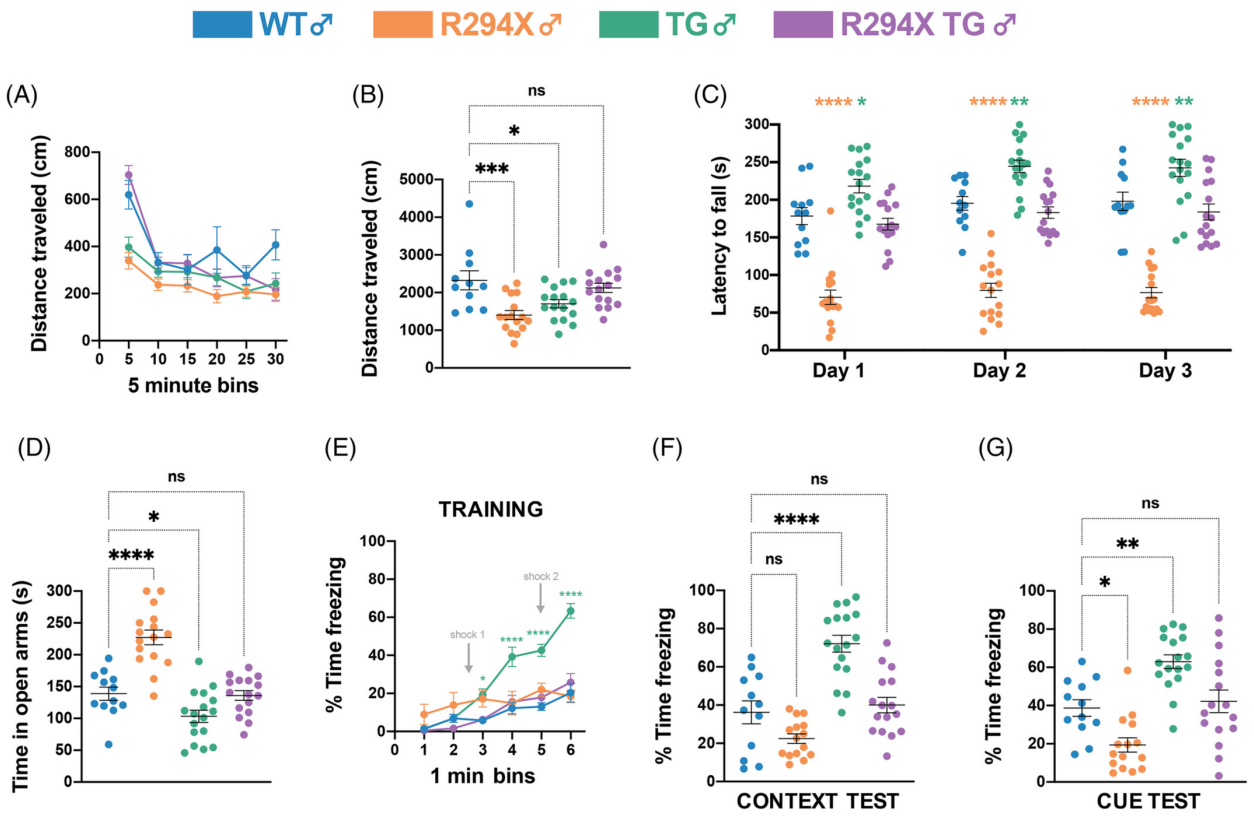

Figure 8. Bidirectionally dosage-sensitive behavioral phenotypes are normalized with *MECP2* transgene in male R294X mice

(A,B) Both male R294X and TG mice have decreased locomotor activity in the open field assay compared with WT littermates. Locomotor activity of male R294X TG mice is not different from WT littermates. (A) depicts distance traveled in centimeters across 5-min bins. (B) quantifies total distance traveled across the 30-min assay. (Age: 20 weeks. WT n = 11; R294X n = 16; TG n = 16; R294X TG n = 16) (C) Male R294X mice have reduced motor coordination in the rotarod assay, while male TG mice have enhanced motor coordination, compared with WT littermates. Motor coordination in male R294X TG mice is not different from that of WT littermates, indicating normalization of phenotypes. (Age: 20 weeks. WT n = 12; R294X n = 16; TG n = 17; R294X TG n = 16) (D) Male R294X mice have decreased anxiety-like behavior in the elevated zero maze assay, while male TG mice display increased anxiety-like behavior, compared with WT littermates. Addition of *MECP2* transgene normalizes anxiety-like behavior in male R294X TG mice. (Age: 20 weeks. WT n = 12; R294X n = 16; TG n = 17; R294X TG n = 16) (E–G) During the training session of the fear conditioning assay (E), male TG mice display increased freezing after the first shock compared with WT mice, which is rescued in R294X TG mice. In the context (F) and cue (G) tests of the fear conditioning assay, male TG mice display increased freezing compared with WT littermates. Male R294X mice display decreased freezing relative to WT littermates in the cue test. Freezing levels of male R294X TG mice are not different from that of WT littermates. (Age: 22 weeks. WT n = 12; R294X n = 15; TG n = 17; R294X TG n = 16)

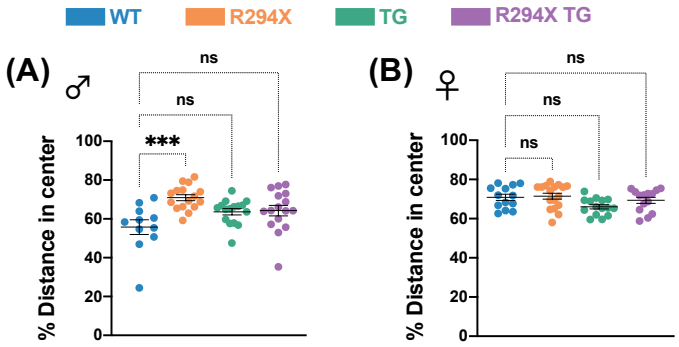

Figure 9. Male R294X exhibit a decreased anxiety-like behavior phenotype in the open field assay

(A) Male R294X mice have a higher percentage of distance travelled in the center of the open field arena, indicating decreased anxiety-like behavior. Addition of *MECP2* transgene rescues anxiety-like behavior in male R294X TG mice. (Age: 20 weeks. WT n=11; R294X n=16; TG n=16; R294X TG n=16) (B) Female R294X, TG, and R294X TG mice have a percentage of distance travelled in the center of the open field arena that is not different from WT littermates. (Age: 30 weeks. WT n=13; R294X n=17; TG n=15; R294X TG n=14)

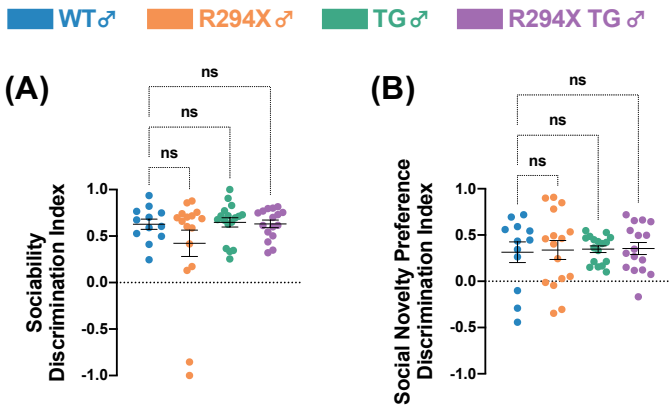

Figure 10. Neither R294X nor TG male mice exhibit deficits in social behavior

(A) Sociability in the Crawley 3-chamber assay (Stage 2) in male R294X, TG, and R294X TG mice is not different from WT. (Age: 21 weeks. WT n=12; R294X n=16; TG n=17; R294X TG n=16) (B) Social novelty preference in the Crawley 3-chamber assay (Stage 3) in male R294X, TG, and R294X TG mice is not different from WT. (Age: 21 weeks. WT n=12; R294X n=16; TG n=17; R294X TG n=16)

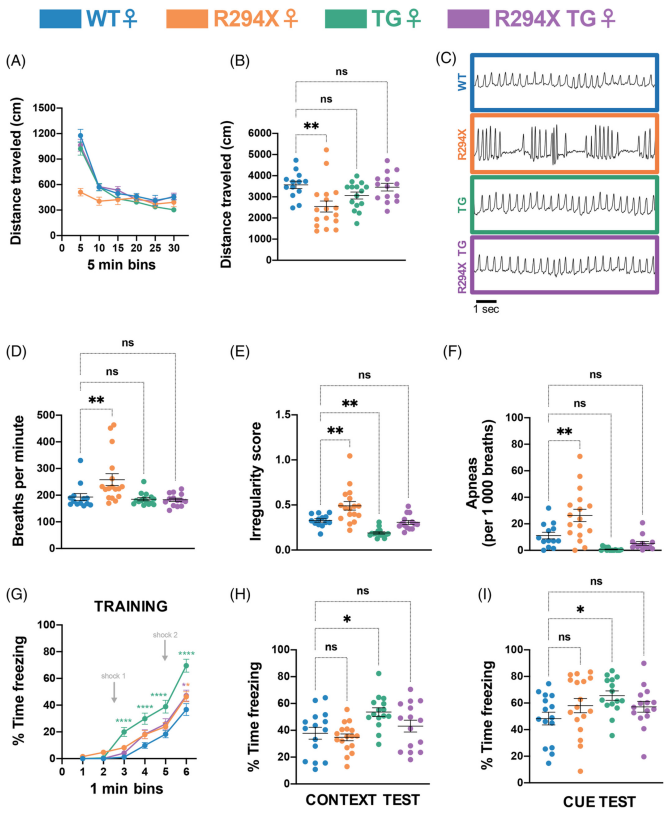

Figure 11. RTT- and MDS-like behavioral phenotypes are rescued in female R294X TG mice

(A,B) Female R294X mice have decreased locomotor activity in the open field assay compared with WT littermates, which is rescued by addition of *MECP2* transgene. (A) depicts distance traveled in centimeters across 5-min bins. (B) quantifies total distance traveled across the 30-min assay. (Age: 30 weeks. WT n = 13; R294X n = 17; TG n = 15; R294X TG n = 14) (C) *Mecp2*$^{R294X/+}$ mice have an altered breathing pattern compared with WT littermates at 30 weeks of age, which is rescued by addition of *MECP2* transgene in female R294X TG mice. (D) Basal breathing rate is elevated in female R294X mice compared with WT littermates, which is rescued by addition of *MECP2* transgene. (Age: 30 weeks. WT n = 13; R294X n = 17; TG n = 15; R294X TG n = 14) (E) Breathing irregularity score, which reflects the instantaneous rate of change in total breath time, is elevated in female R294X mice and reduced in female TG mice compared with WT littermates. These phenotypes are rescued by addition of *MECP2* transgene. (Age: 30 weeks. WT n = 13; R294X n = 17; TG n = 15; R294X TG n = 14) (F) Female R294X mice have increased apneic events compared with WT littermates, which is rescued by addition of *MECP2* transgene. (Age: 30 weeks. WT n = 13; R294X n = 17; TG n = 15; R294X TG n = 14) (G–I) During the training session of the fear conditioning assay (G), female TG mice display increased freezing after the first shock compared with WT littermates, which is rescued in female R294X TG mice. In the context (H) and cue (I) tests of the fear conditioning assay, female TG mice display increased freezing compared with WT mice. Freezing levels of female R294X TG mice are not different from that of WT mice. (Age: 31 weeks. WT n = 15; R294X n = 17; TG n = 15; R294X TG n = 15)

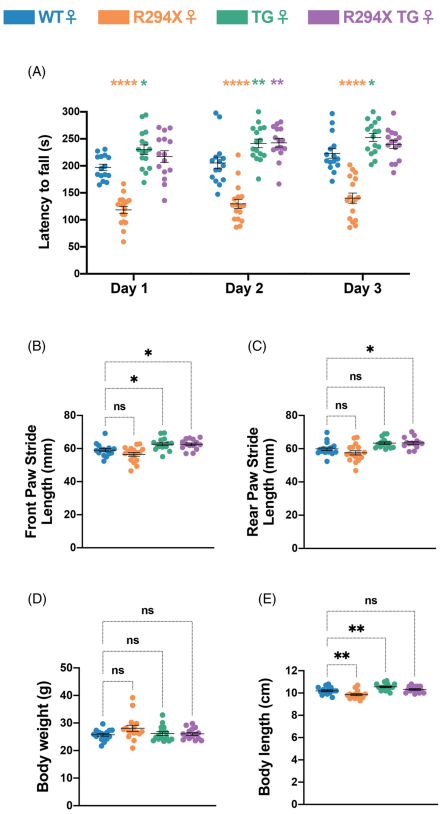

Figure 12. Transgenic *MECP2* supplementation leads to an MDS-like motor coordination phenotype in female R294X mice

(A) Female R294X mice have reduced motor coordination in the rotarod assay, while female TG mice have enhanced motor coordination, compared with WT littermates. Motor coordination of female R294X TG mice is elevated compared with WT. (Age: 31 weeks. WT n = 15; R294X n = 17; TG n = 16; R294X TG n = 15) (B,C) In the forced gait assay, front paw stride length in millimeters (B) is increased in both female TG and R294X TG mice compared with WT littermates. Rear paw stride length (C) is increased in female R294X TG mice compared with WT littermates. (Age: 34–40 weeks. WT n = 15; R294X n = 17; TG n = 16; R294X TG n = 14) (D) There are no differences in body weights of female R294X,TG or R294X TG mice compared with WT littermates. (Age: 34–40 weeks. WT n = 15; R294X n = 16; TG n = 16; R294X TG n = 15) (E) The body length of female R294X mice is decreased relative to WT littermates, while body length of female TG mice is relatively increased. Body length of female R294X TG mice is not different from that of WT. (Age: 34–40 weeks. WT n = 15; R294X n = 16; TG n = 16; R294X TG n = 15)

CHAPTER 3

Modeling the C-terminal X487R *MECP2* mutation in conditionally immortalized human neural progenitors

Introduction

Rett syndrome (RTT) is an X-linked neurodevelopmental disorder and a leading genetic cause of disability in girls worldwide[227]. Girls with RTT develop typically for 6-18 months, at which time the disease causes loss of purposeful hand movements, loss of speech, and autistic features[2,3]. RTT is predominantly caused by mutations in the gene encoding transcriptional modulator methyl-CpG-binding protein 2 (*MECP2*)[12]. However, despite this knowledge, no disease-modifying therapies are available, and treatment is limited to symptomatic management. Given the prevalence and severity of RTT, finding viable therapeutic approaches to restore MeCP2 function is critical. Fundamental to this goal is understanding the pathophysiological mechanism of *MECP2* mutations. Thus far, disease modeling in cellular and mouse models has shown that *MECP2* mutations within the two functional domains of MeCP2 – the MBD and NID – act through partial loss-of-function to cause RTT[110,129,132–134]. The T158M *MECP2* mutation in the MBD, for instance, impairs the ability of MeCP2 to bind DNA and carry out its function as a transcriptional modulator[132,207]. Other mutations, such as R255X, likely act through complete loss-of-function, as model mice lack expression of detectable MeCP2[134]. While these most common point mutations have been functionally well-characterized, a group of C-terminal *MECP2* mutations at the 3' end of the gene has not. This heterogeneous group of mutations accounts for approximately 10% of cases of typical RTT, and yet studies investigating their pathophysiological mechanism are few[16,228].

The MeCP2 C-terminus is a highly unstructured region, and so it is unfortunately poorly understood from both structural and functional perspectives. Additionally, CTD mutations are relatively heterogeneous – while some mutations span the CTD at low frequency, approximately 60% of mutations occur within a deletion "hotspot" region near amino acid 386[228]. Previous studies of the CTD have reported mixed functional results. Structural work has implicated the CTD in facilitating chromatin binding independent of the MBD and in directing proper chromatin architecture[82,112]. In contrast, work from the Bird lab has suggested that the CTD has no functional significance[111]. In analyzing two common C-terminal frameshift deletion mutations, c.1157-1197Δ41 (CTD1) and c.1164-1207Δ44 (CTD2), authors found that CTD1 and a humanized version of CTD2 led to low protein levels in mouse ESC-derived neurons, proposing that protein instability leads to LOF.

Along with results from cellular and mouse models of *MECP2* mutations, clinical data sheds population-level light on the mechanism of C-terminal *MECP2* mutation. Importantly, type of *MECP2* mutation is significantly associated with clinical

severity of RTT[16,17]. For example, large *MECP2* deletions causing complete LOF tend to confer disease of higher clinical severity, while partial LOF mutation R294X confers disease of lower clinical severity. As a group, C-terminal truncations are also associated with milder disease within this classification of mutations. In the face of mixed disease modeling data, this clinical data suggests some contribution of partial LOF mutations within the group of C-terminal truncations. Interestingly, these mutations are not predicted to disrupt any known functional domain of MeCP2 (MBD or NID). Therefore, whether the C-terminus contributes to protein function, and if so, how, remain open questions.

This Chapter outlines the development of an in vitro system to model *MECP2* mutations using the Lund human mesencephalic (LUHMES) cell line and demonstrates this system's ability to functionally characterize the C-terminal *MECP2* stop-loss mutation X487R in Rett syndrome. Compared to other cellular models, this LUHMES-based system is highly tractable, relatively inexpensive, and permits rapid and homogenous cellular differentiation. LUHMES cells can be genetically engineered with CRISPR/Cas9 technology to model disease-causing mutations and then differentiated to neuron-like cells with molecular features of a dopaminergic state. As proof of its utility, we modelled the C-terminal *MECP2* stop-loss mutation X487R in LUHMES cells and found low protein level as a possible contributor to disease mechanism. Furthermore, in addition to providing a facile platform for characterization of *MECP2* mutations, this system has the potential to be adapted for other purposes of interest, such as high-throughput drug screening, making it highly useful for future research.

Materials and methods

Cloning of overexpression plasmids

The mouse *Mecp2* E1 and E2 transcript isoforms were amplified from mouse hemibrain cDNA using transcript-specific primers and cloned into the Gateway entry vector pDONR221 (Invitrogen Cat. #12536017). R294X, R306C, Q406X, X487R, and X487S *Mecp2* mutations (**Table 5**) were introduced to the pDONR221-*mMecp2-E1* and pDONR221-*mMecp2-E2* constructs using site-directed mutagenesis (**Table 6**). WT and mutant *mMecp2-E1/2* constructs were transferred to the Gateway destination vector pEZY3 (Addgene #18672) for overexpression experiments.

The human *MECP2* E1 transcript isoform was amplified from Human Brain Whole QUICK-Clone cDNA (Takara Cat. #637242) using transcript-specific primers and cloned into Gateway entry vector pDONR221. T158M, R294X, P362HfsX5, L386HfsX5, P389X, T400HfsX5, Q437AfsX49, and X487R *MECP2* mutations (**Table 5**) were introduced to the pDONR221-*hMECP2-E1* construct using site-directed mutagenesis (**Table 6**). WT and mutant *hMECP2-E1* constructs were transferred to the Gateway destination vector pEZY3 for overexpression experiments.

N2a cell culture and transfection

Neuro-2a (N2a) cells were obtained from ATCC (CCL-131) and cultured in DMEM (Gibco Cat. #11965-065), 10% FBS (GeminiBio Cat. #900-108), MEM non-essential amino acids (Gibco Cat. #11140050), and 100 U/ml penicillin with 100 μg/ml streptomycin (Gibco Cat. #15140122). N2a cells were maintained in a 37°C incubator with 5% CO_2 and sub-cultured every two days.

N2a cells were transfected using GenJet In Vitro Transfection Reagent for Neuro-2A cells (GenJet Cat. #SL100489-N2A) according to manufacturer's instructions. Briefly, cells were plated at a density of 200,000 cell per well of a 6-well plate. The next day, media was removed and replaced with 1.2 ml of fresh media 1 hour prior to transfection. Cells were transfected with 1 μg DNA per plasmid, up to a maximum of 2 μg per well, and media was changed 5 hours after transfection. Transfection efficiency was assessed 48 hours after transfection with an EVOS FL inverted microscope (Invitrogen).

LUHMES cell culture and nucleofection

LUHMES cells were obtained from ATCC (CRL-2927) and cultured in accordance with previous reports[229,230]. Culture dishes were pre-coated with 50 μg/ml poly-L-ornithine (PLO, Sigma Cat. #P3655) and 1 μg/ml human fibronectin (Sigma Cat. #F0895) in sterile water for 3 hours or overnight at 37°C. Culture dishes were washed once in sterile water and air dried prior to use. LUHMES cells were grown in proliferation media consisting of Advanced DMEM/Ham's F-12 media (Gibco Cat. #12634028) supplemented with 1% N2 (Gibco Cat. #17502048), 2mM L-glutamine (Gibco Cat. #25030081), and 40 ng/ml human heat stable basic fibroblast growth factor (bFGF, Gibco Cat. #PHG0367). LUHMES cells were maintained in a 37°C incubator with 5% CO_2 and sub-cultured every two days.

LUHMES cells were transfected via nucleofection with a Nucleofector 2b device (Lonza) and Amaxa Basic Nucleofector Kit (Lonza Cat. #VPI-1003) in accordance with previous work[229]. Briefly, confluent LUHMES cells were washed in PBS, dissociated in 0.05% trypsin (Gibco Cat. #25300054) and centrifuged for 5 minutes at 200xg. Cells were resuspended in PBS and counted using a hemacytometer. Aliquots of 2 million cells were transferred into 15 ml conical tubes and re-centrifuged. Cell pellets were resuspended in 100 μl of Nucleofection solution containing plasmid/single-stranded oligodeoxynucleotide (ssODN) and transferred to a nucleofection cuvette. Cells were immediately nucleofected using the D-033 program and resuspended in 500 μl of RPMI 1640 media (Gibco Cat. #11875093) using the pipette provided in the VPI-1003 kit. Cells were transferred to a 15 ml conical tube and incubated at 37°C for 5 minutes to recover. The cell solution

was then added to 2 ml pre-warmed media in wells of a 6-well plate. Media was changed 4 hours after nucleofection. Nucleofection efficiency was assessed 48 hours after transfection with an EVOS FL inverted microscope (Invitrogen).

LUHMES cell differentiation

To differentiate LUHMES cells, 200,000 cells were plated in a 35-mm plate in proliferation media. The next day, proliferation media was aspirated and replaced with differentiation media, consisting of Advanced DMEM/Ham's F-12 media supplemented with 1% N2, 2mM L-glutamine, 1 μg/ml tetracycline (GoldBio Cat. #64-75-5), 1mM dibutyryl cyclic adenosine monophosphate (dbcAMP, Sigma Cat. #D0260), and 2 ng/ml recombinant human glial cell-derived neurotrophic factor (GDNF, PeproTech Cat. #450-10). The next day, differentiating cells were dissociated and replated into coated 10 cm dishes (5 million cells per plate, for collection of protein lysates), into 6-well plates (500,000 cells per well, for collection of genomic DNA), onto coverslips in 12-well plates (250,000 cells per well, for immunocytochemistry), or into 24-well plates (100,000 cells per well, for collection of RNA). Half of the media volume was changed every 3 days during differentiation.

CRISPR/Cas9 engineering

CRISPR single guide RNAs (sgRNAs) were designed using the CRISPOR web tool (http://crispor.tefor.net) for *S. pyogenes* Cas9. sgRNAs were cloned into pX330S-2 (Addgene #58778, mouse sgRNAs) or pX458 (Addgene #48138, human sgRNAs) using Golden Gate assembly as described by the Zhang lab (**Table 7**)[231]. The pDONR221-*mMecp2-E2-R294X* plasmid was used as a homology directed repair (HDR) template to introduce the R294X mutation; the X487R HDR template was designed as a 95 basepair ssODN and ordered from Integrated DNA Technologies as an Ultramer DNA Oligo. (**Table 8**). The X487R ssODN was designed with a synonymous protospacer adjacent motif- (PAM) inactivating point mutation.

Limiting dilution of N2a cells

To isolate individual N2a clones, limiting dilution of N2a cells was performed 2 days after transfection. Cells were washed in PBS, dissociated in 0.05% trypsin, and centrifuged for 4.5 minutes at 200xg. Cells were resuspended in media at a concentration of 100,000 cells/ml and serially diluted to a working concentration of 2.5 cells/ml (0.5 cells/200μl). 200μl of cell at this working concentration was added to each well of a 96-well plate (Corning Cat. #353072). 7 days after limiting dilution, wells were manually scored as having 0, 1, or >1 clone per well. Only wells containing a single clone were propagated further for screening.

FACS sorting of LUHMES cells

To isolate individual LUHMES clones, fluorescence-activated cell sorting (FACS) of LUHMES cells was performed 3 days after nucleofection as previously described[229]. 96-well plates were pre-coated with 50 μg/ml PLO and 1 μg/ml human fibronectin overnight at 37°C, washed once in sterile water, and air dried prior to use. Wells were filled with 100 μl of Advanced DMEM/Ham's F-12 media supplemented with 1x B27 (Sigma Cat. #17504044) and 100 U/ml penicillin with 100 μg/ml streptomycin (Gibco Cat. #15140122). Nucleofected LUHMES cells were washed in PBS, dissociated with 0.05% trypsin, and centrifuged for 5 minutes at 200xg. Cells were resuspended in 1 ml of Advanced DMEM/Ham's F-12 media supplemented with 10 μM HEPES. Cell solutions were passed through a 35 μm cap cell strainer into 5 ml round-bottom flow cytometry tubes (Corning Cat. #352235). 25 ng/ml propidium iodide (PI, Sigma Cat. #P4864) was added to cells as a cell viability marker. GFP+ PI- cells were sorted into individual wells on a FACSAria III machine at room temperature using a 100 μm nozzle. Six days after sorting, 100 μl of Advanced DMEM/Ham's F-12 media supplemented with 1x B27 and penicillin/streptomycin was added to each well of the 96-well plates.

Screening N2a cell clones

When N2a cell clones reached confluency in the 96-well format (approximately 2 weeks), clones were transferred to individual wells of a 24-well plate. After clones reached confluency in the 24-well format, cells were split into two new wells of 24-well plates – half for genomic DNA isolation and half for maintenance. Cells for genomic DNA isolation were washed in PBS and harvested in 135 μl lysis buffer (50mM sodium hydroxide). Lysates were incubated for 2 hours at 65°C with 175 rpm shaking. After shaking, 15 μl Tris-HCl pH 8.0 was added and lysates were stored at room temperature. 1 μl of lysate was used as the input for genomic DNA analysis by PCR using EconoTaq DNA Polymerase (Lucigen Cat. #30033). In experiments to generate a *Mecp2* knockout N2a line, clones were screened for large deletions in exon 3 using primers spanning the region targeted by the CRISPR sgRNA. In experiments to generate a *Mecp2* R294X N2a line, clones were screened for presence of the mutant allele using R294X allele-specific primers[110]. Select clones (i.e. containing a large deletion in exon 3 or demonstrating presence of R294X allele by PCR) were amplified with KAPA HiFi DNA polymerase (Roche Cat. #07958927001) and products were submitted for Sanger sequencing to confirm presence of mutation (Genhunter, TN). All primer pairs used for screening are listed in **Table 9**. Engineered cell lines are listed in **Table 10**. To ensure that no undesired *Mecp2* mutations were present in engineered cell lines, the genomic sequence of *Mecp2* (including exons and splice sites) was amplified piecewise and products were submitted for Sanger sequencing (**Table 11**).

Screening LUHMES cell clones

When LUHMES cell clones reached confluency in the 96-well format (approximately 10 days), clones were transferred to individual wells of a 24-well plate. After clones reached confluency in the 24-well format, half of the cells were frozen for liquid nitrogen storage and half of the cells were transferred to a new well of a 24-well plate for genomic DNA isolation as previously described[229]. Cells for genomic DNA isolation were washed in PBS and harvested in 400 μl lysis buffer (50mM Tris-HCl pH 8.0, 20mM EDTA pH 8.0, 40mM NaCl, 1% SDS, and 0.05 mg/ml proteinase K). Lysates were incubated for 2 hours at 65°C with 175 rpm shaking. 300 μl 5M NaCl was added to each sample, mixed by inversion, and centrifuged for 10 minutes at 13,000xg at room temperature. The supernatant was added to 500 μl isopropanol, mixed by inversion, and centrifuged for 10 minutes at 13,000xg at 4°C. The DNA pellet was washed in 75% ethanol, re-centrifuged, air dried, and resuspended in 50μl TE buffer. Genomic DNA was analyzed by PCR using KAPA HiFi DNA polymerase (Roche Cat. #07958927001). In experiments to generate a *MECP2* knockout LUHMES line, clones were screened for deletions in exon 3 using primers spanning the region targeted by the CRISPR sgRNA. PCR products were submitted for Sanger sequencing to detect presence of homozygous indels. In experiments to generate a *MECP2* X487R LUHMES line, clones were screened for presence of the mutant allele using X487R allele-specific primers[110].

Clones demonstrating presence of X487R allele by PCR of genomic DNA were further subjected to analysis of transcript sequence to determine which X-chromosome (active or inactive) the mutation resided upon. Briefly, LUHMES confluent in wells of a 24-well plate were collected in 250 μl TRIzol reagent (Invitrogen Cat. #15596026). RNA was isolated using the Direct-zol RNA Miniprep Plus Purification Kit (Zymo Cat. #R2071) and eluted in 50 μl of water. cDNA was generated using the SuperScript IV kit (Invitrogen Cat. #18091050) with 200 ng RNA and oligo(dT) priming in a 20 μl reaction. cDNA reactions were diluted 1:5 with water and 5 μl was used as the input for PCR with primers flanking the CRISPR sgRNA binding site. PCR products were submitted for Sanger sequencing to detect presence of mutation. All primer pairs used for screening are listed in **Table 9**. Engineered cell lines are listed in **Table 10**. To ensure that no undesired *MECP2* mutations were present in engineered cell lines, the genomic sequence of *MECP2* (including exons and splice sites) was amplified piecewise and products were submitted for Sanger sequencing (**Table 11**). To determine the *MECP2* sequence of the inactive X-chromosome, the genomic sequence surrounding the *MECP2* stop codon was amplified, transferred into the pCR2.1 TOPO vector using the TOPO TA Cloning kit (Invitrogen Cat. #K4575J10), and submitted for Sanger sequencing.

Quantitative reverse transcription PCR (RT-qPCR)

Upon confluency in wells of a 24-well plate, cells were collected in 250 µl TRIzol reagent (Invitrogen Cat. #15596026). RNA was isolated using the Direct-zol RNA Miniprep Plus Purification Kit (Zymo Cat. #R2071) and eluted in 50 µl of water. cDNA was generated using the SuperScript IV kit (Invitrogen Cat. #18091050) with 200 ng RNA and oligo(dT) priming in a 20 µl reaction. cDNA reactions were diluted 1:5 with water and 2 µl was used as the input for qPCR with primers for *MECP2* and *GAPDH* (**Table 12**). Reactions were run on an Advanced Biosystems 7500 machine using PowerUp SYBR Green Master Mix (Applied Biosystems Cat. #A25742). Relative transcript levels were quantified using the ddC_t method.

Western Blotting

When cells reached confluency in a 10 cm plate, cells were washed in PBS and incubated on ice for 10 minutes in 1 ml buffer containing 10mM HEPES, 1.5mM $MgCl_2$, 10mM KCl, 0.05% NP-40, 0.5mM DTT, and 1x Mammalian Protease Inhibitor Cocktail (Sigma Cat. #P8340), pH 7.9. The cytosolic fraction was removed following centrifugation and nuclear pellets were resuspended in buffer containing 5mM HEPES, 1.5mM $MgCl_2$, 0.2mM EDTA, 25% glycerol, 0.5mM DTT, and 1x Mammalian Protease Inhibitor Cocktail, pH 7.9. Suspended nuclei were treated with benzonase for 1 hour on ice (Sigma Cat. #E1014). Following nuclease treatment, NaCl concentration was increased to 600mM, and nuclei were incubated on ice for 1 hour. Cellular debris was removed by high-speed centrifugation and nuclear protein concentration was determined with the 660nm Protein Assay Reagent (Pierce Cat. #22660). 5 μg of nuclear protein was loaded into individual wells of 10% house-made acrylamide SDS-PAGE gels and subjected to standard Western blotting procedures. An Odyssey CLx (LI-COR) imaging system was used for blot detection and quantification was performed in Image Studio Lite (LI-COR). Full-length MeCP2 was detected with an antibody specific to the amino terminus of MeCP2 (Sigma M7443) and an antibody specific to the carboxy terminus of MeCP2 (Cell Signaling 3456, D4F3), while TBP was detected as a loading control (Westerns using M7443: abcam ab51841) (Westerns using D4F3: Cell Signaling 8515S) (**Table 13**). Secondary antibodies used for detection were goat anti-rabbit 800CW (LI-COR 926-32211) and goat anti-mouse 680RD (LI-COR 926-68070).

Immunocytochemistry (N2a)

N2a cells that reached confluency in a 24-well format were fixed in 4% paraformaldehyde (PFA) for 10 minutes at room temperature. Fixation was quenched with 4 5-minute washes in 0.3M glycine. Heat-induced epitope retrieval (HIER) was essential for achieving robust detection of overexpressed MeCP2. HIER was performed by incubating cells in 0mM trisodium citrate, 0.05% Tween-20 pH 6.0 and heating to 80°C for 30 minutes. Cells were permeabilized in 0.2% Triton X-100 for 10 minutes at room temperature and then blocked in 4% bovine serum albumin (BSA) for 1 hour at room temperature. Cells were incubated in primary antibody overnight at 4°C in a humidified chamber; coverslips were washed

in 0.1% Tween-20 and secondary antibody added for 4 hours at room temperature (**Table 13**). Cells were washed in 0.1% Tween-20 and nuclei stained in 0.1 μg/ml DAPI. Coverslips were mounted onto slides using ProLong Gold Antifade reagent (Invitrogen Cat. #P36930). 40x images of cells were obtained on a Nikon TIRF microscope available through the Cell Imaging Shared Resource at Vanderbilt. Exposure settings were defined using a WT sample and held constant for imaging of mutant samples. Image processing was performed in ImageJ.

Immunocytochemistry (LUHMES)

LUHMES cells that reached confluency in a 24-well format were fixed in 4% PFA for 15 minutes at room temperature. Fixation was quenched with 4 5-minute washes in 0.3M glycine. Cells were permeabilized in 0.2% Triton X-100 for 10 minutes at room temperature and then blocked in 1% BSA for 1 hour at room temperature. Cells were incubated in primary antibody overnight at 4°C in a humidified chamber; coverslips were washed in 0.1% Tween-20 and secondary antibody added for 4 hours at room temperature (**Table 13**). Cells were washed in 0.1% Tween-20 and nuclei stained in 0.1 μg/ml DAPI. Coverslips were mounted onto slides using ProLong Gold Antifade reagent. 40x images of cells were obtained on a Nikon TIRF microscope available through the Cell Imaging Shared Resource at Vanderbilt. Exposure settings were defined using a WT sample and held constant for imaging of mutant samples. Image processing was performed in ImageJ.

Statistical Analysis

Statistical analysis was performed within Prism 9 (GraphPad). RT-qPCR and Western blot experiments were analyzed with either unpaired student's t-test or one-way ANOVA with Dunnett's post-hoc test. All plots display mean ± standard error of the mean. Statistical significance is represented in all plots as follows: *p<0.05, **p<0.01, ***p<0.001, ****p<0.0001.

Results

Generation and validation of a knockout *Mecp2* N2a cell line

N2a cells are a mouse neuroblastoma cell line that has been used to study neurite growth and neuronal differentiation[232,233]. At baseline, N2a cells have an amoeboid morphology and, upon differentiation, develop neurite outgrowths. Differentiation methods vary and include serum deprivation and/or treatment with cAMP, retinoids, bone morphogenetic proteins (BMPs), BDNF, and GDNF[234]. Differentiation occurs on the timescale of several days and results in differentiation method-dependent changes in signaling and gene transcription. Serum deprivation, for example, has been shown to activate epidermal growth factor receptor- (EGFR) mediated signaling and upregulate immediate-early gene transcription[235].

We set out to develop an N2a-based in vitro system to model disease-causing C-terminal *MECP2* mutations. We envisioned using two parallel approaches to functional characterization of these mutations: 1) overexpression of C-terminal mutant MeCP2 in N2a cells, and 2) expression of endogenous C-terminal mutant MeCP2. For the first approach, we generated a *Mecp2* knockout N2a cell line, lacking endogenous MeCP2, to eliminate co-presence of endogenous WT and overexpressed C-terminal mutant MeCP2. CRISPR/Cas9-mediated mutagenesis targeting the shared exon of both *Mecp2* transcript isoforms (exon 3) elicited indel mutations that cause frameshift and knockout of endogenous MeCP2 (**Figure 13A**). After screening 31 N2a clones via PCR and Sanger sequencing, we identified a single knockout clone with a large 213 basepair exon 3 deletion on all X-chromosomes (c.119_332del214/p.E40GfsX14, **Table 10**, **Figure 13B**). We confirmed that this deletion leads to decreased *Mecp2* transcript and loss of protein with RT-qPCR and Western blotting, respectively. Relative quantification of *Mecp2* E1 and E2 transcript isoforms showed that KO N2a cells express approximately 50% of each isoform relative to bulk WT N2a cells (**Figure 13C-D**). Additionally, Western blotting of bulk WT and clonal KO N2a protein lysates demonstrated that KO cells express neither full-length MeCP2 nor truncated MeCP2 protein product (**Figure 13E**).

<u>Q406X and X487R C-terminal mutations produce protein products that localize to heterochromatic foci in the N2a *Mecp2* KO overexpression system</u>

We used this KO N2a cell line to conduct preliminary functional analysis of overexpressed C-terminal mutant MeCP2. We chose to study four C-terminal mutations: R294X – a common truncation mutation that interrupts the NID and eliminates the C-terminus, R306C – a common missense mutation that interrupts the NID and leaves the C-terminus intact, Q406X – a rare late truncation mutation that eliminates part of the C-terminus, and X487R – a rare stop-loss mutation that leaves the MeCP2 protein sequence intact and is predicted to cause addition of a 27-amino acid tail sequence (**Table 5, Figure 14A**). These mutations were introduced to the cDNA sequence of the mouse *Mecp2* E1 transcript isoform via site-directed mutagenesis and constructs were transferred to an expression vector for overexpression experiments.

Protein level of overexpressed C-terminal mutant MeCP2 was determined by Western blotting with an antibody to the N-terminus of MeCP2 and, as a control for transfection efficiency, neomycin phosphotransferase II (NPTII, an enzyme expressed on the overexpression plasmids). We found that the WT overexpression construct produced full-length protein at 75 kDa (**Figure 14B**). Further, truncating mutations R294X and Q406X produced truncation products of lower molecular weight according to their predicted sizes. The R306C mutation, in contrast, produced full-length MeCP2 as expected for a missense mutation. Finally, the stop-loss X487R mutation produced a protein product at a molecular weight similar to that of WT, but at much lower levels.

Given that the C-terminal mutations Q406X and X487R both yielded detectable overexpressed protein products, we then conducted immunocytochemistry to determine whether these protein products localize properly to heterochromatic foci. *Mecp2* KO N2a cells were transfected with C-terminal mutant *Mecp2* overexpression constructs and stained with an antibody to the N-terminus of MeCP2. Using DAPI to visualize nuclei and heterochromatic foci within, we found that each of the four C-terminal mutants appropriately localized to these foci, similar to overexpressed WT MeCP2 (**Figure 14C**).

Generation of two independent *Mecp2* R294X N2a cell lines expressing truncated MeCP2 protein

We aimed to complement these early functional results with a parallel second approach involving analysis of endogenous C-terminal mutant MeCP2. To do so, we used CRISPR/Cas9-mediated mutagenesis of WT N2a cells with an sgRNA targeting the codon for arginine 294 of *Mecp2* and a plasmid-based homology repair template (**Figure 15A**). After screening clones via allele-specific PCR and Sanger sequencing, we identified two independent N2a cell lines with the R294X mutation on all X-chromosomes, 1F6 and 2H2 (c.880C>T;882G>A, **Table 10**, **Figure 15B**). We validated these two R294X lines via RT-qPCR and Western blotting for MeCP2. Using relative quantification of E1 and E2 *Mecp2* transcripts, we found that the 1F6 line expresses E1 *Mecp2* at levels approximately 0.8x that of WT and E2 *Mecp2* at levels similar to WT (**Figure 15C-D**). In contrast, the 2H2 line expresses both E1 and E2 *Mecp2* at approximately 1.5x that of WT. Furthermore, Western blotting of bulk WT and clonal 2H2 R294X N2a protein lysates showed that R294X cells do not express full-length MeCP2 but instead produce a truncated protein product (**Figure 15E**).

Next, we sought to determine whether the R294X truncation product localized to heterochromatic foci, as did the overexpressed truncation product. However, extensive troubleshooting of immunocytochemistry protocols did not elicit detectable endogenous MeCP2 protein, potentially due to low levels of endogenous *Mecp2* expression in N2a cells. With the difficulty in imaging endogenous MeCP2 and the limits it places on cellular phenotyping for these and future experiments, we decided that an N2a-based in vitro system would not be suitable for long-term disease modeling purposes. We conducted an extensive literature search and identified LUHMES cells as an ideal alternative candidate for this purpose.

Generation and characterization of a *MECP2* X487R LUHMES cell line

LUHMES cells are a subclone of MESC2.10, which are a human mesencephalic-derived line originally immortalized with a retroviral vector expressing v-myc in a Tet-Off fashion[236,237]. LUHMES can be differentiated into morphologically and biochemically mature dopamine-like neurons following exposure to tetracycline, GDNF, and dbcAMP[230]. Karyotyping and RNA FISH experiments have shown that LUHMES are female cells and that one of the two X-chromosomes is constitutively inactive[238]. LUHMES cells present several advantages compared to other cellular models. First, the line is highly tractable –

LUHMES are fast-growing and differentiate on a timescale of days. Second, growing LUHMES is relatively inexpensive and less labor-intensive compared to other cellular models. Third, the LUHMES differentiation process is highly efficient. With addition of tetracycline, nearly all cells differentiate and do so in a homogenous manner.

We set out to develop a LUHMES-based in vitro system to model disease-causing C-terminal *MECP2* mutations. This time, however, we focused on studying endogenous C-terminal mutant MeCP2. To do so, we used CRISPR/Cas9-mediated mutagenesis of WT LUHMES cells using a protocol adapted from Shah et al. 2016[229]. Specifically, LUHMES cells were nucleofected with a plasmid encoding Cas9 and the sgRNA along with the HDR template, and then cells underwent FACS to isolate individual transfected cells into wells of a 96-well plate (**Figure 16**). Clones were screened with allele-specific PCR and confirmed with Sanger sequencing of cDNA. We used this protocol to conduct CRISPR/Cas9-mediated mutagenesis of WT LUHMES cells with an sgRNA targeting the stop codon of *MECP2* and an ssODN-based homology repair template with the X487R mutation (**Figure 17A**). After screening 57 clones via allele-specific PCR of genomic DNA, we identified two clones with the X487R mutation on at least one of the X-chromosomes. To determine which X-chromosomes harbored the X487R mutation in these clones, we conducted Sanger sequencing of amplified cDNA and sequencing of TOPO-cloned PCR products surrounding the *MECP2* stop codon. We found that the first clone harbored the X487R mutation on the active X-chromosome and a 70bp insertion on the inactive X-chromosome (c.1459T>C (active) ; c.1145ins70 (inactive)) (**Table 10**, **Figure 17B-C**). The second clone, in contrast, had the X487R mutation on the inactive X-chromosome.

We chose to further characterize the X487R-expressing LUHMES line to determine the effect of this stop-loss mutation on *MECP2* transcript and protein level. First, RT-qPCR for total *MECP2* transcript showed that X487R transcript levels are not different from that of WT (**Figure 17D**). However, Western blotting using antibodies to N- and C-terminal MeCP2 failed to detect protein product in the X487R LUHMES line (**Figure 17E-F**). To further explore whether the stop-loss mutation X487R yielded decreased protein levels, we overexpressed WT and X487R *MECP2* E1 constructs in *Mecp2* KO N2a cells. We found that the X487R *MECP2* construct is expressed at lower levels compared to WT (**Figure 18**), at approximately 25% of overexpressed WT MeCP2.

Finally, we set out to determine if the X487R mutation and loss of full-length protein has phenotypic effects in differentiated LUHMES. Since the dopaminergic system is known to be altered in RTT, we focused on markers of dopaminergic state in differentiated cells[122,127,239,240]. We chose to first analyze levels of tyrosine hydroxylase (TH), an enzyme responsible for the conversion of tyrosine to L-3,4-dihydroxyphenylalanine (L-DOPA)[241]. TH is integral for the biosynthetic pathway of catecholamines dopamine, epinephrine, and norepinephrine and undergoes upregulation in LUHMES after approximately

5 days of differentiation[230]. We differentiated WT and X487R LUHMES for 5 days and collected protein to quantify levels of TH (**Figure 19A**). Preliminary Western blotting shows that while differentiated WT LUHMES express detectable levels of TH at this stage, X487R LUHMES do not express detectable TH (**Figure 19B**).

Discussion

In the past two decades since a genetic cause of Rett syndrome was discovered, more than 200 *MECP2* mutations have been identified in people with RTT (RettBase: http://mecp2.chw.edu.au). A predominant 8 of these mutations have been found to cause approximately 60% of all cases of typical RTT and include R106X, R133C, T158M, R168X, R255X, R270X, R294X, and R306C[16]. Some of these common mutations occur within the functional domains of MeCP2 (MBD, NID) and produce a protein product with partial loss-of-function. Others, such as R255X, do not yield a stable protein product in mice and are predicted to cause complete loss-of-function. While these mutations have been extensively studied, less is known about mutations outside of the main functional domains. Specifically, there is a heterogeneous group of mutations in the C-terminal region of *MECP2* contributing to approximately 5-10% of typical RTT cases. Mostly small deletion-frameshift mutations, CTD mutations span a region more than 500 bp and are highly variable with over 100 different *MECP2* mutations reported (RettBase: http://mecp2.chw.edu.au). Collectively, these mutations are not predicted to disrupt any known functional domain of MeCP2, yet, by an unknown mechanism, they still cause RTT in people.

In this Chapter, we propose a novel in vitro modelling system using the LUHMES cell line and present proof of its utility in investigating the mechanism of a unique C-terminal stoploss mutation, X487R. First, we discuss initial efforts towards using the immortalized N2a cell line as an in vitro modelling system. We describe the generation and characterization of KO and R294X N2a cell lines, as well as demonstrate their utility in studying *MECP2* mutations in an overexpression system. Following consideration of technical challenges specific to N2a cells, we introduce LUHMES cells and develop procedures for their genetic engineering and differentiation. We present evidence of successful introduction of the X487R stop-loss mutation into LUHMES and findings of reduced protein, but not transcript, level compared to WT LUHMES. Given this unexpected finding, we further analyzed protein expression of WT and X487R MeCP2 when overexpressed in the *Mecp2* KO N2a cell line. Consistently, we found that the X487R mutation yields reduced protein expression compared to WT. Finally, we show preliminary evidence of phenotypic differences between differentiated WT and X487R LUHMES, with altered TH expression levels.

We began to develop an in vitro system using the immortalized mouse neuroblastoma N2a cell line. N2a cells are a fast-growing cell line and have been previously used to study neurodevelopment and neurite outgrowth[232,233]. Using

CRISPR/Cas9 technology we first generated an N2a *Mecp2* KO line with a 214-basepair deletion in exon 3 across all X-chromosomes, which should cause frameshift and introduction of an early stop codon in both *Mecp2* transcript isoforms. *Mecp2* KO N2a cells produce approximately 50% of *Mecp2* transcript levels compared to WT and no detectable protein product, making these cells a useful tool to isolate the effect of exogenous overexpressed MeCP2. Indeed, we were able to overexpress exogenous WT, R294X, R306C, Q406X, and X487R MeCP2 without the presence of endogenous MeCP2. Two of these mutations, Q406X and X487R, have not been well-studied in the literature; however, we found that these mutations yield protein products localized to heterochromatic foci in this system.

While the *Mecp2* KO N2a cells could be used to analyze mutations in an overexpression system, this approach cannot capture effects of *Mecp2* mutation under the endogenous promoter and regulatory sequences or at physiological levels of mutant protein. We set out to engineer C-terminal mutations in N2a cells using CRISPR/Cas9. First, we generated two independent R294X N2a lines with the approach previously successful in generating the R294X mouse model[110]. Like male *Mecp2*$^{R294X/Y}$ mice, R294X N2a cells produce a stable truncated protein product of lower molecular weight than WT MeCP2. With this promisingly consistent result, we hoped to develop further experimental assays in endogenously engineered N2a cells. One of these assays, immunocytochemistry to visualize nuclear MeCP2, was unfortunately hampered by low endogenous levels of MeCP2 and high background staining specific to N2a cells. Because of this inability to sufficiently detect endogenous MeCP2, we decided that this cell line would not be ideal for in vitro modelling long-term.

Following this decision, we re-envisioned the in vitro system, considered alternative cell lines, and selected LUHMES cells for this purpose. LUHMES are a subclone of MESC2.10 cells, a human mesencephalon-derived line that was conditionally immortalized with a retroviral vector expressing v-myc in a Tet-OFF system[236,237]. While not as widely used as N2a cells, LUHMES have been shown to be amenable to CRISPR/Cas9 engineering of point mutations and large insertions in *MECP2*[229]. Additionally, LUHMES undergo differentiation within several days upon administration of tetracycline. This process involves morphological changes, such neurite outgrowth, as well as transcriptional changes. Stem cell and neuronal precursor markers such as SOX2 are downregulated with differentiation while neuronal markers such as MAP2, synapsin-1, synaptophysin, and PSD-95 are upregulated[230]. Additionally, supplementation of tetracycline with dbcAMP and GDNF promotes the differentiation of LUHMES towards a dopaminergic phenotype, with expression of transcripts for dopaminergic markers dopamine receptor D2 (DRD2), dopamine transporter (DAT), and TH. Finally, differentiated LUHMES flux dopamine, shown through experiments involving administration of tritiated DAT substrate 1-methyl-4-phenylpyridinium ([^{3}H]-MPP^{+})[230].

Using LUHMES as a basis for an in vitro modelling system is advantageous for several reasons. First, and importantly for RTT work, LUHMES are female cells with a normal diploid chromosome complement. RNA FISH experiments further determined that one of the X-chromosomes is constitutively inactivated in undifferentiated cells, eliminating culture heterogeneity in activity of different X-chromosomes[238]. Second, LUHMES represent a more physiological system compared to other immortalized cell lines such as N2a and SH-SY5Y, which contain many chromosomal aberrations. Additionally, nearly all LUHMES undergo differentiation upon addition of tetracycline within one week, making for a rapid, highly efficient, and homogenous differentiation process. Third, the LUHMES culture system is tractable, relatively inexpensive, and less labor intensive compared to other cellular models such as iPSC-based systems. The major disadvantage to using LUHMES is challenging transfection. Traditional calcium phosphate-based transfection, lipid-based transfection, and electroporation approaches have failed in our hands (data not shown). However, nucleofection with the Amaxa Basic Nucleofector Kit for primary neurons and Program D033 yielded sufficient transfection efficiencies for CRISPR/Cas9 engineering.

Building on previous literature, we developed a protocol to nucleofect LUHMES with CRISPR/Cas9 components, isolate clones via FACS of nucleofected cells, and screen clone with allele-specific PCR. We first designed a guide RNA and homology repair template to introduce the stop-loss X487R mutation. Stop-loss mutations are individually rare but have been identified in a several individuals with RTT. While individual nucleotide changes vary amongst individuals, each stop-loss mutation is predicted to cause no changes to the *MECP2* coding sequence but instead extend the C-terminus by 27 amino acids until the next in-frame stop codon. Since there is limited molecular work on the mechanism of stop-loss mutations in RTT, we set out to introduce the X487R mutation into LUHMES via genetic engineering.

After nucleofection, FACS, and screening of clones, we identified one clone with the X487R mutation on the active *MECP2* allele. The inactive *MECP2* allele of this clone contains a 70-basepair insertion before the typical stop codon. We confirmed that the allele containing the X487R mutation is expressed via amplification of cDNA and Sanger sequencing. Interestingly, there are no differences between WT and X487R LUHMES in *MECP2* transcript level, yet there is no detectable protein product in X487R LUHMES. This result was unexpected, given that later truncating mutations such as R294X and R306C produce stable protein products and that the X487R mutation does not disrupt the full MeCP2 protein sequence. However, this result is not unprecedented. Two other C-terminal mutations have been modelled in mice: c.1157_1197del41 and c.1164_1207del44[111]. Mice with the c.1157_1197del41 mutation display severe RTT-like phenotypes and reduced lifespan. Correspondingly, mice expressed very low levels of truncated MeCP2, and protein instability was proposed as a mechanism for this.

While we cannot deduce the mechanism of reduced protein level from the X487R data, given retained transcript levels possible causes include decreased protein translation (e.g. due to an altered 3'UTR) or increased protein degradation (e.g. due to the presence of an additional C-terminal tail). We further explored this phenomenon by overexpressing WT and X487R *MECP2* E1 in *Mecp2* KO N2a cells, finding that again X487R protein is reduced compared to WT. Given these consistent results, we predict that the X487R mutation is acting through complete loss-of-function due to reduced protein expression. However, future experiments should aim to parse out whether reduced translation or increased protein degradation contribute to these reduced protein levels.

Given that the LUHMES are amenable to genetic engineering of specific *MECP2* mutations, we set out to determine whether differentiated X487R LUHMES exhibit phenotypic differences from differentiated WT LUHMES. We conducted a preliminary first-pass experiment, differentiating WT and X487R LUHMES for 5 days and then quantifying levels of a dopaminergic marker TH. Importantly, the dopaminergic system is known to be altered in RTT; thus, markers of dopaminergic state in differentiated cells presents a relevant potential phenotype[122,127,239,240]. We found that WT LUHMES express detectable TH at this stage of differentiation, while X487R LUHMES do not. While this data supports the notion that there are detectable phenotypes in the LUHMES cells, more work must be done to fully parse out these differences. For example, we have observed that X487R LUHMES undergo high rates of cell death during the differentiation process compared to WT LUHMES. Quantification of cells surviving differentiation, as well as staining with markers for viability and apoptosis, will provide critical insight into baseline differences in differentiation between genotypes. Furthermore, assessment of TH at more timepoints (both before and after 5 days) should be conducted to determine if there are differences in time course of TH expression. Finally, assessment of other pan-neuronal and dopaminergic markers during differentiation and functional assays of dopamine flux could provide greater insight beyond activity of tyrosine hydroxylase.

Table 5. Summary of *MECP2* mutations in this study

Mutation (coding sequence)	Mutation (protein sequence)	Mutation Type	Location in MeCP2	Plasmids with mutation
c.473C>T	p.T158M	Missense	MBD	Human *MECP2-E1-T158M*
c.880C>T	p.R294X	Nonsense	NID	Mouse *Mecp2-E1-R294X* Mouse *Mecp2-E2-R294X* Human *MECP2-E1-R294X*
c.916C>T	p.R306C	Missense	NID	Mouse *Mecp2-E1-R306C* Mouse *Mecp2-E2-R306C* Human *MECP2-E1-R306C*
c.1085_1197del113	p.P362HfsX5	Frameshift (deletion)	C-terminus	Human *MECP2-E1-P362HfsX5*
c.1157_1197del41	p.L386HfsX5	Frameshift (deletion)	C-terminus	Human *MECP2-E1-L386HfsX5*
c.1164_1207del44	p.P389X	Frameshift (deletion)	C-terminus	Human *MECP2-E1-P389X*
c.1197dupC	p.T400HfsX5	Frameshift (insertion)	C-terminus	Human *MECP2-E1-T400HfsX5*
c.1216C>T	p.Q406X	Nonsense	C-terminus	Mouse *Mecp2-E1-Q406X* Mouse *Mecp2-E2-Q406X*
c.1308delTC	p.Q437AfsX49	Frameshift (deletion)	C-terminus	Human *MECP2-E1-Q437AfsX49*
c.1459T>C	p.X487R	Stop-loss	C-terminus	Mouse *Mecp2-E1-X487R* Mouse *Mecp2-E2-X487R* Human *MECP2-E1-X487R*
c.1460G>C	p.X487S	Stop-loss	C-terminus	Mouse *Mecp2-E1-X487S* Mouse *Mecp2-E2-X487S*

Table 6. Site-directed mutagenesis primers For missense mutations, the altered codon is in lowercase letters. Missense mutations and insertions are indicated in red font.

Mutation	Species	Forward Primer (5′ → 3′)	Reverse Primer (5′ → 3′)
T158M	Human	TTTTGACTTCatgGTAACTGGGAG	TCATTAGGGTCCAGGGATG
R294X	Human	GTCTTCTATCtgaTCTGTGCAGG	TCCTTCACGGCTTTCTTTTTG
R294X	Mouse	GTCTTCCATAtgaTCTGTGCA	TCCTTCACGGCTTTCTTTTTG
R306C	Mouse	CATCAAGAAGtgcAAGACCCGGG	GGGAGCACAGTCTCATGC
P362HfsX5	Human	ACCAGCCCCCCTGAGCCC	GGGGTGAGGAGGCGCTGC
L386HfsX5	Human	ACCAGCCCCCCTGAGCCC	GGGGTGGGAGCAGTGGCAC
P389X	Human	CTGAGCCCCAGGACTTGAGCAGC	GGGGGCAGGGGTGGGAGC
T400HfsX5	Human	cACCAGCCCCCCTGAGCCC	GGGGTCCTCGGAGCTCTCG
Q406X	Mouse	CCCTGAGCCTtagGACTTGAGCAG	GGGCTGATGGGGTCCTCA
Q437AfsX49	Human	AGCCCGCGGTTGCCACCG	GTCTTAGCTGGCTCCTTGGGGC
X487R	Human	GAGAGTTAGCcgaCTTTACACGGAGCGGATTGC	TCGGTCACGGGCGTCCGG
X487R	Mouse	GAGAGTTAGCcgaCTTTACATAGAGCGGATTGCAAAGC	TCGGTCACGGGCGTCCGG
X487S	Mouse	GAGAGTTAGCtcaCTTTACATAGAGCGGATTGCAAAG	TCGGTCACGGGCGTCCGG

Table 7. CRISPR sgRNA sequences All sgRNA sequences were designed as 20 basepair oligonucleotides with a 21st 5′ G nucleotide added to increase U6 promoter efficiency.

sgRNA Name	Species	Target	Sequence (5′ → 3′)
mEx3_g2 (sgRNA2)	Mouse	*Mecp2* exon 3 (knockout)	GGTCATCATACATAGGTCCC
mR294X	Mouse	*Mecp2* exon 4 (R294X)	CCGTGAAGGAGTCTTCCATA
hEx3_g2	Human	*MECP2* exon 3 (knockout)	GGTCATCATACATGGGTCCC
hX487R_g2	Human	*MECP2* exon 4 (X487R)	TCAGCTAACTCTCTCGGTCA

Table 8. CRISPR HDR templates Disease-causing point mutations are indicated in bold red font. Synonymous PAM-inactivating point mutations are indicated in bold green font.

Desired mutation	HDR Template	Target	Sequence (5′ → 3′)
Mouse R294X	*Mecp2-E2-R294X* sequence in the pDONR221 plasmid	*Mecp2* exon 4 (R294X)	…AGCTGAGGCCAAAAAGAAAGCCGTGAAGGAGTCTTCCATA**T**G**A**TCTG TGCATGAGACTGTGCTCCCCATCAAGAAGCGCAAGA…
Human X487R	ssODN	*MECP2* exon 4 (X487R)	CCAAACAGAGAGGAGCCTGTGGACAGCCGGACGCC**A**GTGACCGAGAGA GTTAGC**C**GACTTTACACGGAGCGGATTGCAAAGCAAACCAACAAGAA

Table 9. CRISPR clone screening primer pairs Disease-causing point mutations are indicated in bold red font. Destabilizing mismatches are indicated in bold green font.

Target	Purpose	Species	Forward Primer (5′ → 3′)	Reverse Primer (5′ → 3′)	PCR Product Size (bp)
Mecp2 exon 3	Amplify the genomic sequence flanking mEx3_g2 sgRNA	Mouse	ATGTGTGGCACTCAAGCTCA	CTCCCTCTCCCAGTTACCGT	1039 bp
Mecp2 R294X allele	Detect the mouse R294X allele	Mouse	GTGAAGGAGTCTTCCATA**T**G**A**	GGCTGCTCTCCTTGCTTTTA	190 bp
MECP2 exon 3	Amplify the genomic sequence flanking hEx3_g2 sgRNA	Human	CCTCAAGGACAAACCCCTCAA	ACCCTGGGCACATACATTTTC	406 bp
MECP2 X487R allele	Detect the human X487R allele	Human	CGTGACCGAGAGAGTTA**A**C**C**	GGGTAGGGCTCTGACAAAGC	109 bp
MECP2 exon 4	Amplify the transcript sequence flanking hX487R_g2 sgRNA	Human	TCAAACTTCGCCAGGGGG	CCTGACTGTGCTTGTCGGTA	993 bp

Table 10. Summary of genetically engineered cell lines

Cell Line	Mutation (coding sequence)	Mutation (protein sequence)
N2a *Mecp2* knockout (clone P4G5)	c.119_332del214	p.E40GfsX14
N2a *Mecp2* R294X (clone 1F6)	c.880C>T ; 882G>A	p.R294X
N2a *Mecp2* R294X (clone 2H2)	c.880C>T ; 882G>A	p.R294X
LUHMES *MECP2* knockout (clone Ex3 23)	c.268del8	p.D90TfsX4
LUHMES *MECP2* X487R (clone X487R 15)	c.1459T>C (active) ; c.1145ins70 (inactive)	p.X487R

Table 11. *MECP2* genomic sequencing primers

Target	Primer Pairs (5′ → 3′)	PCR Product Sizes (bp)
Mouse genomic *Mecp2*	Exon 1 F: GACTTCCTTAAGCGCCAGAG R: GCCAGTCTGTGTGTGTGAGG	Exon 1 948 bp
	Exon 2 F: GTTCCAAAGTGTTCCCCAGA R: CTGAAAATGCAGCACACCAC	Exon 2 805 bp
	Exon 3 F: CAGAAGCCCTGGATTCAGTC R: TTTTTGGGAAGCCATTTCAG	Exon 3 950 bp
	Exon 4 F: TGGCTTCTGAGCAAGCTGTA R: CCTTCTTAGGTGGGGAGGAG	Exon 4 898 bp
	F: TTGAAAAGGTGGGAGACACC R: TCCACAGGCTCCTCTCTGTT	997 bp
	F: AACAGAGAGGAGCCTGTGGA R: GAGCATGCCTTGTGAACAGA	813 bp
Human genomic *MECP2*	Exon 1 F: TCTCGCCAATTGACGGCAT R: ACGGGAGGCGAAGTGC	Exon 1 793 bp
	Exon 2 F: GCACTGTGTGTTACGTGCC R: CAGATGGCCAAACCAGGACAT	Exon 2 353 bp
	Exon 3 F: CCGAGTCTCTGTTGTCCTGG R: GCACACCTGGTCTCAGTGTT	Exon 3 638 bp
	Exon 4 F: GAGTGGCTTTGGTGACAGGT R: CCTTGACCTCGATGCTGACC	Exon 4 739bp
	F: AGGAGACCGTACTCCCCATC R: TTTGCTTTGCAATCCGCTCC	600 bp
	F: CTGACTTTACACGGAGCGGAT R: TTCAGGCCAGTCTACACCCA	706 bp

Table 12. RT-qPCR primers

Target	Species	Forward Primer (5′ → 3′)	Reverse Primer (5′ → 3′)	PCR Product Size (bp)
Mecp2 E1	Mouse	AGGAGGAGAGACTGGAGGAAAAG	CTTTCTTCGCCTTCTTAAACTTCAG	87 bp
Mecp2 E2	Mouse	GATTCCATGGTAGCTGGGATGT	TCTGAGGCCCTGGAGATCCT	72 bp
Gapdh	Mouse	TGTGTCCGTCGTGGATCTGA	TTGCTGTTGAAGTCGCAGGAG	150 bp
MECP2	Human	CCGGGGACCCATGTATGATG	GGGATGTGTCGCCTACCTTT	179 bp
GAPDH	Human	AGAAGGCTGGGGCTCATTTG	AGGGGCCATCCACAGTCTTC	258 bp

Table 13. Antibodies

Name	Description	Target	Species	Working Concentration
Sigma M7443 (Men8)	Monoclonal	N-terminal MeCP2	Mouse	Western: 1:1,000 Immunocytochemistry: 1:250
Cell Signaling 3456 (D4F3)	Monoclonal	C-terminal MeCP2	Rabbit	Western: 1:5,000
abcam ab51841	Monoclonal	TBP	Mouse	Western: 1:2,000
Cell Signaling 8515	Polyclonal	TBP	Rabbit	Western: 1:2,000
Millipore ABE171	Polyclonal	MeCP2	Chicken	Immunocytochemistry: 1:1000
Millipore AB152	Polyclonal	TH	Rabbit	Western: 1:1,000 Immunocytochemistry: 1:1,000

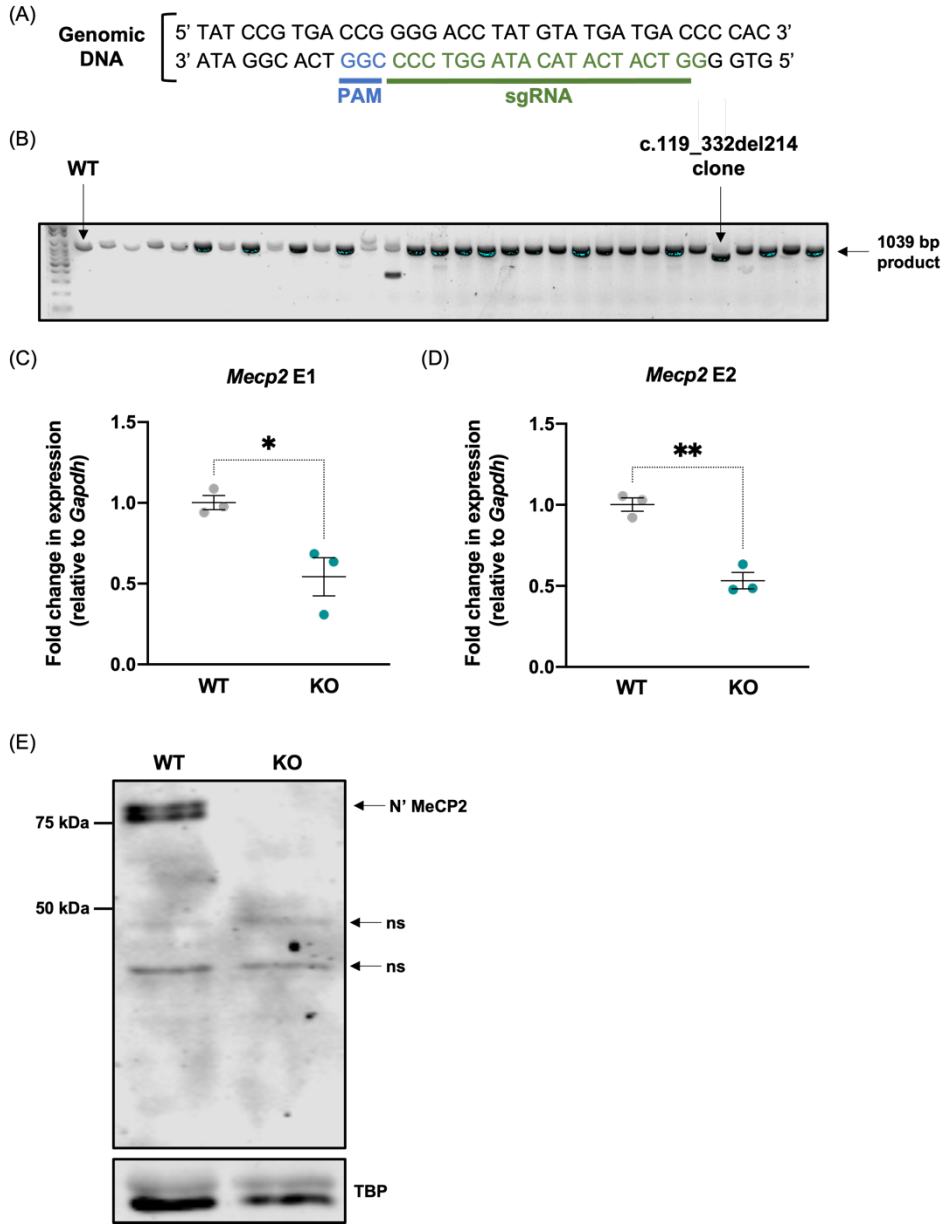

Figure 13. Generation and validation of a *Mecp2* KO N2a cell line

(A) A schematic representation of the CRISPR/Cas9-directed mutagenesis approach to introduce an indel into exon 3 of the endogenous *Mecp2* locus. PAM sequence is indicated in blue font and sgRNA sequence is indicated in green font. (B) Agarose gel image of *Mecp2* exon 3 PCR products from 31 screened N2a clones. WT and selected KO (c.119_332del214) clones are indicated with black arrows. (C-D) *Mecp2* E1 and E2 transcript isoform levels as determined by RT-qPCR in bulk WT and clonal KO N2a cells. (E) Western blotting of bulk WT and clonal KO N2a cells with antibodies to detect the N-terminus of MeCP2 (full-length MeCP2 at 75 kDa) and TBP as a loading control (ns=non-specific).

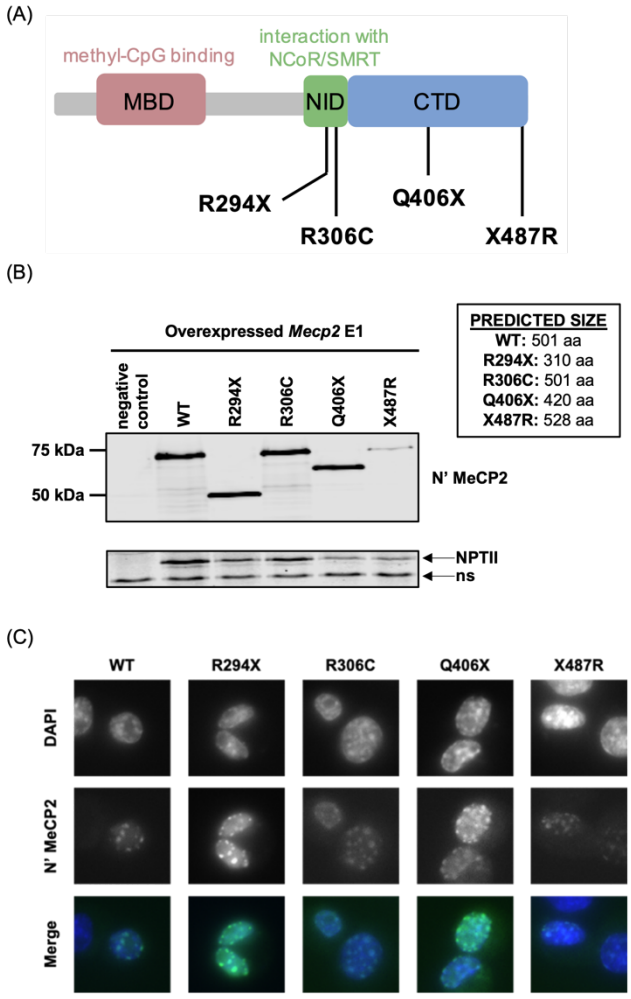

Figure 14. Q406X and X487R C-terminal *MECP2* mutations produce protein products that localize to heterochromatic foci in the N2a *Mecp2* KO overexpression system

(A) Schematic representation of the MeCP2 protein with methyl-binding domain (MBD) in pink, NCoR/SMRT interaction domain (NID) in green, and C-terminal domain (CTD) in blue. The locations of R294X, R306C, Q406X, and X487R mutations are shown below in black. (B) Western blot of overexpressed WT and C-terminal mutant E1 MeCP2 in *Mecp2* KO N2a cells. MeCP2 was detected with an antibody to the N-terminus of the protein and neomycin phosphotransferase II (NPTII) was detected as a control for transfection efficiency (ns=non-specific). Predicted protein product sizes are listed for each mutation. (C) Immunocytochemistry staining of *Mecp2* KO N2a cells overexpressing WT and C-terminal mutant E1 MeCP2. Nuclei are stained with DAPI and MeCP2 is stained with an antibody to the N-terminus of the protein.

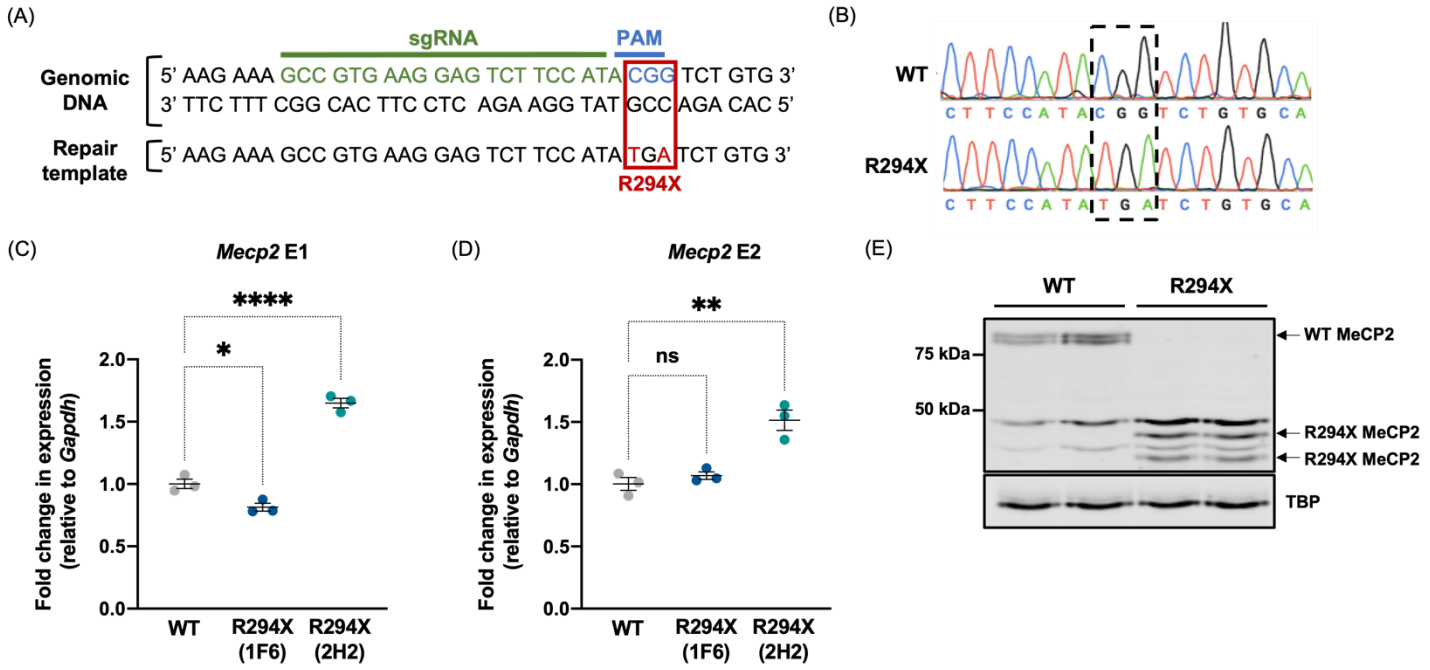

Figure 15. Generation of two independent *Mecp2* R294X N2a cell lines expressing truncated MeCP2 protein

(A) A schematic representation of the CRISPR/Cas9-directed mutagenesis approach to introduce the R294X mutation into exon 4 of the endogenous *Mecp2* locus. PAM sequence is indicated in blue font and sgRNA sequence is indicated in green font. (B) Sanger sequencing chromatogram confirming the c.880C>T and c.882G>A mutations. (C-D) *Mecp2* E1 and E2 transcript isoform levels as determined by RT-qPCR in WT and two R294X (1F6, 2H2) N2a clonal lines. (E) Western blotting of WT and R294X (2H2) N2a clonal lines with antibodies to detect the N-terminus of MeCP2 (full-length MeCP2 at 75 kDa) and TBP as a loading control.

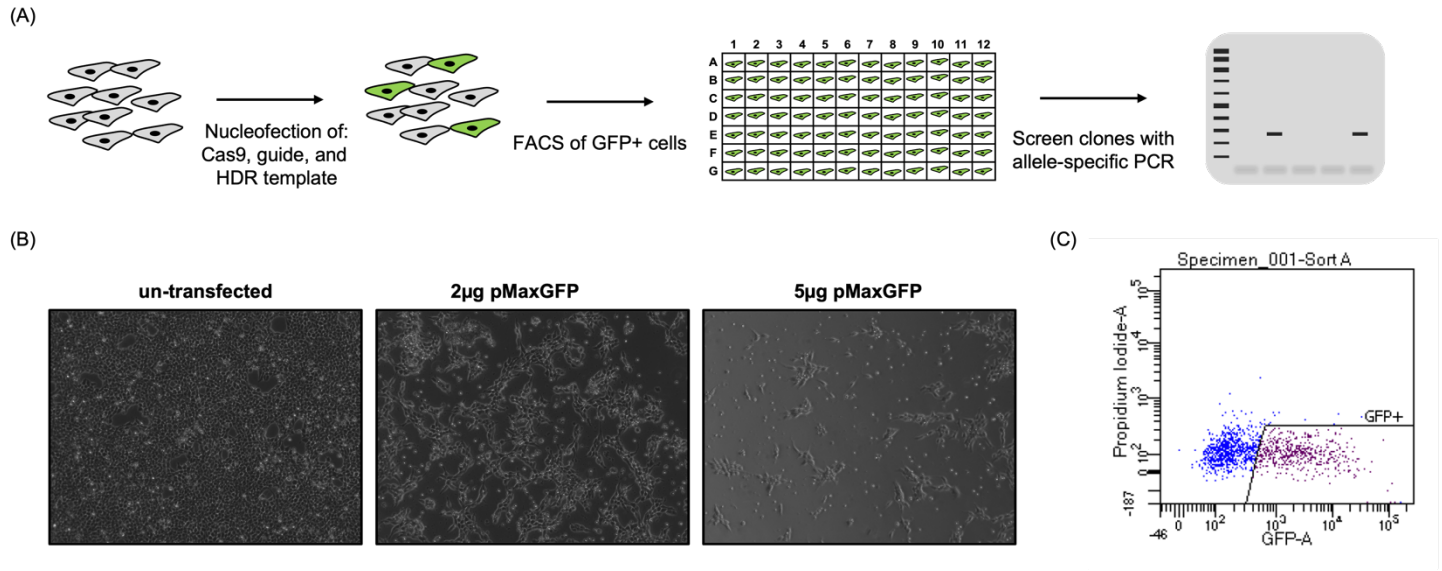

Figure 16. Experimental approach to genetic engineering of LUHMES cells

(A) Schematic representation of experimental approach to engineer LUHMES cells with the CRISPR/Cas9 system, isolate clones, and screen for desired mutation. (B) Representative nucleofection experiment determining the optimal amount of transfected plasmid (2µg) per well of a 6-well plate. Images of cells nucleofected with no plasmid (left), 2µg plasmid (middle), and 5µg plasmid (right). (C) Representative FACS gates to sort GFP+;PI- cells into single wells of a 96-well plate.

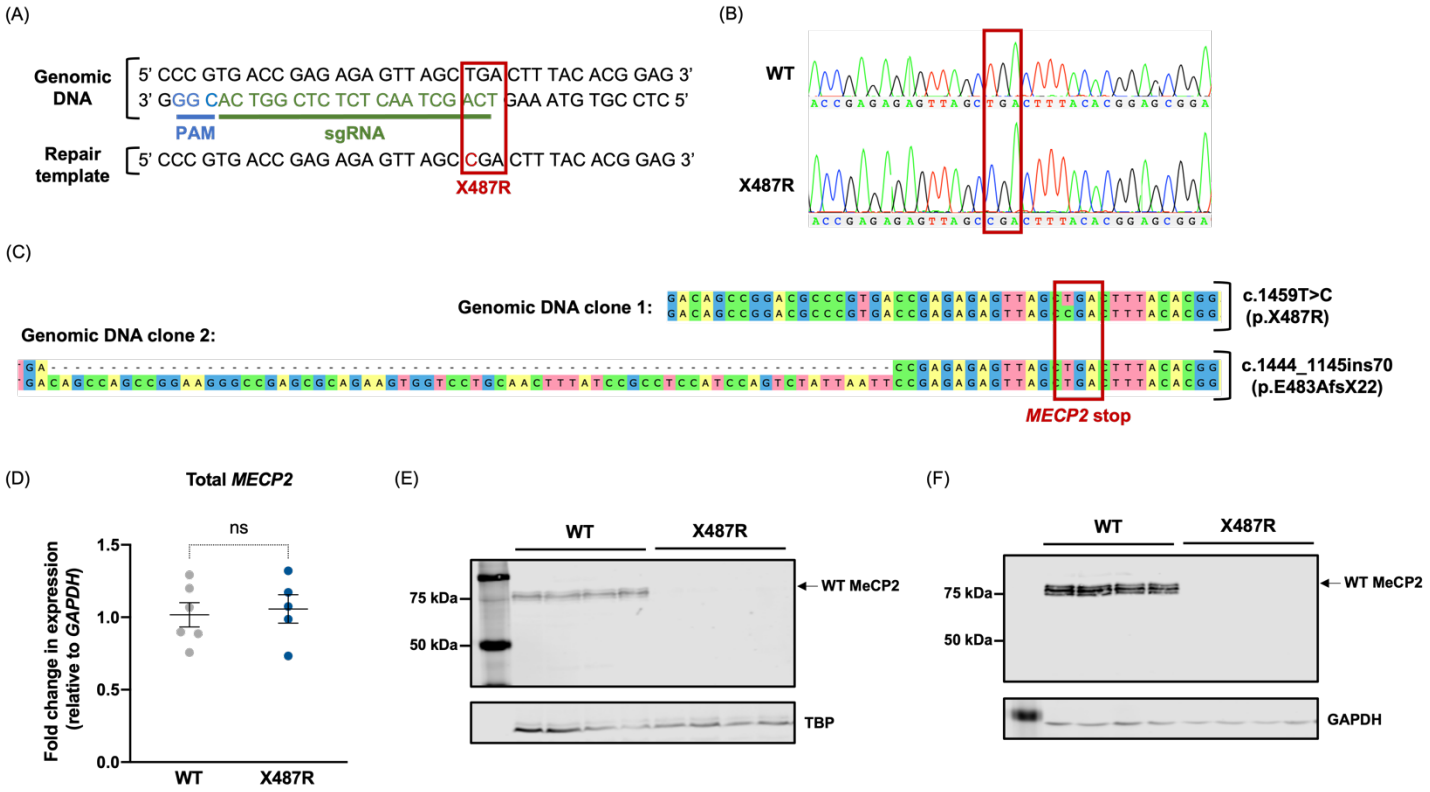

Figure 17. Generation and characterization of a *MECP2* X487R LUHMES cell line

(A) A schematic representation of the CRISPR/Cas9-directed mutagenesis approach to introduce the X487R mutation into exon 4 of the endogenous *Mecp2* locus. PAM sequence is indicated in blue font and sgRNA sequence is indicated in green font. (B) Sanger sequencing chromatogram confirming the c.1459T>C mutation in LUHMES cDNA. (C) Genomic DNA sequences of the two X-chromosomes of X487R cells isolated via TOPO cloning. Top: Active X487R X-chromosome. Bottom: Inactive E483Afs X-chromosome. (D) *MECP2* transcript levels as determined by RT-qPCR in WT and X487R cells. (E) Western blotting of WT and X487R LUHMES with antibodies to detect the N-terminus of MeCP2 (full-length MeCP2 at 75 kDa) and TBP as a loading control. (F) Western blotting of WT and X487R LUHMES with antibodies to detect the C-terminus of MeCP2 (full-length MeCP2 at 75 kDa) and GAPDH as a loading control.

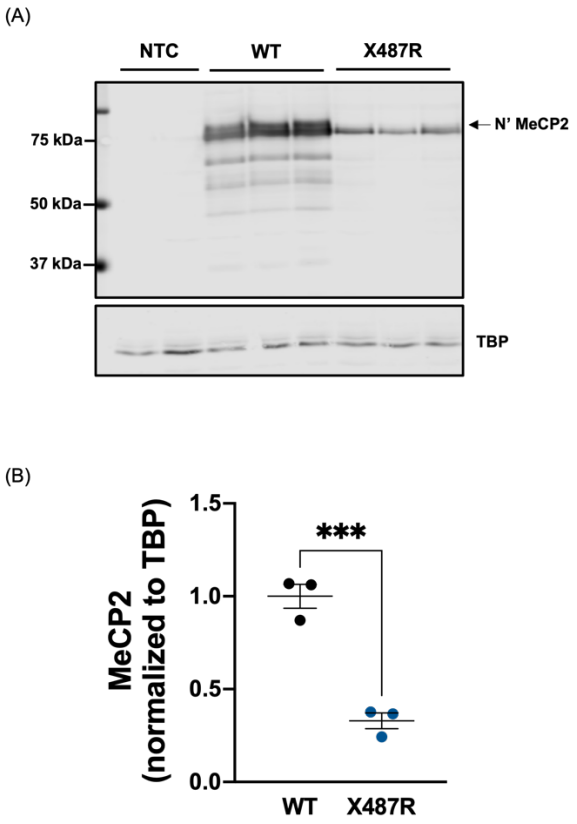

Figure 18. The *MECP2* stop-loss X487R mutation results in reduced protein levels in the N2a *Mecp2* KO overexpression system

(A) Western blotting of protein lysates from *Mecp2* KO N2a cells transfected with either WT or X487R *MECP2* (NTC=no template control). MeCP2 was detected with an antibody to the N-terminus of the protein (full-length protein at 75 kDa) and TBP was detected as a loading control. Each lane contains protein from a single biological replicate. (B) Quantification of MeCP2 levels, normalized to TBP, of the experiment in (A).

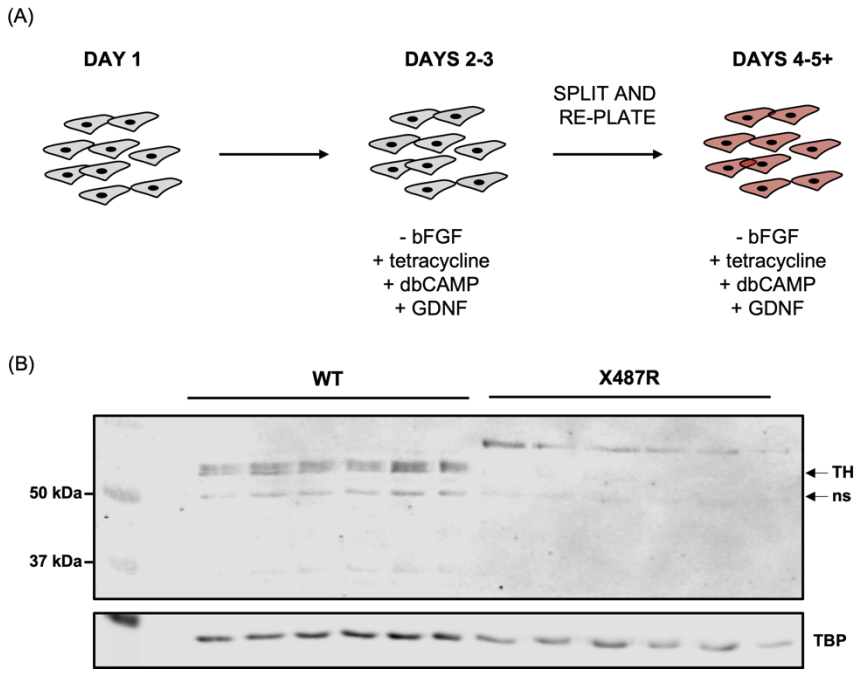

Figure 19. Differentiated *MECP2* X487R LUHMES have altered TH expression

(A) Schematic representation of the LUHMES differentiation process. On Day 2, cells are removed from media containing bFGF and incubated in media containing tetracycline, dbcAMP, and GDNF. On Day 3, cells are split and re-plated. Differentiated cells were harvested for protein on Day 5. (B) Western blotting of differentiated WT and differentiated X487R LUHMES with antibodies to detect TH (60 kDa) and TBP as a loading control (ns=non-specific). Each lane contains protein from a single biological replicate.

CHAPTER 4

Summary and Future Directions

Summary

Together, this dissertation work comprises a functional characterization of R294X and representative C-terminal stop-loss *MECP2* mutations that cause Rett syndrome in people. In Chapter 2, we show that RTT-like phenotypes induced by the partial loss-of-function R294X mutation can be rescued by genetic *MECP2* supplementation in mice. These results dissuade concerns about the potential for dominant negative interactions between full-length MeCP2 and an R294X truncated protein product with altered chromatin binding properties. Additionally, we present evidence of subtle motor-specific MDS-like behavioral effects of genetic *MECP2* supplementation in female mice, suggesting that the motor circuitry is particularly susceptible to elevated gene dosage. With the knowledge that the partial loss-of-function R294X mutation can be genetically rescued, we wondered whether mutations that retain intact MBD and NID functional domains and occur in the C-terminal region of the protein would also be amenable to genetic rescue. In Chapter 3, we develop an in vitro LUHMES-based cellular modelling system and demonstrate its utility in evaluating a unique stop-loss X487R C-terminal mutation. We present evidence that the X487R mutation yields reduced protein levels in an endogenous context and provide preliminary data showing differences in dopaminergic phenotype during differentiation. While there remains much to be explored, this dissertation work advances our understanding of mutation-specific susceptibility to putative genetic supplementation therapy and develops a foundation for mechanistic study of the heterogeneous and understudied group of C-terminal *MECP2* mutations.

An important corollary of this work is its implications for putative genetic MeCP2 supplementation therapy, including approaches such as gene therapy and X-chromosome reactivation. The former, viral delivery of full-length *MECP2* to the CNS, is currently under preclinical evaluation and when modelled in male mice has shown rescue of survival, body weight, and select behavioral phenotypes[174–179]. While there remain concerns over eliciting sufficient transduction and over hepatotoxicity, the literature has not thus far evaluated the potential for adverse effects due to excess MeCP2 in the CNS. We find MeCP2 supplementation to physiological levels is safe and effective in males, with no behavioral evidence of excess MeCP2. However, in females, we find that MeCP2 supplementation leads to approximately 1.5x the level of MeCP2 compared to that in the WT brain, due to the indiscriminate supplementation of cells expressing endogenous WT *Mecp2* and cells expressing endogenous R294X *Mecp2*. We report the presence of subtle motor-specific MDS-like effects associated with this excess MeCP2 and suggest that consideration of motor-specific side effects may be warranted for girls and women

with RTT in the context of genetic supplementation therapy. Importantly, because we do not observe MDS-like effects in males, our findings suggest that this is not a mutation-specific phenomenon but instead a sex-specific phenomenon. Therefore, we expect these findings to extend to other partial loss-of-function *MECP2* mutations as well.

Another important corollary of this dissertation work is that it establishes an in vitro system amenable to further mechanistic or high-throughput screening work. While not yet broadly used in the neuroscience community, LUHMES are a tractable option for disease modelling in labs not familiar with complicated cell culture. We built upon previous work to design culture maintenance, nucleofection, genetic engineering, and cell differentiation protocols. With these, we generated an X487R *MECP2* C-terminal mutation in LUHMES cells and provide preliminary evidence of phenotypic effects of *MECP2* mutation. These tools can be used to investigate the mechanisms underlying other common C-terminal mutations in *MECP2* or mutations in other genes causative of neurodevelopmental disease. Additionally, given their facile propagation and scalability, LUHMES can be leveraged for other purposes including high-throughput screening of potential therapeutic compounds or of genetic modifiers of disease.

Future Directions

Genetic *MECP2* supplementation of the R294X allele

We have shown that global genetic supplementation is capable of rescuing RTT-like phenotypes in the context of the R294X allele and, while there exists precedent in the literature to expect that rescue is dependent on supplementation of neurons in the CNS, our experimental design cannot distinguish between the effects of genetic supplementation in neurons of the CNS or of supplementation in other cells in the body[113,114]. Indeed, MeCP2 is expressed most highly in post-mitotic neurons, but is also expressed at lower levels in other cells of the body[87]. Extensive work has tied many of the RTT-like phenotypes observed in mice to loss of *Mecp2* in various brain regions/circuits (e.g. motor coordination deficits to cortical and striatal regions)[113,121–124]. Additionally, a recent report has shown that MDS-like phenotypes in mice are differentially susceptible to MeCP2 supplementation, suggesting that different brain regions have different thresholds for MeCP2 dosage[242]. It is not fully understood why MeCP2 dosage sensitivity depends on brain region; however, it may depend on subtle differences in MeCP2 access to methylated DNA binding sites across different cell types (e.g. differential methylation patterns, abundance of competing DNA binding proteins, transcriptional milieu, etc.).

To refine our results and control the spatial supplementation of MeCP2, future work could employ the Cre-Lox recombination system to express *MECP2* transgene in specific brain regions. Two different mouse lines would be needed: 1) a line with a *MECP2* transgene with a loxP-flanked (floxed) stop sequence between the promoter and coding sequence,

and 2) a Cre driver line for region/cell type of interest (e.g. Camk2a driver for post-mitotic forebrain neurons). This approach would provide spatial control as the floxed stop sequence will be removed and supplemented *MECP2* will be expressed only in regions that express Cre recombinase. Repeating a broad behavioral battery to evaluate rescue of RTT-like phenotypes and onset of MDS-like phenotypes would determine the impact of genetic MeCP2 supplementation in specific regions or cell types.

Two regions of interest for future work determining region-specific effects of MeCP2 supplementation would be the striatum and cortex. Previous work has shown that region-specific knockout of *Mecp2* in either postnatal forebrain or forebrain GABAergic neurons elicits rotarod deficits at ages consistent with onset of motor phenotypes in global *Mecp2* KO mice[121,122]. Additionally, an enhanced motor coordination phenotype in a mouse model of autism-associated NL3 mutations was determined to occur through decreased synaptic inhibition onto D1-expressing medium spiny neurons in the nucleus accumbens in ventral striatum, causing acquired repetitive motor behavior[226]. Collectively, this work suggests that the striatum and/or cortex may be involved in rotarod overperformance with MeCP2 overexpression in MDS model mice. To test this, future work could use region-specific MeCP2 supplementation, through the approach described above, in the striatum or cortex to determine whether elevated MeCP2 in these regions is associated with rotarod overperformance.

Additionally, our work shows that genetic supplementation throughout development is capable of rescuing RTT-like phenotypes in the context of the R294X allele. Again, while there is precedent in the literature to suggest that addition of MeCP2 after symptom onset can provide symptomatic benefit, the genetic approach we used cannot differentiate between effects of supplemented MeCP2 before and after symptom onset[119,120]. To better control the temporal precision of supplementation of MeCP2, future work could employ the tamoxifen-inducible Cre recombinase system. In this system, Cre recombinase is fused to the mutated ligand-binding domain of the estrogen receptor (Cre-ER), which has high affinity for tamoxifen. Upon binding tamoxifen, Cre-ER translocates to the nucleus and can carry out site-specific recombination. Two different mouse lines would be needed: 1) a line with a *MECP2* transgene with a loxP-flanked (floxed) stop sequence between the promoter and coding sequence, and 2) a Cre-ER line for inducible transgene expression. This would provide temporal control because *MECP2* transgene would only be expressed after administration of tamoxifen. Administration of tamoxifen after symptom onset and then repeating the behavioral battery would permit determination of whether MeCP2 supplementation is required during development for rescue of RTT-like phenotypes and onset of subtle motor-specific MDS-like phenotypes in female mice.

Another limitation of our genetic approach is that it models a single, fixed amount of supplemental MeCP2. However, endogenous modulation of MeCP2 level would provide better control of protein dose and reduce risk of MDS-like adverse effects. There are several ways to control expression level of *MECP2* transgene. However, one approach that is gaining traction involves the addition of microRNA response elements (MREs) to the 3′ UTR of the transgene. Endogenous microRNAs bind MRES in the transgene transcript and decrease protein expression through RNA interference. This approach has been used to generate safer *MECP2* viral vectors for gene therapy models in mice and should remain a priority in the field[243].

Development of a LUHMES-based in vitro disease modelling system for C-terminal *MECP2* mutations

After finding that behavioral effects of the R294X allele can be rescued by MeCP2 supplementation, we wondered whether mutations later in the *MECP2* sequence, that do not interrupt any known functional domain, would similarly be amenable to rescue. We developed a LUHMES-based in vitro modelling system and used it to analyze the functional effects of a specific C-terminal *MECP2* mutation, the stop-loss X487R mutation. While this dissertation work provides an initial toolkit to examine C-terminal mutations, there remains much to be explored.

First, our results suggest that the *MECP2* X487R mutation yields low protein levels compared to WT when expressed endogenously in LUHMES. However, it is not clear what process is leading to reduced MeCP2 levels. Two broad possibilities are 1) decreased translation and 2) increased protein degradation. To test the former, polysome profiling experiments could determine whether the X487R transcript is undergoing active translation. To test the latter, future work could involve a cycloheximide chase experiment to determine steady state protein stability. In this experiment, cells are treated with the translational inhibitor cycloheximide, and protein is collected at several times afterwards to observe protein degradation over time[244]. A mutant protein undergoing increased degradation would be expected to show a faster decline in protein levels relative to the WT protein. Additionally, to test involvement of specific degradation pathways, proteasomal inhibitors such as MG132 or lactacystin could be administered to determine whether they are able to elevate mutant protein levels. Preliminary MG132 experiments have been conducted with no detected differences in X487R MeCP2 expression; however, optimization of dosage and treatment time is still needed (**Figure 20**).

Another remaining question regarding the *MECP2* X487R LUHMES is to what extent they differ from WT LUHMES during differentiation. We have observed that fewer *MECP2* X487R LUHMES survive the differentiation process, whereas virtually no cell death is observed in WT LUHMES during differentiation. Future work should focus on quantifying a potential survival phenotype, using either immunocytochemistry to stain surviving cells, or flow cytometry with a viability stain

such as PI, after differentiation. We further found that, while WT LUHMES express TH by day 5 of differentiation, *MECP2* X487R LUHMES do not. To evaluate this phenotype further, time course experiments should be conducted to see whether *MECP2* X487R LUHMES express TH earlier or later than day 5 of differentiation, if at all. Additionally, TH is only one marker of differentiation. Evaluation of other markers, both pan-neuronal and dopaminergic, may provide greater insight into phenotypic differences between WT and *MECP2* X487R LUHMES. Finally, previous work has shown that differentiated LUHMES are capable of fluxing dopamine[230]. An intriguing future direction could focus on functional effects of the stop-loss mutation by analyzing dopamine transport.

A last, broad remaining question for the LUHMES system is whether it can be leveraged to provide insight as to how C-terminal mutations as a whole cause RTT syndrome. While these mutations are many and heterogeneous, a good starting place would be to model the most common C-terminal mutations. These are three main deletion-frameshift mutations in a mutation hotspot within the *MECP2* C-terminus: 1) c.1157_1197del41 (CTD1, p.L386HfsX5, where X=HQPP*), 2) c.1157_1200del44 (CTD2, p.L386HfsX4, where X=QPP*), and 3) c.1164_1207del44 (CTD3, p.P389X). Two of these have been modelled in mice: CTD1 and CTD3. CTD1 mice developed RTT-like phenotypes and exhibited decreased survival[111]. A CTD1 truncation product was present at very low levels and authors of the work proposed that overall lower MeCP2 levels were sufficient to cause these RTT-like phenotypes in mice. However, CTD3 mice did not display any progression of RTT-like phenotypes and exhibited normal survival. Only when authors of the work "humanized" the CTD3 sequence did they find protein instability. It is possible that there are important sequence differences between mice and humans at this mutation hotspot, and the LUHMES system provides the opportunity to isolate any human-specific effects of CTD3. Together, these three common CTD mutations may be acting in unique ways to cause RTT. For example, while CTD1 may cause protein instability, CTD3 may cause disruption of other MeCP2 functions. CTD2 is highly similar to CTD1, with only a single amino acid difference in the predicted tail protein. Given this, I would hypothesize that CTD1 and CTD2 have similar functional effects on MeCP2; however, molecular characterization is necessary to determine this. Finally, given that C-terminal mutations are associated with lower clinical severity in people, I would predict that these three mutations are not all complete loss-of-function mutations caused by protein instability.

Concluding Remarks

The work contained in this dissertation advances our understanding of how specific mutations in *MECP2* – R294X and the representative C-terminal mutation X487R – cause Rett syndrome in people. It provides hope that even late truncating mutations like R294X, which produces a truncation product with altered binding properties, could be amenable to genetic MeCP2 supplementation therapy. Further, this work demonstrates the utility of LUHMES cells in modelling C-terminal

MECP2 mutations. Future work should refine the mechanism of stop-loss mutations by investigating how mutations like X487R yield reduced protein levels, as well as model the three predominant C-terminal mutations (c.1157_1197del41, c.1157_1200del44, c.1164_1207del44) to determine similarities and/or differences in mechanism given an overall relatively low clinical severity of individuals with this group of mutations.

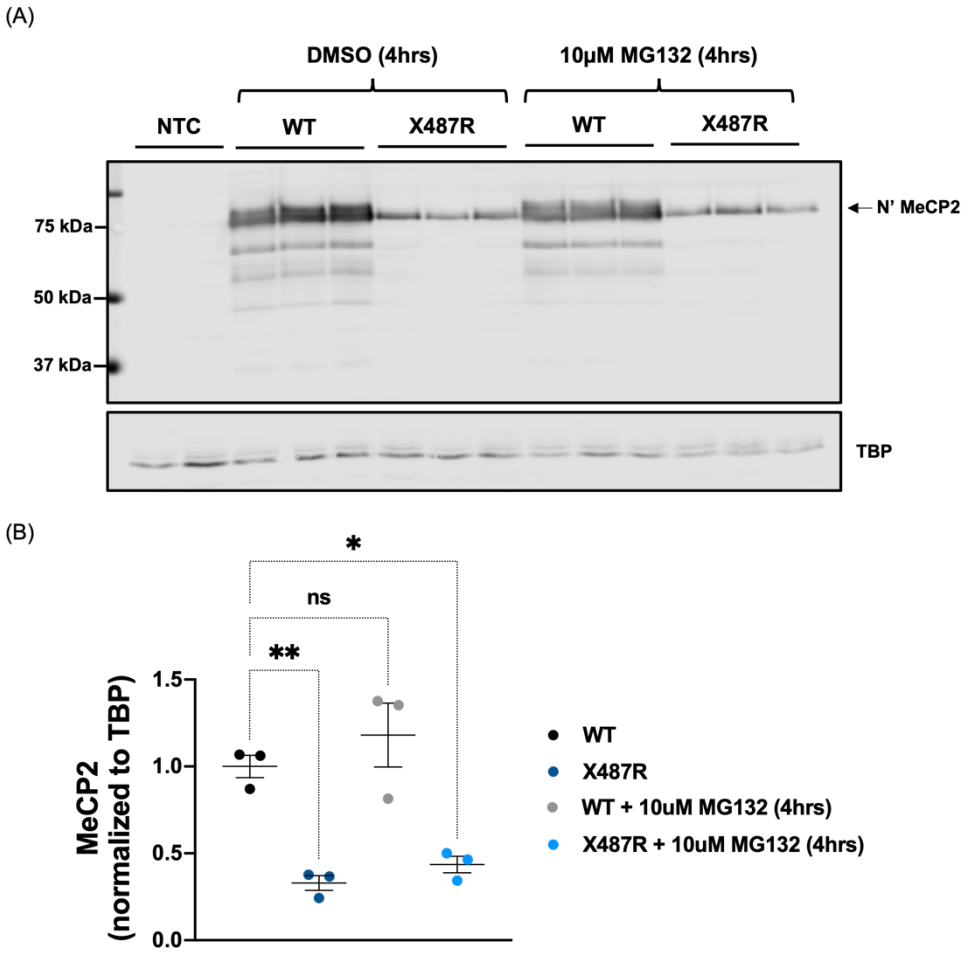

Figure 20. The proteasome inhibitor MG132 does not affect overexpressed X487R protein level at 10 μM for 4 hours

(A) Western blotting of protein lysates from *Mecp2* KO N2a cells transfected with either WT or X487R *MECP2* and treated with either DMSO or 10 μM MG132 for 4 hours (NTC=no template control). MeCP2 was detected with an antibody to the N-terminus of the protein (full-length protein at 75 kDa) and TBP was detected as a loading control. Each lane contains protein from a single biological replicate. (B) Quantification of MeCP2 levels, normalized to TBP, of the experiment in (A).

REFERENCES

1. Haas, R. H. The History and Challenge of Rett Syndrome. *J. Child Neurol.* **3**, S3–S5 (1988).
2. Rett, A. On a unusual brain atrophy syndrome in hyperammonemia in childhood. *Wiener Medizinische Wochenschrift* **116**, 723–726 (1966).
3. Hagberg, B., Aicardi, J., Dias, K. & Ramos, O. A Progressive Syndrome of Autism, Dementia, Ataxia, and Loss of Purposeful Hand Use in Girls: Rett's Syndrome: Report of 35 Cases. *Ann. Neurol.* **14**, 471–479 (1983).
4. Hagberg, B. & Witt-Engerström, I. Rett Syndrome: A suggested staging system for describing impairment profile with increasing age towards adolescence. *Am. J. Med. Genet.* **1**, 47–59 (1986).
5. Neul, J. L. *et al.* Rett syndrome: Revised Diagnostic Criteria and Nomenclature. *Ann. Neurol.* **68**, 944–950 (2010).
6. Laurvick, C. L. *et al.* Rett syndrome in Australia: A review of the epidemiology. *J. Pediatr.* **148**, 347–352 (2006).
7. Zoghbi, H. Genetic Aspects of Rett Syndrome. *J. Child Neurol.* **3**, S76–S78 (1988).
8. Zoghbi, H. Y., Percy, A. K., Schultz, R. J. & Fill, C. Patterns of X Chromosome Inactivation in the Rett Syndrome. *Brain Dev.* **12**, 131–135 (1990).
9. Schanen, C. & Francke, U. A Severely Affected Male Born into Rett Syndrome Kindred Supports X-linked Inheritance and Allows Extension of the Exclusion Map. *Am J Hum Genet* **63**, 267–269 (1998).
10. Schanen, N. C. *et al.* A New Rett Syndrome Family Consistent with X-Linked Inheritance Expands the X chromosome Exclusion Map. *Am. J. Hum. Genet.* **61**, 634–641 (1997).
11. Ellison, K. A. *et al.* Examination of X chromosome Markers in Rett Syndrome: Exclusion Mapping with a Novel Variation on Multilocus Linkage Analysis. *Am. J. Hum. Genet.* **50**, 278–287 (1992).
12. Amir, R. E. *et al.* Rett syndrome is caused by mutations in X-linked MECP2, encoding methyl-CpG-binding protein 2. *Nat. Genet.* **23**, 185–188 (1999).
13. Sirianni, N., Naidu, S., Pereira, J., Pillotto, R. F. & Hoffman, E. P. Rett Syndrome: Confirmation of X-linked Dominant Inheritance, and Localization of the Gene to Xq28. *Am. J. Hum. Genet.* **63**, 1552–1558 (1998).
14. Curtis, A. R. J. *et al.* X chromosome linkage studies in familial Rett syndrome. *Hum Genet* **90**, 551–555 (1993).
15. Archidiacono, N. *et al.* Rett syndrome: exclusion mapping following the hypothesis of germinal mosaicism for new X-linked mutations. *Hum. Genet.* **86**, 604–606 (1991).
16. Neul, J. L. *et al.* Specific mutations in Methyl-CpG-Binding Protein 2 confer different severity in Rett syndrome. *Neurology* **70**, 1313–1321 (2008).
17. Cuddapah, V. A. *et al.* Methyl-CpG-binding protein 2 (MECP2) mutation type is associated with disease severity in Rett syndrome. *J. Med. Genet.* **51**, 152–158 (2014).

18. Trappe, R. *et al.* MECP2 Mutations in Sporadic Cases of Rett Syndrome Are Almost Exclusively of Paternal Origin. *Am. J. Hum. Genet.* **68**, 1093–1101 (2001).

19. Wan, M. *et al.* Rett Syndrome and Beyond: Recurrent Spontaneous and Familial MECP2 Mutations at CpG Hotspots. *Am. J. Hum. Genet.* **65**, 1520–1529 (1999).

20. Girard, M. *et al.* Parental origin of de novo MECP2 mutations in Rett syndrome. *Eur. J. Hum. Genet.* **9**, 231–236 (2001).

21. Zhu, X. *et al.* Analysis of the Parental Origin of De Novo MECP2 Mutations and X chromosome Inactivation in 24 Sporadic Patients With Rett Syndrome in China. *J. Child Neurol.* **25**, 842–848 (2010).

22. Duncan, B. K. & Miller, J. H. Mutagenic deamination of cytosine residues in DNA. *Nature* **287**, 560–561 (1980).

23. Oakes, C. C., La Salle, S., Smiraglia, D. J., Robaire, B. & Trasler, J. M. A unique configuration of genome-wide DNA methylation patterns in the testis. *PNAS* **104**, 228–233 (2007).

24. Augenstein, K., Lane, J. B., Horton, A., Schanen, C. & Percy, A. K. Variable phenotypic expression of a MECP2 mutation in a family. *J. Neurodev. Disord.* **1**, 313–317 (2009).

25. Vorsanova, S. G. *et al.* Cytogenetic and molecular-cytogenetic studies of Rett syndrome (RTT): a retrospective analysis of a Russian cohort of RTT patients (the investigation of 57 girls and three boys). *Brain Dev.* **23**, S196–S201 (2001).

26. Schwartzman, J. S., Bernardino, A., Nishimura, A., Gomes, R. R. & Zatz, M. Rett Syndrome in a Boy with a 47,XXY Karyotype Confirmed by a Rare Mutation in the MECP2 Gene. *Neuropediatrics* **32**, 162–164 (2001).

27. Clayton-Smith, J., Watson, P., Ramsden, S. & Black, G. Somatic mutation in MECP2 as a non-fatal neurodevelopmental disorder in males. *Lancet* **356**, 830–832 (2000).

28. Dayer, A. G. *et al.* MECP2 mutant allele in a boy with Rett syndrome and his unaffected heterozygous mother. *Brain Dev.* **29**, 47–50 (2007).

29. Cohen, D. *et al.* MECP2 Mutation in a Boy With Language Disorder and Schizophrenia. *Am. J. Psychiatry* **159**, 148–149 (2002).

30. Neul, J. L. *et al.* The array of clinical phenotypes of males with mutations in Methyl-CpG binding protein 2. *Am. J. Med. Genet. - Neuropsychiatr. Genet.* **180**, 55–67 (2019).

31. Meins, M. *et al.* Submicroscopic duplication in Xq28 causes increased expression of the MECP2 gene in a boy with severe mental retardation and features of Rett syndrome. *J. Med. Genet.* **42**, e12 (2005).

32. Van Esch, H. *et al.* Duplication of the MECP2 Region is a Frequent Cause of Severe Mental Retardation and Progressive Neurological Symptoms in Males. *Am. J. Hum. Genet.* **77**, 442–453 (2005).

33. Collins, A. L. *et al.* Mild overexpression of MeCP2 causes a progressive neurological disorder in mice. *Hum. Mol. Genet.* **13**, 2679–2689 (2004).

34. Bauters, M. *et al.* Nonrecurrent MECP2 duplications mediated by genomic architecture-driven DNA breaks and break-induced replication repair. *Genome Res.* **18**, 847–858 (2008).

35. Carvalho, C. M. B. *et al.* Complex rearrangements in patients with duplications of MECP2 can occur by fork stalling and template switching. *Hum. Mol. Genet.* **18**, 2188–2203 (2009).

36. Zhang, F. *et al.* The DNA replication FoSTeS/MMBIR mechanism can generate genomic, genic and exonic complex rearrangements in humans. *Nat. Genet.* **41**, 849–853 (2009).

37. Sanlaville, D. *et al.* Functional disomy of the Xq28 chromosome region. *Eur. J. Hum. Genet.* **13**, 579–585 (2005).

38. Friez, M. J. *et al.* Recurrent Infections, Hypotonia, and Mental Retardation Caused by Duplication of MECP2 and Adjacent Region in Xq28. *Pediatrics* **118**, e1687–e1695 (2006).

39. Yang, T. *et al.* Overexpression of Methyl-CpG Binding Protein 2 Impairs TH1 Responses. *Sci. Transl. Med.* **4**, 163ra158 (2012).

40. Ramocki, M. B. *et al.* Autism and Other Neuropsychiatric Symptoms Are Prevalent in Individuals With MECP2 Duplication Syndrome. *Ann. Neurol.* **66**, 771–782 (2009).

41. Peters, S. U. *et al.* The Behavioral Phenotype in MECP2 Duplication Syndrome: A Comparison with Idiopathic Autism. *Autism Res.* **6**, 42–50 (2013).

42. Van Esch, H. MECP2 Duplication Syndrome. *Mol. Syndromol.* **2**, 128–136 (2012).

43. Lugtenberg, D. *et al.* Structural variation in Xq28: MECP2 duplications in 1% of patients with unexplained XLMR and in 2% of male patients with severe encephalopathy. *Eur. J. Hum. Genet.* **17**, 444–453 (2009).

44. Reardon, W. *et al.* Progressive cerebellar degenerative changes in the severe mental retardation syndrome caused by duplication of MECP2 and adjacent loci on Xq28. *Eur. J. Pediatr.* **169**, 941–949 (2010).

45. Schwoerer, J. S. *et al.* MECP2 Duplication: Possible Cause of Severe Phenotype in Females. *Am. J. Med. Genet. Part A* **164A**, 1029–1034 (2014).

46. Peters, S. *et al.* Characterizing the Phenotypic Effect of Xq28 Duplication Size in MECP2 Duplication Syndrome. *Clin. Genet.* **95**, 575–581 (2019).

47. Clayton-Smith, J. *et al.* Xq28 duplication presenting with intestinal and bladder dysfunction and a distinctive facial appearance. *Eur. J. Hum. Genet.* **17**, 434–443 (2009).

48. Nakagawa, O. *et al.* Centronuclear myopathy in mice lacking a novel muscle-specific protein kinase transcriptionally regulated by MEF2. *Genes Dev.* **19**, 2066–2077 (2005).

49. Vandewalle, J. *et al.* Dosage-Dependent Severity of the Phenotype in Patients with Mental Retardation Due to a Recurrent Copy-Number Gain at Xq28 Mediated by an Unusual Recombination. *Am. J. Hum. Genet.* **85**, 809–822 (2009).

50. Vanmarsenille, L. *et al.* Increased Dosage of RAB39B Affects Neuronal Development and Could Explain the Cognitive Impairment in Male Patients with Distal Xq28 Copy Number Gains. *Hum. Mutat.* **35**, 377–383 (2014).

51. Smith, Z. D. & Meissner, A. DNA methylation: roles in mammalian development. *Nat. Rev. Genet.* **14**, 204–220 (2013).

52. Jones, P. A. Functions of DNA methylation: islands, start sites, gene bodies and beyond. *Nat. Rev. Genet.* **13**, 484–492 (2012).

53. Ehrlich, M. *et al.* Amount and distribution of 5-methylcytosine in human DNA from different types of tissues or cells. *Nucleic Acids Res.* **10**, 2709–2721 (1982).

54. Meehan, R. R., Lewis, J. D. & Bird, A. P. Characterization of MeCP2, a vertebrate DNA binding protein with affinity for methylated DNA. *Nucleic Acids Res.* **20**, 5085–5092 (1992).

55. Saxonov, S., Berg, P. & Brutlag, D. L. A genome-wide analysis of CpG dinucleotides in the human genome distinguishes two distinct classes of promoters. *PNAS* **103**, 1412–1417 (2006).

56. Ball, M. P. *et al.* Targeted and genome-scale strategies reveal gene-body methylation signatures in human cells. *Nat. Biotechnol.* **27**, 361–368 (2009).

57. Xie, W. *et al.* Base-Resolution Analyses of Sequence and Parent-of-Origin Dependent DNA Methylation in the Mouse Genome. *Cell* **148**, 816–831 (2012).

58. Varley, K. E. *et al.* Dynamic DNA methylation across diverse human cell lines and tissues. *Genome Res.* **23**, 555–567 (2013).

59. Lister, R. *et al.* Global Epigenomic Reconfiguration During Mammalian Brain Development. *Science* **341**, 1237905 (2013).

60. Huttenlocher, P. R. & Dabholkar, A. S. Regional Differences in Synaptogenesis in Human Cerebral Cortex. *J. Comp. Neurol.* **387**, 167–178 (1997).

61. De Felipe, J., Marco, P., Fairén, A. & Jones, E. G. Inhibitory Synaptogenesis in Mouse Somatosensory Cortex. *Cereb. Cortex* **7**, 619–634 (1997).

62. Shahbazian, M. D., Antalffy, B. A., Armstrong, D. L. & Zoghbi, H. Y. Insight into Rett syndrome: MeCP2 levels display tissue- and cell-specific differences and correlate with neuronal maturation. *Hum. Mol. Genet.* **11**, 115–124 (2002).

63. Guo, J. U., Su, Y., Zhong, C., Ming, G. L. & Song, H. Hydroxylation of 5-Methylcytosine by TET1 Promotes Active DNA Demethylation in the Adult Brain. *Cell* **145**, 423–434 (2011).

64. Tahiliani, M. *et al.* Conversion of 5-Methylcytosine to 5-Hydroxymethylcytosine in Mammalian DNA by MLL Partner TET1. *Science* **324**, 930–935 (2009).

65. Globisch, D. *et al.* Tissue Distribution of 5-Hydroxymethylcytosine and Search for Active Demethylation

Intermediates. *PLoS One* **5**, e15367 (2010).

66. Kriaucionis, S. & Heintz, N. The Nuclear DNA Base 5-Hydroxymethylcytosine Is Present in Purkinje Neurons and the Brain. *Science* **324**, 929–930 (2009).

67. Mellén, M., Ayata, P., Dewell, S., Kriaucionis, S. & Heintz, N. MeCP2 Binds to 5hmC Enriched within Active Genes and Accessible Chromatin in the Nervous System. *Cell* **151**, 1417–1430 (2012).

68. Mellén, M., Ayata, P. & Heintz, N. 5-Hydroxymethylcytosine accumulation in postmitotic neurons results in functional demethylation of expressed genes. *PNAS* **114**, E7812–E7821 (2017).

69. Lewis, J. D. *et al.* Purification, Sequence, and Cellular Localization of a Novel Chromosomal Protein That Binds to Methylated DNA. *Cell* **69**, 905–914 (1992).

70. Nan, X., Meehan, R. R. & Bird, A. Dissection of the methyl-CpG binding domain from the chromosomal protein MeCP2. *Nucleic Acids Res.* **21**, 4886–4892 (1993).

71. Guo, J. U. *et al.* Distribution, recognition and regulation of non-CpG methylation in the adult mammalian brain. *Nat. Neurosci.* **17**, 215–222 (2014).

72. Chen, L. *et al.* MeCP2 binds to non-CG methylated DNA as neurons mature, influencing transcription and the timing of onset for Rett syndrome. *PNAS* **112**, 5509–5514 (2015).

73. Gabel, H. W. *et al.* Disruption of DNA-methylation-dependent long gene repression in Rett syndrome. *Nature* **522**, 89–93 (2015).

74. Ho, K. L. *et al.* MeCP2 Binding to DNA Depends upon Hydration at Methyl-CpG. *Mol. Cell* **29**, 525–531 (2008).

75. Wakefield, R. I. D. *et al.* The Solution Structure of the Domain from MeCP2 that Binds to Methylated DNA. *J. Mol. Biol.* **291**, 1055–1065 (1999).

76. Nan, X., Campoy, F. J. & Bird, A. MeCP2 is a transcriptional repressor with abundant binding sites in genomic chromatin. *Cell* **88**, 471–481 (1997).

77. Lyst, M. J. *et al.* Rett syndrome mutations abolish the interaction of MeCP2 with the NCoR/SMRT co-repressor. *Nat. Neurosci.* **16**, 898–902 (2013).

78. Kruusvee, V. *et al.* Structure of the MeCP2–TBLR1 complex reveals a molecular basis for Rett syndrome and related disorders. *Proc. Natl. Acad. Sci.* **114**, E3243–E3250 (2017).

79. Ben-Shachar, S., Chahrour, M., Thaller, C., Shaw, C. A. & Zoghbi, H. Y. Mouse models of MeCP2 disorders share gene expression changes in the cerebellum and hypothalamus. *Hum. Mol. Genet.* **18**, 2431–2442 (2009).

80. Chahrour, M. *et al.* MeCP2, a Key Contributor to Neurological Disease, Activates and Represses Transcription. *Science* **320**, 1224–1229 (2008).

81. Li, Y. *et al.* Global Transcriptional and Translational Repression in Human-Embryonic-Stem-Cell-Derived Rett

Syndrome Neurons. *Cell Stem Cell* **13**, 446–458 (2013).

82. Adams, V. H., McBryant, S. J., Wade, P. A., Woodcock, C. L. & Hansen, J. C. Intrinsic Disorder and Autonomous Domain Function in the Multifunctional Nuclear Protein, MeCP2. *J. Biol. Chem.* **282**, 15057–15064 (2007).

83. Ghosh, R. P. *et al.* Unique Physical Properties and Interactions of the Domains of Methylated DNA Binding Protein 2. *Biochemistry* **49**, 4395–4410 (2010).

84. Aravind, L. & Landsman, D. AT-hook motifs identified in a wide variety of DNA-binding proteins. *Nucleic Acids Res.* **26**, 4413–4421 (1998).

85. Baker, S. A. *et al.* An AT-hook Domain in MeCP2 Determines the Clinical Course of Rett Syndrome and Related Disorders. *Cell* **152**, 984–996 (2013).

86. Lyst, M. J., Connelly, J., Merusi, C. & Bird, A. Sequence-specific DNA binding by AT-hook motifs in MeCP2. *FEBS Lett.* **590**, 2927–2933 (2016).

87. Kishi, N. & Macklis, J. D. MECP2 is progressively expressed in post-migratory neurons and is involved in neuronal maturation rather than cell fate decisions. *Mol. Cell. Neurosci.* **27**, 306–321 (2004).

88. Skene, P. J. *et al.* Neuronal MeCP2 Is Expressed at Near Histone-Octamer Levels and Globally Alters the Chromatin State. *Mol. Cell* **37**, 457–468 (2010).

89. Yasui, D. H. *et al.* Integrated epigenomic analyses of neuronal MeCP2 reveal a role for long-range interaction with active genes. *PNAS* **104**, 19416–19421 (2007).

90. Boxer, L. D. *et al.* MeCP2 Represses the Rate of Transcriptional Initiation of Highly Methylated Long Genes. *Mol. Cell* **77**, 294-309.e9 (2020).

91. Clemens, A. W. *et al.* MeCP2 Represses Enhancers through Chromosome Topology-Associated DNA Methylation. *Mol. Cell* **77**, 279-293.e8 (2020).

92. Zhou, Z. *et al.* Brain-specific Phosphorylation of MeCP2 Regulates Activity-Dependent Bdnf Transcription, Dendritic Growth, and Spine Maturation. *Neuron* **52**, 255–69 (2006).

93. Ebert, D. H. *et al.* Activity-dependent phosphorylation of MeCP2 threonine 308 regulates interaction with NCoR. *Nature* **499**, 341–345 (2013).

94. Georgel, P. T. *et al.* Chromatin Compaction by Human MeCP2. *J. Biol. Chem.* **278**, 32181–32188 (2003).

95. Ghosh, R. P., Horowitz-Scherer, R. A., Nikitina, T., Shlyakhtenko, L. S. & Woodcock, C. L. MeCP2 Binds Cooperatively to Its Substrate and Competes with Histone H1 for Chromatin Binding Sites. *Mol. Cell. Biol.* **30**, 4656–4670 (2010).

96. Zappella, M. *et al.* Study of MECP2 Gene in Rett Syndrome Variants and Autistic Girls. *Am. J. Med. Genet. - Neuropsychiatr. Genet.* **119B**, 102–107 (2003).

97. Mount, R. H., Charman, T., Hasting, R. P., Reilly, S. & Cass, H. Features of Autism in Rett Syndrome and Severe Mental Retardation. *J. Autism Dev. Disord.* **33**, 435–442 (2003).

98. Carney, R. M. *et al.* Identification of MeCP2 Mutations in a Series of Females with Autistic Disorder. *Pediatr. Neurol.* **28**, 205–211 (2003).

99. Shibayama, A. *et al.* MECP2 Structural and 3′-UTR Variants in Schizophrenia, Autism and Other Psychiatric Diseases: A Possible Association with Autism. *Am. J. Med. Genet. - Neuropsychiatr. Genet.* **128B**, 50–53 (2004).

100. Hitchins, M. P. *et al.* Investigation of UBE3A and MECP2 in Angelman syndrome (AS) and Patients With Features of AS. *Am. J. Med. Genet.* **125A**, 167–172 (2004).

101. Watson, P. *et al.* Angelman syndrome phenotype associated with mutations in MECP2, a gene encoding a methyl CpG binding protein. *J. Med. Genet.* **38**, 224–228 (2001).

102. Couvert, P. *et al.* MECP2 is highly mutated in X-linked mental retardation. *Hum. Mol. Genet.* **10**, 941–946 (2001).

103. Lyon, M. F. Gene Action in the X-chromosome of the Mouse (Mus musculus L.). *Nature* **190**, 372–373 (1961).

104. Young, J. I. & Zoghbi, H. Y. X-Chromosome Inactivation Patterns Are Unbalanced and Affect the Phenotypic Outcome in a Mouse Model of Rett Syndrome. *Am. J. Hum. Genet.* **74**, 511–520 (2004).

105. Enikanolaiye, A. *et al.* Suppressor mutations in Mecp2-null mice implicate the DNA damage response in Rett syndrome pathology. *Genome Res.* **30**, 540–552 (2020).

106. Achilly, N. P., Wang, W. & Zoghbi, H. Y. Presymptomatic training mitigates functional deficits in Rett syndrome mice. *Nature* **592**, 596–600 (2021).

107. Downs, J. *et al.* Environmental enrichment intervention for Rett syndrome: an individually randomised stepped wedge trial. *Orphanet J. Rare Dis.* **13**, 3 (2018).

108. Brown, K. *et al.* The molecular basis of variable phenotypic severity among common missense mutations causing Rett syndrome. *Hum. Mol. Genet.* **25**, 558–570 (2016).

109. Ibrahim, A. *et al.* MeCP2 is a microsatellite binding protein that protects CA repeats from nucleosome invasion. *Science* **372**, eabd5581 (2021).

110. Merritt, J. K., Collins, B. E., Erickson, K. R., Dong, H. & Neul, J. L. Pharmacological read-through of R294X Mecp2 in a novel mouse model of Rett syndrome. *Hum. Mol. Genet.* **29**, 2461–2470 (2020).

111. Guy, J. *et al.* A mutation-led search for novel functional domains in MeCP2. *Hum. Mol. Genet.* **27**, 2531–2545 (2018).

112. Nikitina, T. *et al.* Multiple Modes of Interaction between the Methylated DNA Binding Protein MeCP2 and Chromatin. *Mol. Cell. Biol.* **27**, 864–877 (2007).

113. Chen, R. Z., Akbarian, S., Tudor, M. & Jaenisch, R. Deficiency of methyl-CpG binding protein-2 in CNS neurons results in a Rett-like phenotype in mice. *Nat. Genet.* **27**, 327–331 (2001).

114. Guy, J., Hendrich, B., Holmes, M., Martin, J. E. & Bird, A. A mouse Mecp2-null mutation causes neurological symptoms that mimic Rett syndrome. *Nat. Genet.* **27**, 322–326 (2001).

115. Lioy, D. T. *et al.* A role for glia in the progression of Rett's syndrome. *Nature* **475**, 497–500 (2011).

116. Cronk, J. C. *et al.* Methyl-CpG Binding Protein 2 Regulates Microglia and Macrophage Gene Expression in Response to Inflammatory Stimuli. *Immunity* **42**, 679–691 (2015).

117. Wang, J. *et al.* Wild-type microglia do not reverse pathology in a mouse models of Rett syndrome. *Nature* **521**, E1–E4 (2015).

118. McGraw, C. M., Samaco, R. C. & Zoghbi, H. Y. Adult neural function requires MeCP2. *Science* **333**, 186 (2011).

119. Guy, J., Gan, J., Selfridge, J., Cobb, S. & Bird, A. Reversal of Neurological Defects in a Mouse Model of Rett Syndrome. *Science* **315**, 1143–1147 (2007).

120. Robinson, L. *et al.* Morphological and functional reversal of phenotypes in a mouse model of Rett syndrome. *Brain* **135**, 2699–2710 (2012).

121. Gemelli, T. *et al.* Postnatal Loss of Methyl-CpG Binding Protein 2 in the Forebrain is Sufficient to Mediate Behavioral Aspects of Rett Syndrome in Mice. *Biol. Psychiatry* **59**, 468–476 (2006).

122. Su, S.-H., Kao, F.-C., Huang, Y.-B. & Liao, W. MeCP2 in the Rostral Striatum Maintains Local Dopamine Content Critical for Psychomotor Control. *J. Neurosci.* **35**, 6209–6220 (2015).

123. Fyffe, S. L. *et al.* Deletion of Mecp2 in Sim1-Expressing Neurons Reveals a Critical Role for MeCP2 in Feeding Behavior, Aggression, and the Response to Stress. *Neuron* **59**, 947–958 (2008).

124. Achilly, N. P. *et al.* Deleting Mecp2 from the cerebellum rather than its neuronal subtypes causes a delay in motor learning in mice. *Elife* **10**, 1–20 (2021).

125. Meng, X. *et al.* Manipulations of MeCP2 in glutamatergic neurons highlight their contributions to Rett and other neurological disorders. *Elife* **5**, e14199 (2016).

126. Chao, H.-T. *et al.* Dysfunction in GABA signalling mediates autism-like stereotypies and Rett syndrome phenotypes. *Nature* **468**, 263–269 (2010).

127. Samaco, R. C. *et al.* Loss of MeCP2 in aminergic neurons causes cell-autonomous defects in neurotransmitter synthesis and specific behavioral abnormalities. *PNAS* **106**, 21966–21971 (2009).

128. Ito-Ishida, A., Ure, K., Chen, H., Swann, J. W. & Zoghbi, H. Y. Loss of MeCP2 in Parvalbumin-and Somatostatin-Expressing Neurons in Mice Leads to Distinct Rett Syndrome-like Phenotypes. *Neuron* **88**, 651–658 (2015).

129. Heckman, L. D., Chahrour, M. H. & Zoghbi, H. Y. Rett-causing mutations reveal two domains critical for MeCP2 function and for toxicity in MECP2 duplication syndrome mice. *Elife* **3**, e02676 (2014).

130. Rangasamy, S. *et al.* Reduced neuronal size and mTOR pathway activity in the Mecp2 A140V Rett syndrome mouse

model. *F1000Research* **5**, 1–16 (2016).

131. Johnson, B. *et al.* Biotin tagging of MeCP2 in mice reveals contextual insights into the Rett syndrome transcriptome. *Nat. Med.* **23**, 1203–1214 (2017).

132. Goffin, D. *et al.* Rett syndrome mutation MeCP2 T158A disrupts DNA binding, protein stability and ERP responses. *Nat. Neurosci.* **15**, 274–283 (2012).

133. Wegener, E. *et al.* Characterization of the MeCP2R168X Knockin Mouse Model for Rett Syndrome. *PLoS One* **9**, e115444 (2014).

134. Pitcher, M. R. *et al.* Rett syndrome like phenotypes in the R255X Mecp2 mutant mouse are rescued by MECP2 transgene. *Hum. Mol. Genet.* **24**, 2662–2672 (2015).

135. Brendel, C. *et al.* Readthrough of nonsense mutations in Rett syndrome: evaluation of novel aminoglycosides and generation of a new mouse model. *J. Mol. Med.* **89**, 389–398 (2011).

136. Ghosh, R. P., Horowitz-Scherer, R. A., Nikitina, T., Gierasch, L. M. & Woodcock, C. L. Rett Syndrome-causing Mutations in Human MeCP2 Result in Diverse Structural Changes That Impact Folding and DNA Interactions. *J. Biol. Chem.* **283**, 20523–20534 (2008).

137. Asaka, Y., Jugloff, D. G. M., Zhang, L., Eubanks, J. H. & Fitzsimonds, R. M. Hippocampal synaptic plasticity is impaired in the Mecp2-null mouse model of Rett syndrome. *Neurobiol. Dis.* **21**, 217–227 (2006).

138. Moretti, P. *et al.* Learning and Memory and Synaptic Plasticity are Impaired in a Mouse Model of Rett Syndrome. *J. Neurosci.* **26**, 319–327 (2006).

139. Nelson, E. D., Bal, M., Kavalali, E. T. & Monteggia, L. M. Selective impact of MeCP2 and associated histone deacetylases on the dynamics of evoked excitatory neurotransmission. *J. Neurophysiol.* **106**, 193–201 (2011).

140. Na, E. S., Nelson, E. D., Kavalali, E. T. & Monteggia, L. M. The Impact of MeCP2 Loss-or Gain-of-Function on Synaptic Plasticity. *Neuropsychopharmacology* **38**, 212–219 (2013).

141. Liu, L. *et al.* Role of NMDA Receptor Subtypes in Governing the Direction of Hippocampal Synaptic Plasticity. *Science* **304**, 1021-1024. (2004).

142. Qiu, Z. *et al.* The Rett Syndrome Protein MeCP2 Regulates Synaptic Scaling. *J. Neurosci.* **32**, 989–994 (2012).

143. Blackman, M. P., Djukic, B., Nelson, S. B. & Turrigiano, G. G. A critical and cell-autonomous role for MeCP2 in synaptic scaling up. *J. Neurosci.* **32**, 13529–13536 (2012).

144. Fukuda, T., Itoh, M., Ichikawa, T., Washiyama, K. & Goto, Y. I. Delayed Maturation of Neuronal Architecture and Synaptogenesis in Cerebral Cortex of Mecp2-Deficient Mice. *J. Neuropathol. Exp. Neurol.* **64**, 537–544 (2005).

145. Marchetto, M. C. N. *et al.* A Model for Neural Development and Treatment of Rett Syndrome Using Human Induced Pluripotent Stem Cells. *Cell* **143**, 527–539 (2010).

146. Chapleau, C. A. *et al.* Dendritic spine pathologies in hippocampal pyramidal neurons from Rett syndrome brain and after expression of Rett-associated MECP2 mutations. *Neurobiol. Dis.* **35**, 219–233 (2010).

147. Schüle, B., Armstrong, D. D., Vogel, H., Oviedo, A. & Francke, U. Severe congenital encephalopathy caused by MECP2 null mutations in males: central hypoxia and reduced neuronal dendritic structure. *Clin. Genet.* **74**, 116–126 (2008).

148. Luikenhuis, S., Giacometti, E., Beard, C. F. & Jaenisch, R. Expression of MeCP2 in postmitotic neurons rescues Rett syndrome in mice. *PNAS* **101**, 6033–6038 (2004).

149. Na, E. S. *et al.* A Mouse Model for MeCP2 Duplication Syndrome: MeCP2 Overexpression Impairs Learning and Memory and Synaptic Transmission. *J. Neurosci.* **32**, 3109–3117 (2012).

150. Sztainberg, Y. *et al.* Reversal of phenotypes in MECP2 duplication mice using genetic rescue or antisense oligonucleotides. *Nature* **528**, 123–126 (2015).

151. Samaco, R. C. *et al.* Crh and Oprm1 mediate anxiety-related behavior and social approach in a mouse model of MECP2 duplication syndrome. *Nat. Genet.* **44**, 206–211 (2012).

152. Yu, B. *et al.* Reversal of Social Recognition Deficit in Adult Mice with MECP2 Duplication via Normalization of MeCP2 in the Medial Prefrontal Cortex. *Neurosci. Bull.* **36**, 570–584 (2020).

153. Na, E. S., Morris, M. J., Nelson, E. D. & Monteggia, L. M. GABAa Receptor Antagonism Ameliorates Behavioral and Synaptic Impairments Associated with MeCP2 Overexpression. *Neuropsychopharmacology* **39**, 1946–1954 (2014).

154. Chao, H. T., Zoghbi, H. Y. & Rosenmund, C. MeCP2 Controls Excitatory Synaptic Strength by Regulating Glutamatergic Synapse Number. *Neuron* **56**, 58–65 (2007).

155. Nageshappa, S. *et al.* Altered neuronal network and rescue in a human MECP2 duplication model. *Mol. Psychiatry* **21**, 178–188 (2016).

156. Jiang, M. *et al.* Dendritic Arborization and Spine Dynamics are Abnormal in the Mouse Model of MECP2 Duplication Syndrome. *J. Neurosci.* **33**, 19518–19533 (2013).

157. Ash, R. T., Fahey, P. G., Park, J., Zoghbi, H. Y. & Smirnakis, S. M. Increased axonal bouton stability during learning in the mouse model of MECP2 duplication syndrome. *eNeuro* **5**, (2018).

158. Ash, R. T., Park, J., Suter, B., Smirnakis, S. M. & Zoghbi, H. Y. Excessive formation and stabilization of dendritic spine clusters in the mecp2-duplication syndrome mouse model of autism. *eNeuro* **8**, 1–13 (2021).

159. Ash, R. T. *et al.* Inhibition of Elevated Ras-MAPK Signaling Normalizes Enhanced Motor Learning and Excessive Clustered Dendritic Spine Stabilization in the MECP2-Duplication Syndrome Mouse Model of Autism. *eNeuro* **8**, ENEURO.0056-21.2021 (2021).

160. Renthal, W. *et al.* Characterization of human mosaic Rett syndrome brain tissue by single-nucleus RNA sequencing.

Nat. Neurosci. **21**, 1670–1679 (2018).

161. Chang, Q., Khare, G., Dani, V., Nelson, S. & Jaenisch, R. The Disease Progression of Mecp2 Mutant Mice Is Affected by the Level of BDNF Expression. *Neuron* **49**, 341–348 (2006).

162. Ogier, M. *et al.* Brain-Derived Neurotrophic Factor Expression and Respiratory Function Improve After Ampakine Treatment in a Mouse Model of Rett Syndrome. *J. Neurosci.* **27**, 10912–10917 (2007).

163. Deogracias, R. *et al.* Fingolimod , a sphingosine-1 phosphate receptor modulator, increases BDNF levels and improves symptoms of a mouse model of Rett syndrome. *PNAS* **109**, 14230–14235 (2012).

164. Naegelin, Y. *et al.* Fingolimod in children with Rett syndrome: the FINGORETT study. *Orphanet J. Rare Dis.* **16**, 19 (2021).

165. D'Ercole, A. J., Ye, P., Calikoglu, A. S. & Gutierrez-Ospina, G. The role of the insulin-like growth factors in the central nervous system. *Mol. Neurobiol.* **13**, 227–255 (1996).

166. Zheng, W. & Quirion, R. Comparative signaling pathways of insulin-like growth factor-1 and brain-derived neurotrophic factor in hippocampal neurons and the role of the PI3 kinase pathway in cell survival. *J. Neurochem.* **89**, 844–852 (2004).

167. O'Kusky, J. R., Ye, P. & D'Ercole, A. J. Insulin-like growth factor-I promotes neurogenesis and synaptogenesis in the hippocampal dentate gyrus during postnatal development. *J. Neurosci.* **20**, 8435–8442 (2000).

168. Tropea, D. *et al.* Partial reversal of Rett syndrome-like symptoms in MeCP2 mutant mice. *Proc. Natl. Acad. Sci.* **106**, 2029–2034 (2009).

169. Glaze, D. G. *et al.* A Double-Blind, Randomized, Placebo-Controlled Clinical Study of Trofinetide in the Treatment of Rett Syndrome. *Pediatr. Neurol.* **76**, 37–46 (2017).

170. Glaze, D. G. *et al.* Double-blind, randomized, placebo-controlled study of trofinetide in pediatric Rett syndrome. *Neurology* **92**, e1912–e1925 (2019).

171. Autry, A. E. *et al.* NMDA receptor blockade at rest triggers rapid behavioural antidepressant responses. *Nature* **475**, 91–96 (2011).

172. Kron, M. *et al.* Brain activity mapping in Mecp2 mutant mice reveals functional deficits in forebrain circuits, including key nodes in the default mode network, that are reversed with ketamine treatment. *J. Neurosci.* **32**, 13860–13872 (2012).

173. Lombardi, L. M., Baker, S. A. & Zoghbi, H. Y. MECP2 disorders: from the clinic to mice and back. *J. Clin. Invest.* **125**, 2914–2923 (2015).

174. Garg, S. K. *et al.* Systemic Delivery of MeCP2 Rescues Behavioral and Cellular Deficits in Female Mouse Models of Rett Syndrome. *J. Neurosci.* **33**, 13612–13620 (2013).

175. Gadalla, K. K. *et al.* Improved Survival and Reduced Phenotypic Severity Following AAV9/MECP2 Gene Transfer to Neonatal and Juvenile Male Mecp2 Knockout Mice. *Mol. Ther.* **21**, 18–30 (2013).

176. Gadalla, K. K. E. *et al.* Development of a Novel AAV Gene Therapy Cassette with Improved Safety Features and Efficacy in a Mouse Model of Rett Syndrome. *Mol. Ther. - Methods Clin. Dev.* **5**, 180–190 (2017).

177. Sinnett, S. E. *et al.* Improved MECP2 Gene Therapy Extends the Survival of MeCP2-Null Mice without Apparent Toxicity after Intracisternal Delivery. *Mol. Ther. - Methods Clin. Dev.* **5**, 106–115 (2017).

178. Matagne, V. *et al.* A codon-optimized Mecp2 transgene corrects breathing deficits and improves survival in a mouse model of Rett syndrome. *Neurobiol. Dis.* **99**, 1–11 (2017).

179. Matagne, V. *et al.* Severe offtarget effects following intravenous delivery of AAV9-MECP2 in a female mouse model of Rett syndrome. *Neurobiol. Dis.* **149**, 105235 (2021).

180. Przanowski, P. *et al.* Pharmacological reactivation of inactive X-linked Mecp2 in cerebral cortical neurons of living mice. *PNAS* **115**, 7991–7996 (2018).

181. Huong Le, T. T. *et al.* Efficient and Precise CRISPR/Cas9-Mediated MECP2 Modifications in Human-Induced Pluripotent Stem Cells. *Front. Genet.* **10**, (2019).

182. Sinnamon, J. R. *et al.* Site-directed RNA repair of endogenous Mecp2 RNA in neurons. *PNAS* **114**, E9395–E9402 (2017).

183. Sinnamon, J. R. *et al.* In Vivo Repair of a Protein Underlying a Neurological Disorder by Programmable RNA Editing. *Cell Rep.* **32**, 107878 (2020).

184. Nan, X. *et al.* Interaction between chromatin proteins MECP2 and ATRX is disrupted by mutations that cause inherited mental retardation. *PNAS* **104**, 2709–2714 (2007).

185. Kernohan, K. D. *et al.* ATRX Partners with Cohesin and MeCP2 and Contributes to Developmental Silencing of Imprinted Genes in the Brain. *Dev. Cell* **18**, 191–202 (2010).

186. Kernohan, K. D., Vernimmen, D., Gloor, G. B. & Bérubé, N. G. Analysis of neonatal brain lacking ATRX or MeCP2 reveals changes in nucleosome density, CTCF binding and chromatin looping. *Nucleic Acids Res.* **42**, 8356–8368 (2014).

187. Harikrishnan, K. N. *et al.* Brahma links the SWI/SNF chromatin-remodeling complex with MeCP2-dependent transcriptional silencing. *Nat. Genet.* **37**, 254–264 (2005).

188. Kokura, K. *et al.* The Ski Protein Family Is Required for MeCP2-mediated Transcriptional Repression. *J. Biol. Chem.* **276**, 34115–34121 (2001).

189. Ballas, N., Grunseich, C., Lu, D. D., Speh, J. C. & Mandel, G. REST and Its Corepressors Mediate Plasticity of Neuronal Gene Chromatin throughout Neurogenesis. *Cell* **121**, 645–657 (2005).

190. Kimura, H. & Shiota, K. Methyl-CpG-binding Protein, MeCP2, is a Target Molecule for Maintenance DNA Methyltransferase, Dnmt1. *J. Biol. Chem.* **278**, 4806–4812 (2003).

191. Fuks, F. *et al.* The Methyl-CpG-Binding Protein MeCP2 Links DNA Methylation to Histone Methylation. *J. Biol. Chem.* **278**, 4035–4040 (2003).

192. Agarwal, N. *et al.* MeCP2 interacts with HP1 and modulates its heterochromatin association during myogenic differentiation. *Nucleic Acids Res.* **35**, 5402–5408 (2007).

193. Jones, P. L. *et al.* Methylated DNA and MeCP2 recruit histone deacetylase to repress transcription. *Nat. Genet.* **19**, 187–191 (1998).

194. Nan, X. *et al.* Transcriptional repression by the methyl-CpG-binding protein MeCP2 involves a histone deacetylase complex. *Nature* **393**, 386–389 (1998).

195. Zhou, J. *et al.* Disruption of MeCP2-TCF20 complex underlies distinct neurodevelopmental disorders. *PNAS* **119**, e2119078119 (2022).

196. Young, J. I. *et al.* Regulation of RNA splicing by the methylation-dependent transcriptional repressor methyl-CpG binding protein 2. *Proc. Natl. Acad. Sci.* **102**, 17551–17558 (2005).

197. Forlani, G. *et al.* The MeCP2/YY1 interaction regulates ANT1 expression at 4q35: novel hints for Rett syndrome pathogenesis. *Hum. Mol. Genet.* **19**, 3114–3123 (2010).

198. Samaco, R. C. *et al.* Female Mecp2+/- mice display robust behavioral deficits on two different genetic backgrounds providing a framework for pre-clinical studies. *Hum. Mol. Genet.* **22**, 96–109 (2013).

199. Lawson-Yuen, A. *et al.* Ube3a mRNA and protein expression are not decreased in Mecp2R168X mutant mice. *Brain Res.* **1180**, 1–6 (2007).

200. Shahbazian, M. D. *et al.* Mice with Truncated MeCP2 Recapitulate Many Rett Syndrome Features and Display Hyperacetylation of Histone H3. *Neuron* **35**, 243–254 (2002).

201. Guideri, F., Acampa, M., DiPerri, T., Zappella, M. & Hayek, Y. Progressive Cardiac Dysautonomia Observed in Patients Affected by Classic Rett Syndrome and Not in the Preserved Speech Variant. *J. Child Neurol.* **16**, 370–373 (2001).

202. Tarquinio, D. C. *et al.* The course of awake breathing disturbances across the lifespan in Rett syndrome. *Brain Dev.* **40**, 515–529 (2018).

203. Glaze, D. G. *et al.* Epilepsy and the natural history of Rett syndrome. *Neurology* **74**, 909–912 (2010).

204. Giacometti, E., Luikenhuis, S., Beard, C. & Jaenisch, R. Partial rescue of MeCP2 deficiency by postnatal activation of MeCP2. *PNAS* **104**, 1931–1936 (2007).

205. del Gaudio, D. *et al.* Increased MECP2 gene copy number as the result of genomic duplication in

neurodevelopmentally delayed males. *Genet. Med.* **8**, 784–792 (2006).

206. Sandweiss, A. J., Brandt, V. L. & Zoghbi, H. Y. Advances in understanding of Rett syndrome and MECP2 duplication syndrome: prospects for future therapies. *Lancet Neurol.* **19**, 689–698 (2020).

207. Lamonica, J. M. *et al.* Elevating expression of MeCP2 T158M rescues DNA binding and Rett syndrome–like phenotypes. *J. Clin. Invest.* **127**, 1889–1904 (2017).

208. Moy, S. S. *et al.* Sociability and preference for social novelty in five inbred strains: an approach to assess autistic-like behavior in mice. *Genes, Brain Behav.* **3**, 287–302 (2004).

209. Ramirez, J.-M., Ward, C. S. & Neul, J. L. Breathing challenges in Rett Syndrome: Lessons learned from humans and animal models. *Respir. Physiol. Neurobiol.* **189**, 280–287 (2013).

210. Ward, C. S. *et al.* MeCP2 is Critical within HoxB1-Derived Tissues of Mice for Normal Lifespan. *J. Neurosci.* **31**, 10359–10370 (2011).

211. Huang, T.-W. *et al.* Progressive Changes in a Distributed Neural Circuit Underlie Breathing Abnormalities in Mice Lacking MeCP2. *J. Neurosci.* **36**, 5572–5586 (2016).

212. Ward, C. S. *et al.* Loss of MeCP2 Function Across Several Neuronal Populations Impairs Breathing Response to Acute Hypoxia. *Front. Neurol.* **11**, (2020).

213. Sansom, D., Krishnan, V. H. R., Corbett, J. & Kerr, A. Emotional and behavioural aspects of Rett syndrome. *Dev. Med. Child Neurol.* **35**, 340–345 (1993).

214. Mount, R. H., Charman, T., Hastings, R. P., Reilly, S. & Cass, H. The Rett Syndrome Behaviour Questionnaire (RSBQ): refining the behavioural phenotype of Rett syndrome. *J. Child Psychol. Psychiatry* **43**, 1099–1110 (2002).

215. Kerr, B., Alvarez-Saavedra, M., Sáez, M. A., Saona, A. & Young, J. I. Defective body-weight regulation, motor control and abnormal social interactions in Mecp2 hypomorphic mice. *Hum. Mol. Genet.* **17**, 1707–1717 (2008).

216. Schaevitz, L. R., Moriuchi, J. M., Nag, N., Mellot, T. J. & Berger-Sweeney, J. Cognitive and social functions and growth factors in a mouse model of Rett syndrome. *Physiol. Behav.* **100**, 255–263 (2010).

217. Braunschweig, D., Simcox, T., Samaco, R. C. & LaSalle, J. M. X-Chromosome inactivation ratios affect wild-type MeCP2 expression within mosaic Rett syndrome and Mecp2-/+ mouse brain. *Hum. Mol. Genet.* **13**, 1275–1286 (2004).

218. Shahbazian, M. D., Sun, Y. & Zoghbi, H. Y. Balanced X Chromosome Inactivation Patterns in the Rett Syndrome Brain. *Am. J. Med. Genet.* **111**, 164–168 (2002).

219. Amir, R. E. *et al.* Influence of Mutation Type and X Chromosome Inactivation on Rett Syndrome Phenotypes. *Ann. Neurol.* **47**, 670–679 (2000).

220. Knudsen, G. P. S. *et al.* Increased skewing of X chromosome inactivation in Rett syndrome patients and their mothers. *Eur. J. Hum. Genet.* **14**, 1189–1194 (2006).

221. Gogliotti, R. G. *et al.* mGlu7 potentiation rescues cognitive, social, and respiratory phenotypes in a mouse model of Rett syndrome. *Sci. Transl. Med.* **9**, eaai7459 (2017).

222. Gogliotti, R. G. *et al.* Total RNA Sequencing of Rett Syndrome Autopsy Samples Identifies the M4 Muscarinic Receptor as a Novel Therapeutic Target. *J. Pharmacol. Exp. Ther.* **365**, 291–300 (2018).

223. Katz, D. M. *et al.* Preclinical research in Rett syndrome: setting the foundation for translational success. *Dis. Model. Mech.* **5**, 733–745 (2012).

224. Javed, S., Selliah, T., Lee, Y.-J. & Huang, W.-H. Dosage-sensitive genes in autism spectrum disorders: From neurobiology to therapy. *Neurosci. Biobehav. Rev.* **118**, 538–567 (2020).

225. El Chehadeh, S. *et al.* Xq28 duplication including MECP2 in six unreported affected females: what can we learn for diagnosis and genetic counselling? *Clin. Genet.* **91**, 576–588 (2017).

226. Rothwell, P. E. *et al.* Autism-Associated Neuroligin-3 Mutations Commonly Impair Striatal Circuits to Boost Repetitive Behaviors. *Cell* **158**, 198–212 (2014).

227. Weaving, L., Ellaway, C., Gécz, J. & Christodoulou, J. Rett syndrome: clinical review and genetic update. *J. Med. Genet.* **42**, 1–7 (2005).

228. Bebbington, A. *et al.* Updating the profile of C-terminal MECP2 deletions in Rett syndrome. *J. Med. Genet.* **47**, 242–248 (2010).

229. Shah, R. R. *et al.* Efficient and versatile CRISPR engineering of human neurons in culture to model neurological disorders. *Wellcome Open Res.* **1**, (2016).

230. Scholz, D. *et al.* Rapid, complete and large-scale generation of post-mitotic neurons from the human LUHMES cell line. *J. Neurochem.* **119**, 957–971 (2011).

231. Ran, F. A. *et al.* Genome engineering using the CRISPR-Cas9 system. *Nat. Protoc.* **8**, 2281–2308 (2013).

232. Mao, A. J. *et al.* Neuronal Differentiation and Growth Control of Neuro-2a Cells After Retroviral Gene Delivery of Connexin43. *J. Biol. Chem.* **275**, 34407–34414 (2000).

233. Dasgupta, B. & Milbrandt, J. Resveratrol stimulates AMP kinase activity in neurons. *PNAS* **104**, 7217–7222 (2007).

234. Tremblay, R. G. *et al.* Differentiation of mouse Neuro 2A cells into dopamine neurons. *J. Neurosci. Methods* **186**, 60–67 (2010).

235. Evangelopoulos, M. E., Weis, J. & Krüttgen, A. Signalling pathways leading to neuroblastoma differentiation after serum withdrawal: HDL blocks neuroblastoma differentiation by inhibition of EGFR. *Oncogene* **24**, 3309–3318 (2005).

236. Lotharius, J. *et al.* Effect of Mutant α-Synuclein on Dopamine Homeostasis in a New Human Mesencephalic Cell Line. *J. Biol. Chem.* **277**, 38884–38894 (2002).

237. Lotharius, J. *et al.* Progressive Degeneration of Human Mesencephalic Neuron-Derived Cells Triggered by

Dopamine-Dependent Oxidative Stress Is Dependent on the Mixed-Lineage Kinase Pathway. *J. Neurosci.* **25**, 6329–6342 (2005).

238. Paul, G. *et al.* Tyrosine hydroxylase expression is unstable in a human immortalized mesencephalic cell line - Studies in vitro and after intracerebral grafting in vivo. *Mol. Cell. Neurosci.* **34**, 390–399 (2007).

239. Gantz, S. C., Ford, C. P., Neve, K. A. & Williams, J. T. Loss of Mecp2 in Substantia Nigra Dopamine Neurons Compromises the Nigrostriatal Pathway. *J. Neurosci.* **31**, 12629–12637 (2011).

240. Panayotis, N. *et al.* Morphological and functional alterations in the substantia nigra pars compacta of the Mecp2-null mouse. *Neurobiol. Dis.* **41**, 385–397 (2011).

241. Molinoff, P. B. & Axelrod, J. Biochemisry of Catecholamines. *Annu. Rev. Biochem.* **40**, 465–500 (1971).

242. Shao, Y. *et al.* Antisense oligonucleotide therapy in a humanized mouse model of MECP2 duplication syndrome. *Sci. Transl. Med.* **13**, eaaz7785 (2021).

243. Sinnett, S. E., Boyle, E., Lyons, C. & Gray, S. J. Engineered microRNA-based regulatory element permits safe high-dose miniMECP2 gene therapy in Rett mice. *Brain* **144**, 3005–3019 (2021).

244. Schneider-Poetsch, T. *et al.* Inhibition of Eukaryotic Translation Elongation by Cycloheximide and Lactimidomycin. *Nat. Chem. Biol.* **6**, 209–217 (2010).